2012

Porous silicon platform technologies for transmembrane protein investigation

Khalid Hasan Tantawi

POROUS SILICON PLATFORM TECHNOLOGIES FOR TRANSMEMBRANE PROTEIN INVESTIGATION

by

KHALID HASAN TANTAWI

A DISSERTATION

Submitted in partial fulfillment of the requirements
for the degree of Doctor of Philosophy
in
The Electrical Engineering Program
to
The School of Graduate Studies
of
The University of Alabama in Huntsville

HUNTSVILLE, ALABAMA

2012

In presenting this dissertation in partial fulfillment of the requirements for a doctoral degree from The University of Alabama in Huntsville, I agree that the Library of this University shall make it freely available for inspection. I further agree that permission for extensive copying for scholarly purposes may be granted by my advisor or, in his/her absence, by the Chair of the Department or the Dean of the School of Graduate Studies. It is also understood that due recognition shall be given to me and to The University of Alabama in Huntsville in any scholarly use which may be made of any material in this dissertation.

June 8, 2012

(Khalid Hasan Tantawi) (date)

DISSERTATION APPROVAL FORM

Submitted by Khalid Hasan Tantawi in partial fulfillment of the requirements for the degree of Doctor of Philosophy in Electrical Engineering and accepted on behalf of the Faculty of the School of Graduate Studies by the dissertation committee.

We, the undersigned members of the Graduate Faculty of The University of Alabama in Huntsville, certify that we have advised and/or supervised the candidate on the work described in this dissertation. We further certify that we have reviewed the dissertation manuscript and approve it in partial fulfillment of the requirements for the degree of Doctor of Philosophy in Electrical Engineering.

6/8/12 Committee Chair
(Date)

6/28/2012

6/28/12

6/29/12

Department Chair

College Dean

7/26/12 Graduate Dean

ABSTRACT

The School of Graduate Studies
The University of Alabama in Huntsville

Degree Doctor of Philosophy College/Dept. Engineering/Electrical and Computer Engineering.

Name of Candidate Khalid Hasan Tantawi

Title Porous Silicon Platform Technologies for Transmembrane Protein Investigation

This work presents the research in which a device is fabricated to investigate the functionalities of transmembrane proteins and artificial lipid membranes. The device is composed of a supported porous silicon membrane which in turn is a backbone that supports a lipid bilayer membrane (LBM) fused with epithelial sodium channel (ENaC) proteins. The electrochemically-fabricated porous silicon membrane had pore diameters in the range 0.2~2 μm. Lipid bilayer membranes were composed of two synthetic phospholipids: 1,2-diphytanoyl-*sn*-glycero-3-phosphoserine and 1,2-diphytanoyl-*sn*-glycero-3-phosphoethanolamine. The lipid bilayer membrane was formed from the two phospholipids by means of the Langmuir-Blodgett and Langmuir- Schaefer techniques, at a monolayer surface tension of 26 mN/m at room temperature, and on a deionized water subphase, which resulted in an average molecular area of 0.68-0.73 nm^2. The resulting device demonstrates the functionality of the transmembrane ion channels and the lipid bilayer membranes. The device provides full visual and physical accessibility to the biological membranes and proteins from both sides. The photoluminescence, biocompatibility, and biodegradability properties of porous silicon as well as availability, make it superior over other porous materials, and thus suitable for *in-vivo* monitoring. Characterization of the porous silicon-LBM-ENaC system was performed using atomic

force microscopy (AFM), electrical impedance spectroscopy (EIS), contact angle measurements, and optical microscopy. The porous silicon membrane was also investigated using scanning electron microscopy (SEM). The measured capacitance and resistance of the system composed of the 0.1M NaCl electrolyte and the porous silicon membrane were about 1.39 $\mu F/cm^2$ and 3.25×10^4 $\Omega.cm^2$, respectively. The lipid bilayer membrane had a capacitance of about 0.194 $\mu F/cm^2$, and a resistance of about 2.35×10^5 $\Omega.cm^2$. The epithelial sodium channel proteins resulted in a capacitance of about 0.222 $\mu F/cm^2$ and a resistance of about 1.81×10^5 $\Omega.cm^2$. This technology can be used for investigating functionalities of numerous other lipid membranes and transmembrane proteins.

Abstract Approval: Committee Chair

Department Chair

Graduate Dean Rhonda Kay Gaede 7/26/12

ACKNOWLEDGEMENTS

"What a piece of work is a man, how noble in reason, how infinite in faculties . . . how express and admirable in action."[*] Now that I stand at the end of the road, of my four years at UAHuntsville, I have been honored to know and work with many faculty, colleagues, and friends. For them, I would like to say thank you.

Of those I am gratefully indebted to, I would like to thank my advisor Dr. John D. Williams, for his infinite patience, and expressive support, and more importantly, because he taught me the skills, determination, and the thinking perspective that I need to continue on my journey in life from a new path and in a new career henceforth.

I would also like to thank Dr. Ramon Cerro from the Chemical Engineering Department for his tremendous help and support, and for allowing me to freely perform experiments in his laboratory. I am also indebted to Dr. Emanuel Waddell from the Department of Chemistry and Material Science for his support, advices, and helpfulness in performing research and utilizing the lab equipment in the Chemistry Department.

This research would not have been finished in this form without the help and collaboration from Dr. Bakhrom Berdiev from the Department of Microbiology in the University of Alabama at Birmingham, for supplying me with the purified proteins that I used in this research, as well as Dr. Elena Diaz Martin and Dr. Francisco J. Montez from the University of Salamanca for the help in performing lipid bilayer membrane experiments. I extremely appreciate the tremendous help from Dr. Darayas Patel at the Department of Mathematics and Computer Sciences in Oakwood University for the help in performing atomic force microscopy (AFM) in his lab.

[*] W. Shakespeare, *The Tragedy of Hamlet*, Act II

I gratefully thank every member of my research committee: Dr. Robert Lindquist, Dr. Jennifer English, Dr. Richard Fork, Dr. Sivaguru Ravindran, as well as Dr. Ramon Cerro and Dr. John Williams.

I owe a special thanks to the Alabama EPSCoR Graduate Research Scholars Program for supporting me with the research award to perform this work.

Although four years have passed quickly “like a shooting star”, I have had the honor to know many people, of whom I would especially mention Dr. Malek Abunaemeh, Sandeep Bettadapura, Mohammed Alzaybak, Jennifer Dover, and Anna Green and her family.

Finally, I am thankful to the two people, to whom, until I die, I owe thanks, my father Dr. Hasan M. Tantawi who is currently an engineering faculty at Hashemite University, and my mother Maram Balbaisi.

TABLE OF CONTENTS

LIST OF TABLES

Table **Page**

LIST OF FIGURES

Figure **Page**

LIST OF EQUATIONS

Equation **Page**

CHAPTER 1

INTRODUCTION

1.1. Project Scope and Demand

Artificial black lipid membranes have been studied significantly in literature for their remarkable ability to mimic biological membranes [1] allowing biologists to perform studies on membrane proteins [2] [3]. The importance of membrane proteins stems from the fact that they are the prime targets of most drugs [4]. Membrane proteins also constitute about 50% of the mass of a plasma membrane [5]. Also it is estimated that transmembrane proteins comprise 20% of the proteins in an organism [5]. In addition, membrane proteins claim one third of all gene codes [4]. Hence, addressing membrane protein functionalities in relation to their structures in environments, similar to their native ones, is vital for inventing new drugs.

Studying functionalities and structures of transmembrane ion channels in particular, can be tremendously challenging if performed in their native tissues [6], for which the solution was artificial black lipid membrane environments. Nonetheless, lack of strength in black lipid membranes and their high vulnerability to rupture present a great challenge to biologists.

For the reasons mentioned above, recent efforts to understand the structure and function of intercellular membrane proteins have become reliant on lipid bilayers supported on micro and nanofabricated template technologies, such as sol gel, porous alumina [7], mica-based microarrays [8], and porous silicon templates [9] [10] [11] [12] [13]. However, one drawback of these technologies is the difficulty associated with studying transmembrane proteins, due to the contact of the substrate with the lower membrane side of the proteins, which leads to protein denaturation and conformational changes [9]. To overcome this difficulty, researchers have investigated technologies based on porous materials, such as porous silicon, to support lipid bilayer membranes for studying transmembrane proteins and biosensing applications [10] [11] [12] [13] [4]. However, none of these technologies offers the ability to fully address transmembrane proteins from underneath.

Since the discovery of the Epithelial Sodium Channel (ENaC)/Degenerin family of proteins in the 1990's, considerable research has been done to understand the functionality and structure of these ion channels. Unlike other channels, such as the potassium and chloride channels, the ENaC family of proteins is only found in animal organs [14]. This protein family should not be confused with the Na^+ channel proteins which selectively allow Na^+ ion transport, whereas the Epithelial sodium channel permits ion flow resulting from an ion gradient across the apical membrane of a polarized epithelial cell [14].

Porous silicon and transmembrane proteins offer a high potential of applications, because of the biological advantages of porous silicon over other materials and the extreme importance of transmembrane proteins in medical applications; however, functional transmembrane proteins fused into LBMs that are supported on porous silicon

have not been well-demonstrated in literature. To the best that is known, this is the first work to analyze a transmembrane ion channel fused into an artificial lipid bilayer membrane (LBM) and supported on porous silicon.

1.2. Porous Structures in Medical Applications

Silicon is currently the dominant material in semiconductor technologies. Semiconductor-based nanostructures have paved the way to many biomedical applications such as using semiconductor quantum dots as biological labels [15] and protein-bound nanostructures for drug delivery [16]. Porous silicon (PS) and porous carbon have found applications as extremely sensitive biosensors [17] [18]. For example, porous silicon is used for sensing DNA and protein strands [19]. Porous silicon in particular has four features that make it stand out over other materials for medical applications: its high surface area-to-volume ratio, allowing for larger capacities of biological payloads to be handled; its biocompatibility, thus not being rejected by the body's immune system; its biodegradability to a nontoxic material (orthosilicic acid H_4SiO_4) [10]; and its luminescence property which allows for an *in-vivo* monitoring of the drug cargo being delivered, if used in drug delivery [11].

Likewise, supported lipid bilayer membranes have been investigated in literature for studying protein-protein interactions in environments similar to the *in vivo* ones [12]. They have also been used as biosensors [13] [9]. Investigation of native membrane layers of C. Glutamicum, supported on a silicon surface with holes in it, was shown by Gonçalves et. al [4]. Recently Thibault et al [12] produced a silicon membrane with e-beam patterned holes that are interconnected inside the membrane. This design allows

for access to the water solution in the holes from side openings made for that purpose, but no investigation of lipid bilayers was done. Similarly, Buchholz et. al showed that lipid bilayer membranes can span e-beam patterned holes with diameters in the range 220 nm – 2 μm. They used reactive ion etching techniques to pattern holes in an SOI wafer [20]. None of these works uses the electrochemically-fabricated porous silicon; hence they lack the capabilities offered by porous silicon such as *in-vivo* monitoring. Furthermore, the previously demonstrated silicon structures were made using electron-beam lithography and reactive ion etching, which is expensive and time-consuming. Even with state-of-the-art technologies, the electrochemically-fabricated porous silicon remains, by far, superior in porosity, minimum pore diameters, and pore depths.

In their work, Simion et. al [21] used porous silicon substrates for protein immobilization, but without the presence of any lipid membranes. Worsfold et.al [9] utilized lipid bilayers supported on porous silicon for biosensing human umbilical vein endothelial cells. They used vesicle spreading techniques to coat a lipid bilayer with Arginine-glycine-aspartate that contained peptides of integrin $\alpha_v\beta_3$ on the porous silicon. This effort did not involve proteins that are naturally incorporated into lipid bilayers, but rather peptide sequences attached to a lipid-soluble dye prior to lipid deposition.

The technology presented here is composed of two chambers separated by a porous silicon membrane and allows for full access to both chambers simultaneously. A comparative illustration between the currently available technologies listed above and the technology presented in this work is shown in **Figure 1.1**.

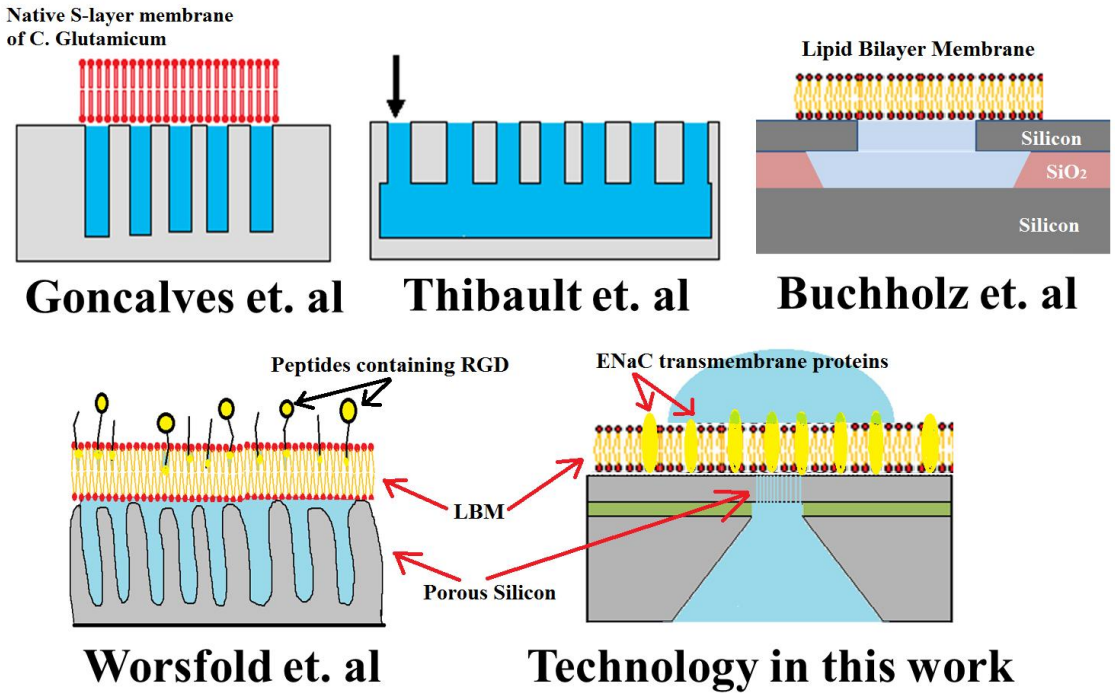

Figure 1.1 A comparative illustration of the currently available silicon technologies for supported lipid bilayer membranes and the technology presented in this work.

We present a method to fabricate a porous silicon platform suitable to investigate the structure of any transmembrane protein fused into an artificially formed lipid bilayer membrane. In this work, the lipid bilayer is deposited using the Langmuir-Blodgett and Langmuir-Schaefer techniques and is supported on porous silicon structures. This technology allows for the study of transmembrane ion flux using native membrane proteins as well as biosensors using peptides attached to a lipid-soluble dye as previously discussed [9].

An analysis is performed on the average molecular area of the deposited lipid monolayers. Membrane fusion techniques previously demonstrated by Berdiev and Benos [2] and Ismailov et al [3] were used for protein fusion. They applied a

combination of synthetic negatively charged phosphatidylserine and the neutral phosphatidylethanolamine lipids to sustain an Amiloride-sensitive Na^+ channel of the epithelial sodium channel (ENaC)/Degenerin family of proteins on a self-supported lipid bilayer.

ENaC was chosen for this experiment due to the availability of expertise in forming black lipid bilayers and incorporating ENaC proteins into them. Furthermore, there is considerable research interests associated with the effects of ENaC proteins on Liddle syndrome, a condition that causes hypertension, and the pseudohypoaldosteronism type-1 syndrome that results in salt loss [22]. Finally, ENaC is a typical ion channel that is voltage–activated and, therefore, can be integrated with electronic components for biological circuits.

1.3. Significance of the Research

In this research, a lipid bilayer membrane of several nanometers in thickness is formed over a 3µm-thick porous silicon layer, to host transmembrane protein channels. The impact of this research is seen on two fields: engineering and molecular biology.

Impact on engineering: In the device resulting from this research, ions are transported through transmembrane channel proteins, leading to electrical conductivity. This research presents the fundamentals for studying biological transistors and bio-electronic switches.

Impact on molecular biology: The prime advantage of this research lies in nanobiology, where numerous transmembrane proteins can ban be investigated. As mentioned earlier,

studying membrane proteins in environments that are fully accessible visually and physically, and as close as possible to the native environments is a cornerstone for the advancements in the pharmaceutical industry. This importance is due to the fact that membrane proteins are the destinations of most drugs [4]. Also they comprise 20% of the proteins in an organism [5]. It is estimated that about one third of gene codes are dedicated for membrane proteins [4].

Full access to functional membrane proteins is achieved by allowing protein functionalities to occur that are similar to those naturally occurring in cellular membranes, while both sides of the transmembrane proteins are physically accessible simultaneously, rather than one side at a time. For example, using atomic force microscopy (AFM) to visualize the proteins, allows the protein activity to be monitored with electrochemical impedance spectroscopy (EIS) techniques. This allows for structural and functional studies of membrane proteins such as conformational changes that occur during transport of ions [4].

1.4. Fabrication of the Device

This technology is fabricated in three stages:

1. Fabrication of a 3-μm-thick porous silicon membrane that is supported from the sides.
2. Deposition of the lipid bilayer membrane.
3. Incorporation of the transmembrane proteins.

The final device is a square-shaped porous silicon membrane that is supported from the sides and used as a backbone that supports a lipid bilayer membrane with ion channels

fused into it. The side length of the porous silicon membrane is less than 0.20 mm, the thickness of the lipid bilayer membranes is on the order of a few nanometers.

In the first stage of the process, porous silicon is fabricated in a n-type silicon on insulator (SOI). Pores are formed electrochemically in an ethanoic Hydrofluoric (HF) acid solution. The fabrication procedure starts by depositing silicon nitride layers on both sides of the SOI wafer to isolate to the silicon layer. A pattern of an array of 36 squares is transferred to the lower nitride layer, followed by anisotropic etching of the silicon substrate forming the lower compartment of the structure of one hole of the array. This stage is detailed in Chapter 2. **Figure 1.2** illustrates a system composed of the device with two compartments. In the figure, a water drop constitutes the top compartment of the system.

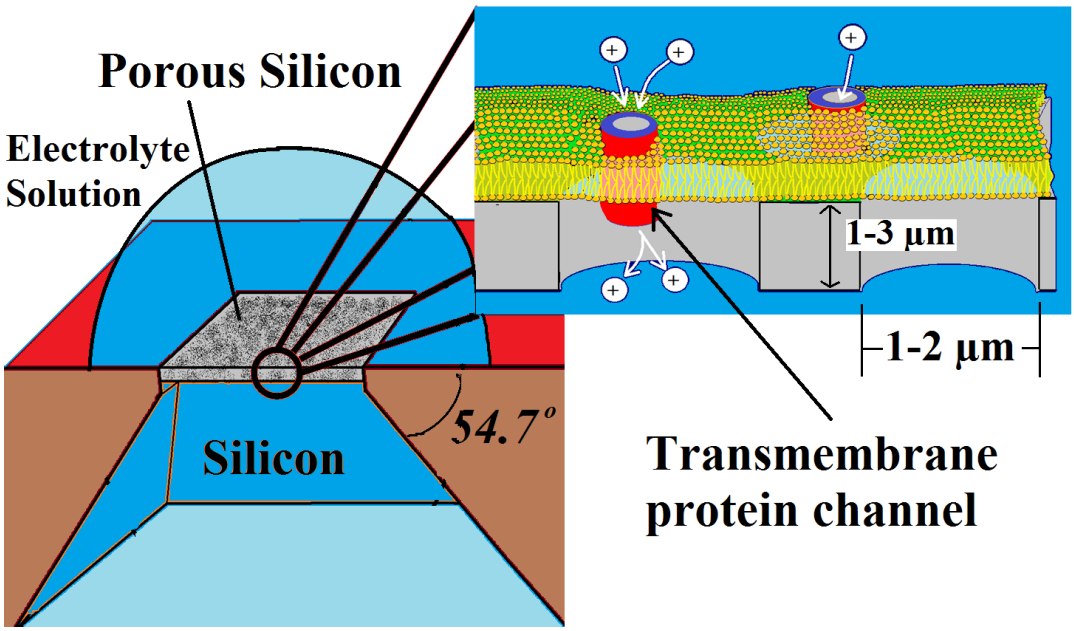

Figure 1.2 An illustration of the device that is built in this project (not drawn to scale).

A Langmuir-Blodgett trough is used to deposit a compact lipid bilayer membrane of synthetic phospholipids. Chapter 3 discusses lipid bilayer membranes and phospholipids, along with and an analysis of the deposited membrane and contact angle measurements.

The transmembrane proteins that are used in this work are the three proteins that constitute the epithelial sodium channel (ENaC) [2]. Vesicles containing the ENaC proteins were prepared and supplied by Dr. Bakhrom Berdiev from the University of Alabama at Birmingham. Chapter 4 discusses preparation and fusion of the ENaC transmembrane channel proteins. Analysis is performed using atomic force microscopy.

Finally, to characterize the functionality of the device, electrochemical impedance spectroscopy (EIS) techniques were used. Details and results of the EIS measurements are presented in Chapter 5.

CHAPTER 2

FORMATION OF THE POROUS SILICON MEMBRANE

2.1. Introduction to Porous Silicon

Porous silicon has received much attention after the discovery of the light-emitting capability of porous silicon in 1990 by Canham [23]. More attention came to it in medical applications for its high surface area-to-volume ratio, biocompatibility, and biodegradability to the nontoxic silicic acid $Si(OH)_4$ [10]. These features allow technologies based on porous silicon to be used for applications in which large capacities of biological molecules are to be handled, and at the same time not being rejected by the body's immune system, such as in drug delivery applications.

There are several properties that make porous silicon more attractive over porous alumina and other porous media. These properties result in a large number of applications of this material. Some of these features include the following:

1. **Optical Properties:** Several active and passive optical properties are present in porous silicon that depend mainly on the orientation of the pores, pore diameters, depth of pores and porosity (percentage of pore to the total volume of the material) [24] [25]. These properties include:
   - Photoluminescence [26]
   - Electroluminescence [27]

- Ability to change the index of refraction with depth [25] and porosity [24].

These properties of porous silicon permit this material to be used for numerous applications such as waveguides [28], optical cavities [29], broadband antireflection coating [30], and rugate filters [24]. As the material becomes more porous, the refractive index decreases due to the replacement of more dielectric material by air as porosity increases.

2. **Biological properties:** These properties are inherited from the dielectric material, they are mainly two properties:
   - Biological Compatibility [10]
   - Biological degradability: it degrades to the nontoxic orthosilicic acid H_4SiO_4 [10]

3. **High surface-area-to-volume ratio:** this property allows porous silicon microstructures to carry large cargo quantities if used in drug delivery applications [10].

4. **Microelectronic Compatibility**: silicon is currently, and most likely will continue to be the single most used material in microelectronics and MEMS industries.

5. **Low-cost and simple fabrication:** simple electromechanical etching techniques are used to fabricate porous silicon [31].

2.2. Formation Mechanisms of Porous Silicon

When p-type silicon is forward biased properly in a solution that contains Hydrofluoric (HF) acid, micro or macropores are formed on the silicon electrode, the size of which depends on the biasing conditions. There are many models that suggest theoretical explanations of the formation of porous silicon [32] [33]. For p-type silicon under anodization conditions, the silicon acts like a forward-biased Schottcky diode. If a pore is initially present, the field and diffusion currents in the pore tip are found to be larger than the currents on the pore walls, resulting in a further deepening of the pore [34]. In the case of a polished silicon surface, studies suggest that surface defects are the cause of the formation of the pores [35]. In n-type silicon under anodization conditions, the silicon is reverse-biased, therefore holes (the defect electrons) are the minority carriers. To increase the number of holes, ultra violet (UV) light illumination is used. In p-type silicon, etching of the pore walls stops when the wall separation becomes less than two times the width of the space charge region. However, in n-type silicon, this limit does not exist. Instead, wall etching stops when the minority carriers are depleted in the walls [34].

Porous silicon may be classified as microporous if the pore diameters are less than 2 nm, or mesoporous if the pore diameters are less than 50 nm, or macroporous if the pore diameters are larger than 50 nm, as defined by the Compendium of Chemical Terminology of the International Union of Pure and Applied Chemistry (IUPAC) [36]. In this work, the porous silicon structure needs to be as porous as possible in order to increase the probability of free suspension of protein channels on the solution subphase that would be filling the pores, rather than on the dielectric material. Also the pores

should be deep enough to form channels from one side of the silicon membrane to the other. The pore depths and heavy porosity in the n-type silicon result in a macroporous structure. At the same time, pores need to be as narrow and as uniform in direction as possible in order to avoid the collapse of the porous silicon membrane under the different stresses, and more importantly, to support the lipid bilayers and the proteins over them.

When plotting the current versus the applied potential on a silicon substrate in an electrochemical cell containing the HF electrolyte, a relationship similar to that of a Schottcky diode is achieved, as was mentioned previously. The current-voltage (IV) relationships that results for n-type and p-type silicon substrates of the same area are shown in **Figure 2.1** and **Figure 2.2** respectively. It can be seen that the anodic IV-relationship in the dark is different from the relationship that results under light illumination for n-type silicon.

The current-voltage relationship for the p-type silicon does not show any significant difference under light illumination from that in the dark, when anodic etching is performed. In contrast to the n-type silicon, a dependence on light illumination occurs in cathodic conditions for p-type silicon. Only anodic etching results in silicon dissolution [32], therefore porous silicon does not form under cathodic conditions for neither n-type nor p-type silicon.

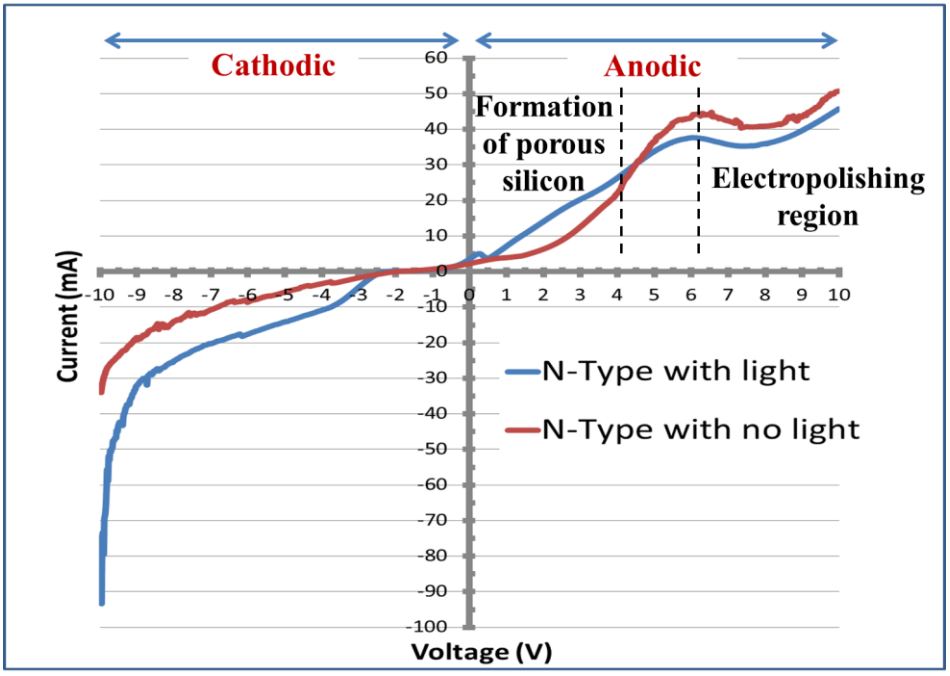

Figure 2.1 The current-voltage relationship of an n-type silicon sample. Silicon dissolution only occurs in the anodic conditions, in which formation of porous silicon occurs at low-voltage levels and silicon electropolishing at higher voltage levels.

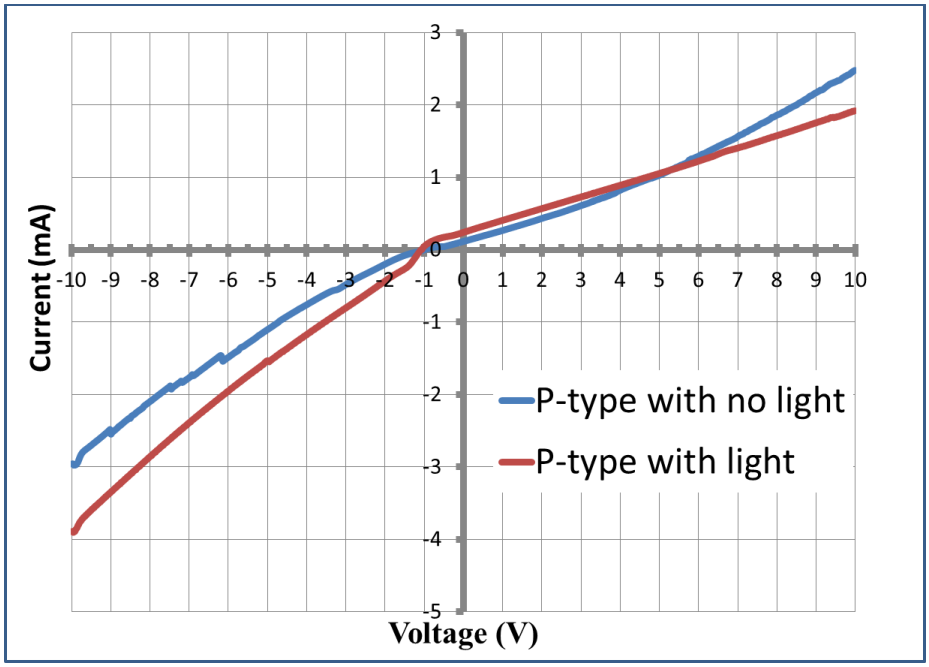

Figure 2.2 The current-voltage relationship of a p-type silicon sample. Contrary to n-type silicon, light illumination has no significant effect under anodic conditions for p-type silicon, thence anodic etching may be performed in the dark or under light illumination to achieve porous silicon.

In the anodic region, porous silicon only forms when etching is performed under light illumination when n-type silicon is used. An electrochemical cell in which porous silicon is formed by anodic etching in ethanoic HF acid, is illustrated in **Figure 2.3**. In the cell, an n-type silicon sample is connected to the cell's anode, and the cathode is a platinum mesh.

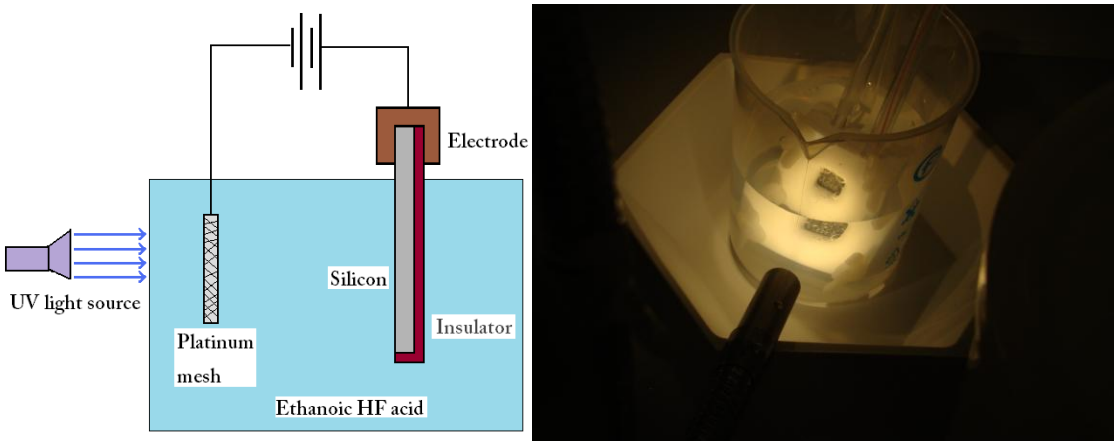

Figure 2.3 A schematic of the electrochemical cell for porous silicon formation (left). The cell in the lab (right), notice the hydrogen bubbles that form at the silicon surface.

In this research, n-type silicon is used to fabricate the porous silicon membrane. N-type silicon is preferred over p-type silicon due to the ability to control the etch process of n-type silicon using light illumination, as well as the strong tendency of n-type silicon to form straight pores with less branching than in p-type silicon [32]. **Figure 2.4** shows a porous silicon structure with straight pores that are about 10-µm-deep.

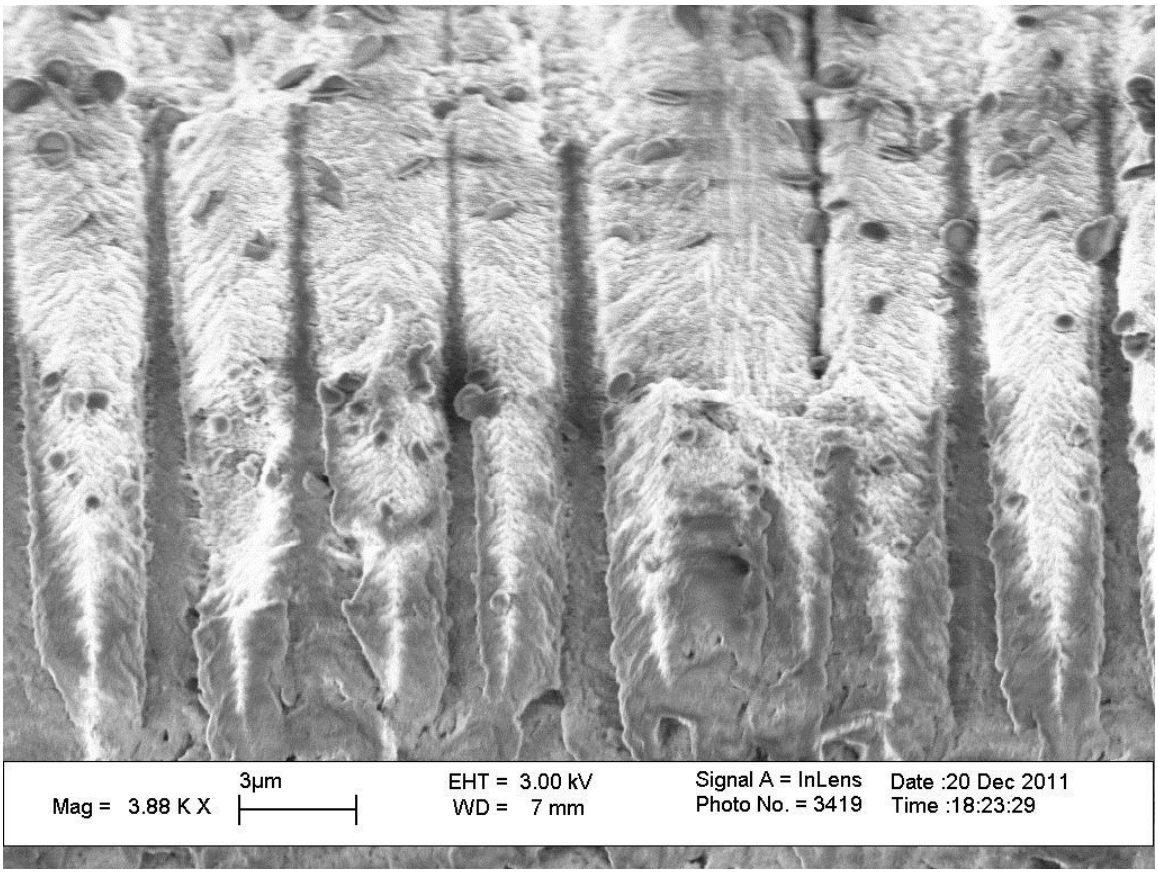

Figure 2.4 Straight non-branching pores deeper than 10 µm with pore openings about 1~2 µm in diameter are easily obtained in n-type silicon.

Some of the factors that must be controlled when fabricating porous silicon are the porosity, pore branching, and average pore diameters. Many parameters control these three requirements, and almost all these parameters are coupled with each other. They are shown in **Table 1**. For example, pore homogeneity may be improved by using pulsed current. Presence of a wetting agent such as ethanol in the electrolyte improves pore uniformity and reduces branching. HF concentration and current density are strongly coupled, generally the higher the HF concentration the higher the current density that can be used and keep the system in the pore formation region as was discussed before.

Table 1. Parameters that control the formation of Porous Silicon and their effects

CONTROL PARAMETER	EFFECT
HF acid concentration	Coupled with current density, determine whether pore formation occurs (at higher concentrations) or polishing (at lower concentrations) for a given current density [32].
Doping type	Determines the voltage polarity, the needed current density, and light illumination [37] [38]. Determines pore width, n-type wafers make larger pores than p-type.
Doping level	- Determines the needed current density and light illumination, n-type silicon needs light illumination in anodic etching while n+ silicon does not need so [37]. - The higher the resistivity the larger the pores [37] [38] [32] - The higher the resistivity the lower the pore density [32]
Current density	- Depending on the HF concentration, if the current density exceeds a certain limit, pore formation stops and electropolishing takes place. This limit increases as HF concentration increases [37]. - The higher the current density, the more the anisotropy of the pores, and the less branching [38] [32]. This is explained as resulting from an increase in the electric field perpendicular to wafer surface. - It is also observed that the higher the current density, the larger the pores, and the thinner the walls [38]. - The higher the current density, the lower is the refractive index [24].
Direct vs. pulsed current	- Direct current results in a gradient in pore distribution, Pulsed current improves pore homogeneity, this is due to the diffusion limit of HF inside the pores [32]. - A current that alternates between high and low values results in two layers of porous silicon of low and high indices of refraction [24].
Presence of organic solvents	- Presence of ethanol improves uniformity and reduces branching [38]. - Ethanol improves wettability, and reduces possibility of pore damaging due to the water capillary effect [11] [9]. - It is suggested that organic solvents have no significance in macropore formation [32].
Light illumination	No pores are formed for low resistivity n-type Si if not uv light illuminated in anodic etching [37].
Temperature	Pore etch rate increases with increasing temperature in macroporous n-type silicon [32]. Affects the critical current density after which polishing rather than pore forming occurs [32]. Aggressiveness of Si etching increases with increasing temperature.
Time	Uniformity improves as time increases, due to the favorable etching of the pore tips over the pore walls. Porosity increases resulting in a higher possibility of the collapse of porous mesh.

Macropores with widths in the range 50~100 nm are produced for this research, mainly because macropores are the easiest to fabricate and to control using light illumination when n-type silicon is used in anodic etching. Also macropores are easily capable of forming tunnels as deep as 3 µm. Tunnels of this depth also continuously guarantee the flow of ions through them. Features and physics of Macroporous silicon are discussed by Lehmann et. al. in [34].

2.3. Fabrication of the Porous Silicon Structure

The preparation of the porous silicon structure starts with coating an n-type 3µm/1.1µm/500µm SOI wafer of <100> orientation with a 2 µm thick silicon nitride on both sides. Previous literature suggests that when forming porous silicon, the pores propagate only in the <100> directions, at least for the n-type silicon [39] [32].

Plasma Enhanced Chemical Vapor Deposition (PECVD) was used for coating the nitride layer. The n-type was chosen to make use of the light illumination control parameter while fabricating porous silicon; however, a disadvantage of the n-type silicon is that the resulting pores are on the meso or macro scale. Although the PECVD nitride layer has a lower density than that deposited by Low Pressure Chemical Vapor Deposition (LPCVD) [14], PECVD nitride is chosen due to availability at Auburn University. It also has a lower risk of damaging the extremely delicate 3µm-thick porous silicon layer that will form in the later stages of the process. The deposition of the PECVD nitride layers was performed at the labs of Auburn University. The wafer was then diced into 20 mm x 20 mm sections. A pattern of 0.90 mm x 0.90 mm squares was lithographically transferred to the back side of the 20 mm x 20 mm SOI wafer, this

pattern transfer is done by spin-coating a 10 µm layer of the SPR®220 photoresist on the SOI wafer. This thickness of the photoresist is achieved by spinning the wafer with the photoresist on it to a speed of 1800 rpm for 40 seconds. To improve uniformity of the deposited film, the spinner is programmed to increase its speed at intervals of 100 rpm per second up to 500 rpm, then increasing it by 400 rpm per second intervals to 1800 rpm. The wafer is then soft baked at 90°C for three minutes, and then it is exposed to Near Ultra Violet (NUV) light for 200 seconds through a mask that contains the desired pattern on a conventional UV-contact aligner, as shown in **Figure 2.5** and **Figure 2.6**.

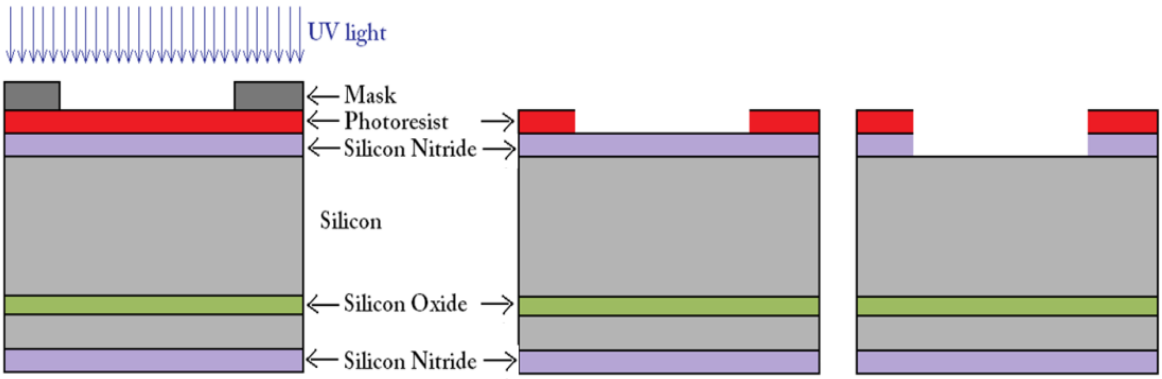

Figure 2.5 Photolithographically transferring the pattern to the back of a nitride-coated SOI wafer, then removing the nitride layer underneath by Reactive Ion Etching.

After that, the wafer is post-exposure baked for 180 seconds at 120°C, and finally the photoresist is developed in MF®-24A for five minutes at room temperature. The exposed silicon nitride layer is then removed by reactive ion etching using the fluorine-based gas composition CF_4 and SF_6 at a pressure of 75 mtorr as etchant for 42 minutes. After removing the photoresist layer with acetone and isopropanol, the silicon substrate is etched in 20% Potassium Hydroxide (KOH) for four hours at 55°C followed by for 5

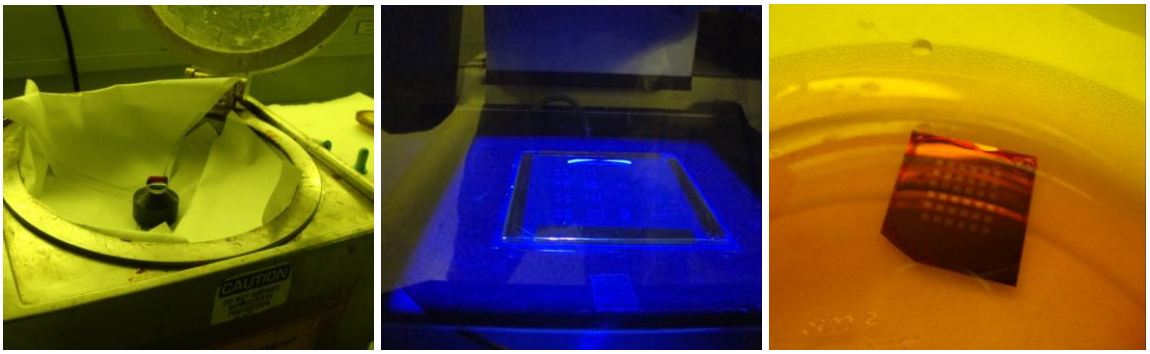

Figure 2.6 Conventional Photolithographic techniques are used to form a 6 x 6 array pattern of 0.90 mm x 0.90 mm holes on the back side of the SOI wafer. The sample on the spinner for photoresist coating (left). UV contact lithography (center). The pattern is visible on the sample during photoresist development (right).

days at room temperature. The 20% concentration is chosen because the <100> oriented silicon has the fastest etch rate at this concentration [15]. The etch rate increases with higher temperatures, but the surface roughness of the etched silicon increases significantly, putting the 1.1-um-thick oxide layer underneath the silicon substrate at risk of being etched or having pinholes in it. To avoid these defects, the KOH etch process is initially etched at 55 ^{o}C then completed at room temperature. KOH etching of silicon is a form of wet anisotropic etching in which sidewalls with angles of 54.74^{o} are formed when the silicon wafer with crystal orientation <100> is etched. This angle results because the etch stops at the {111} planes which form the sidewalls of the etched cavity [40]. Therefore, for the 0.90 mm x 0.90 mm square patterns that were transferred to the wafer, the resulting area at the bottom of the etched well is given by the equation:

$$Area = \left(0.90 - 2\frac{0.500}{\tan 54.74}\right)^2 = 0.037\ mm^2 \qquad \textbf{Equation 2.1}$$

The area calculated above is the final area of the porous silicon layer that will form in the later stages.

Next, the wafer is dipped in 5% Hydrofluoric Acid (HF) for 2 minutes to remove the oxide layer, then after it is cleaned with water. Contact between the electrode and the 3-µm-thick embedded silicon layer is achieved by removing the nitride layer that is at the corners of the structure using 20% HF acid. The etching time is at least 40 minutes to guarantee the removal of nitride residues. An access hole about 2-5 mm^2 is made at the edge of the nitride layer. These two stages are shown in **Figure 2.7**.

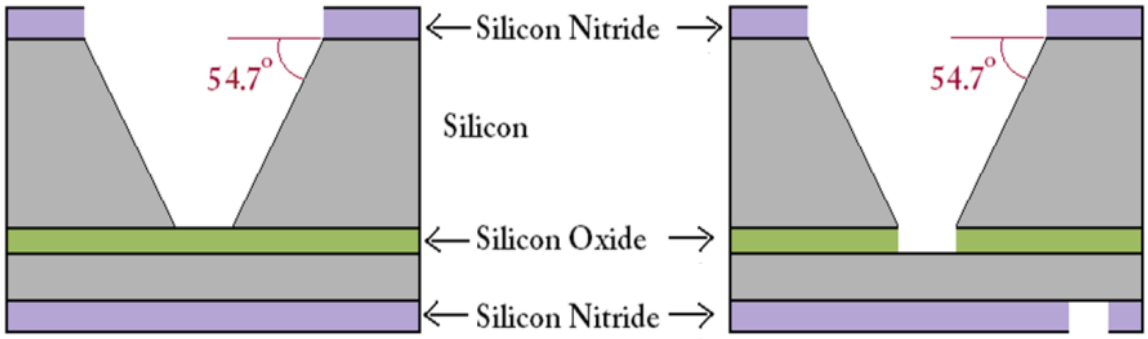

Figure 2.7 The resulting structure after the KOH etching stage (left), the structure being prepared for electrochemical etching (right).

The structure is now ready for the last stage, electrochemical etching to form the porous silicon membrane. The electrochemical cell for forming porous silicon was hand-built and is sketched in **Figure 2.8**. The Porous silicon layer is formed in an ethanoic HF acid with a volumetric concentration of 30:15:55 of 49% HF acid: 95% Ethanol: water consecutively. HF acid is a highly toxic material requiring extra safety precautions to be taken when handled. The silicon substrate was light-illuminated at room temperature. A

current density of approximately 15 mA/cm^2 was applied anodically for 30 minutes. To be certain that the nitride layer is etched away completely, the structure was left in the HF solution for about 20 minutes. Then It was immediately immersed in Ethanol for about 10 minutes to reduce the damage induced by the water capillary effect when drying.

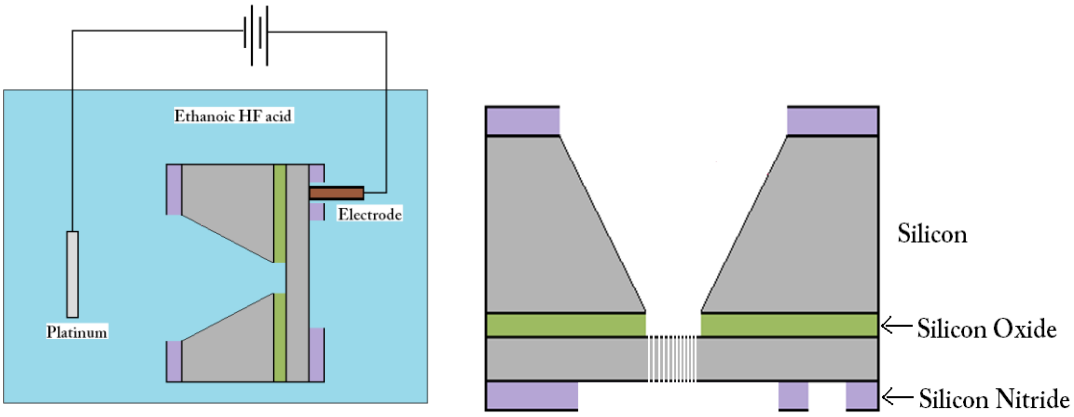

Figure 2.8 The electrochemical cell for forming the porous silicon membrane (left). The final structure achieved by this process (right).

2.4. Results and Discussion

The porous silicon structures are best characterized by scanning electron microscopy (SEM). Images were taken of porous silicon formed on silicon substrates, over which early measurements were performed. Images were also taken of free standing porous silicon layers of the final design.

2.4.1. Effects on Porous Silicon Structure and Surface Morphology

A typical voltage-current curve of a 1-cm^2 anodically-etched n-type silicon is shown in **Figure 2.9** below. The solution used was an ethanoic HF electrolyte solution of 49% HF: Deionized water: 95% ethanol equal to 2:1:1. The resulting structure had pores

of about 5-10 µm deep and 1-2 µm wide at the top. The applied current density of 15 mA/cm^2 was anodically applied for 30 minutes; the relationship is similar to the known schottcky diode voltage-current relationship. Light illumination is required for porous silicon formation in n-type silicon to provide minority carriers. The corresponding porous silicon structure that forms when operating the electrochemical cell at the operating point in the figure is displayed in **Figure 2.10**. The top view of the structure is shown in **Figure 2.11**. The images were taken using a LEO 1550 Gemini® scanning electron microscope (SEM). The effect of the different control parameters on the surface morphology and porosity of porous silicon are shown in the figures that follow.

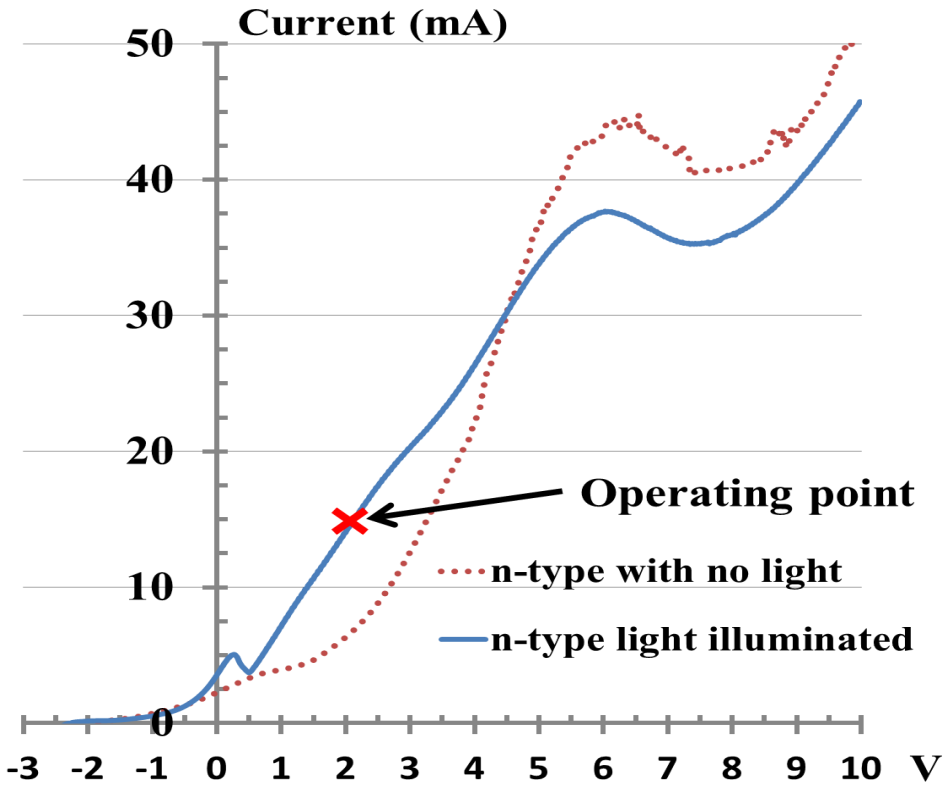

Figure 2.9 The anodic relationship between the current and the voltage for an n-type silicon in a HF solution under light illumination and in the dark.

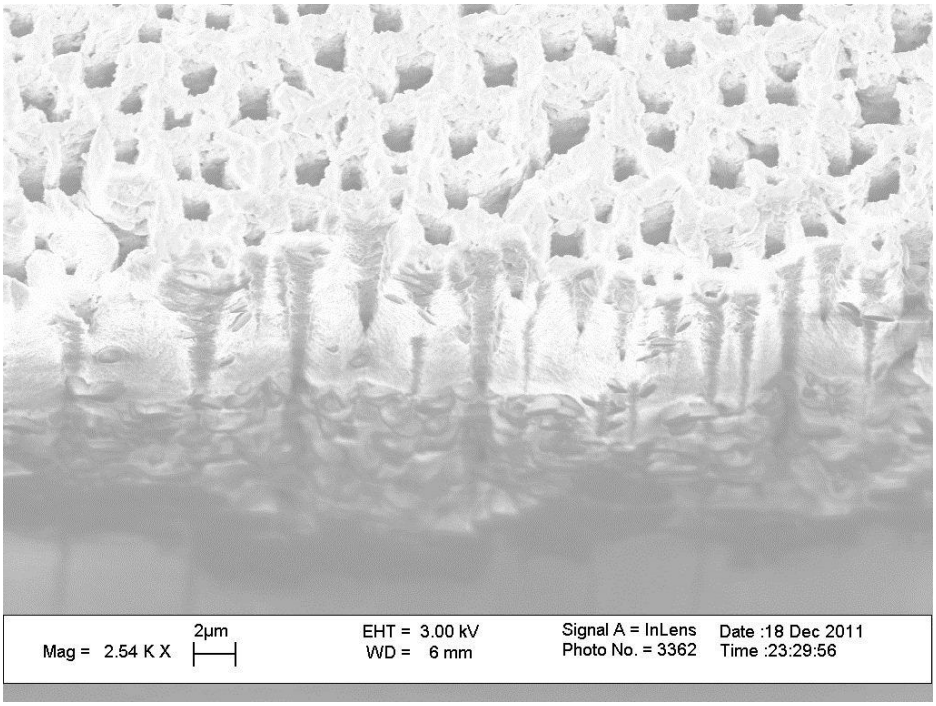

Figure 2.10 A side view of a n-type porous silicon structure that was formed using the operating conditions of current and voltage shown in Figure 2.9.

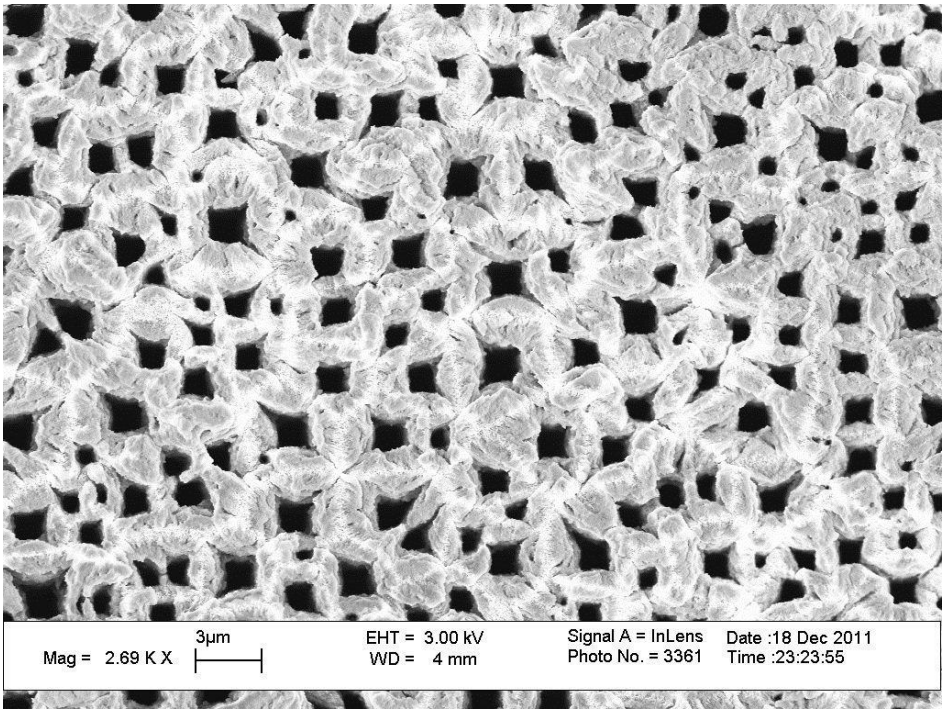

Figure 2.11 The top surface of the porous silicon substrate.

Decreasing the concentration of HF acid for a given current density may result in pushing the operating point away from the pore formation to the electropolishing region of the IV-curve. **Figure 2.12** shows an example of a porous silicon structure formed in n-type silicon and a volumetric concentration of 49% HF: 95% Ethanol: Deionized Water equal to 15:15:55 and a current density of 10 mA/cm^2 applied for 20 minutes. Pores have diameters of about 100 nm.

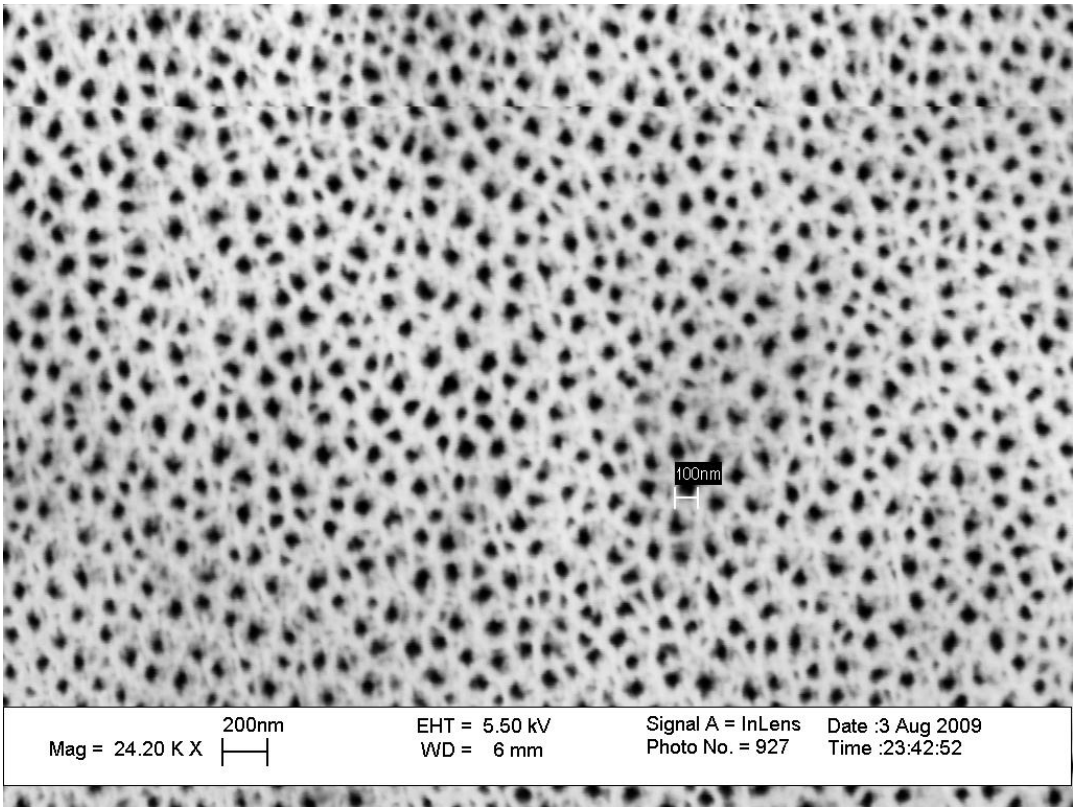

Figure 2.12 A porous silicon structure formed in n-type silicon and a volumetric concentration of 49% HF: 95% Ethanol: Deionized Water equal to 15:15:55 and a current density of 10 mA/cm^2 applied for 20 minutes.

In the case when a concentration of 5% of HF acid is used with a high current density, large pores formed as shown in **Figure 2.13**. Nonuniformity and damage in the pore openings can be seen, and is due to electropolishing and pore formation taking place simultaneously. However, pore formation can still be achieved under these process conditions by using a higher conduction n-doped silicon wafer. The results presented in **Figure 2.14** show less pore branching when a 5 Ω.cm wafer is used.

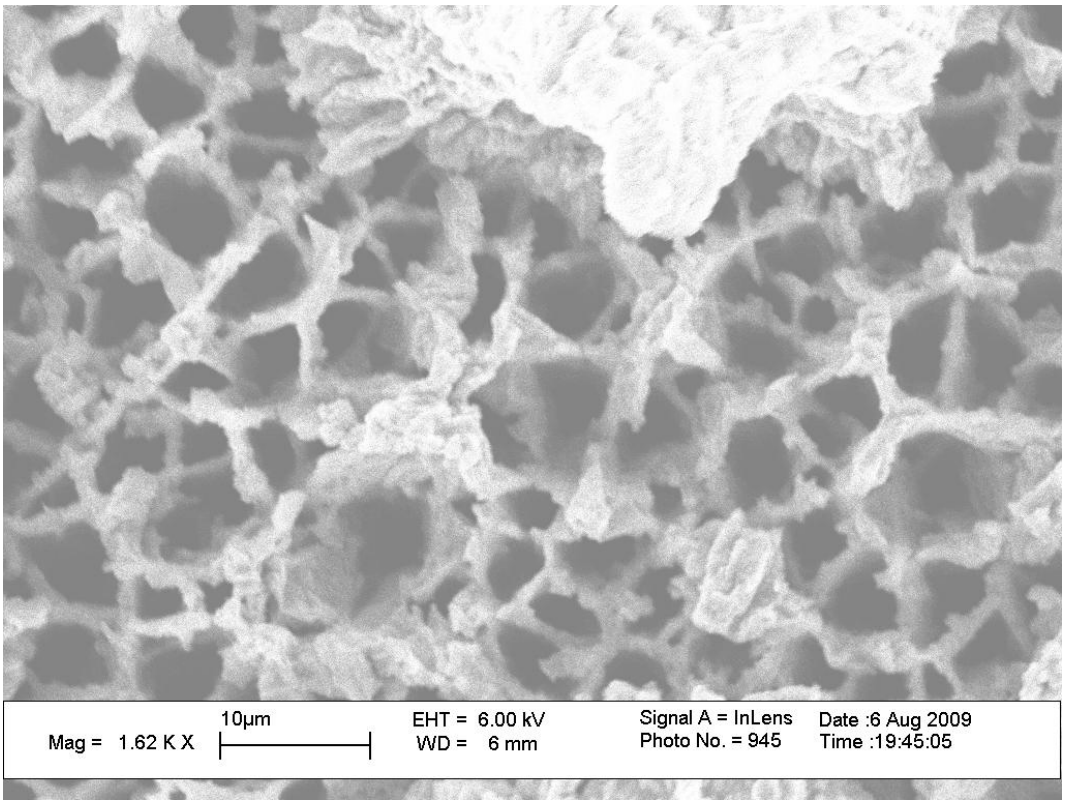

Figure 2.13 Large pores with average diameters of about 5~7 µm are observed in a porous silicon structure formed in n-type silicon with an aquous HF solution of 5% and a current density of 20 mA/cm^2 for 30 minutes.

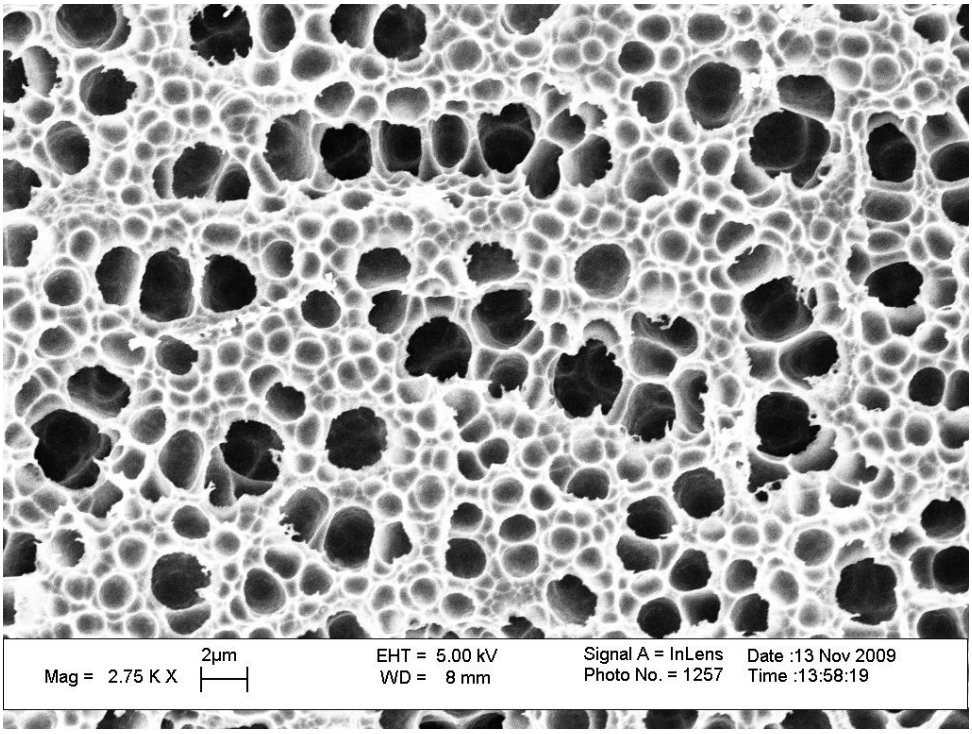

Figure 2.14 Etching a low-resistivity n-type silicon in 5% aquous HF acid and a current density of 20 mA/cm^2 for 30 minutes results in pores with diameters of about 2~3 µm.

Finally, one can show that pore uniformity is significantly improved and pore diameters are reduced after the addition of ethanol, increasing the HF acid concentration slightly, and decreasing the current density (see **Figure 2.15**). Here, a low-resistivity n-type silicon is etched in an electrolyte with a volumetric concentration of 49% HF: 95% Ethanol: DI Water equal to 15:15:55 and a current density of 10 mA/cm^2 applied for 20 minutes. The results are small, dispersed pores that do not branch significantly. The sample presented in **Figure 2.15** has 200 nm pores covering approximately 15% of the membrane surface area.

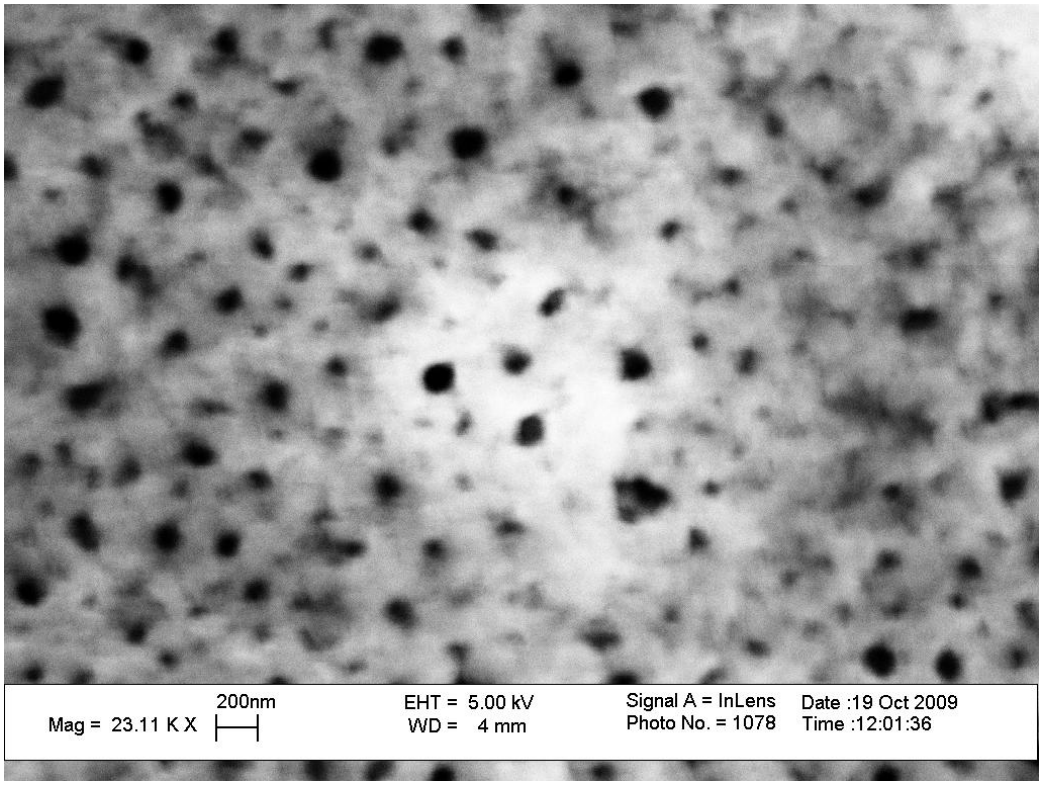

Figure 2.15 Pores that result in a low-resistivity n-type silicon etched in ethanoic HF acid with a volumetric concentration of 49% HF: 95% Ethanol: DI Water equal to 15:15:55 and a current density of 10 mA/cm^2 applied for 20 minutes.

2.4.2. Crystallographic Orientation Dependence

In n-type silicon, rectangular-shaped pore domains result with sidewalls along the {100} planes. Within these domains, pores originate perpendicular to the walls in the <100> directions [32]. The formation of rectangular domains with their sidewalls along the {100} planes is reasoned to be due to the formation of more Si-F (or Si-H) bonds at the silicon-electrolyte interface in the crystal plane (100) [32] than in other planes. These rectangular domains suggest that pore formation is dependent on the crystallographic orientation, and that the mechanism is anisotropic to some degree [32]. These pore domains are shown in **Figure 2.16**, and one of them is shown at a larger magnification in **Figure 2.17**.

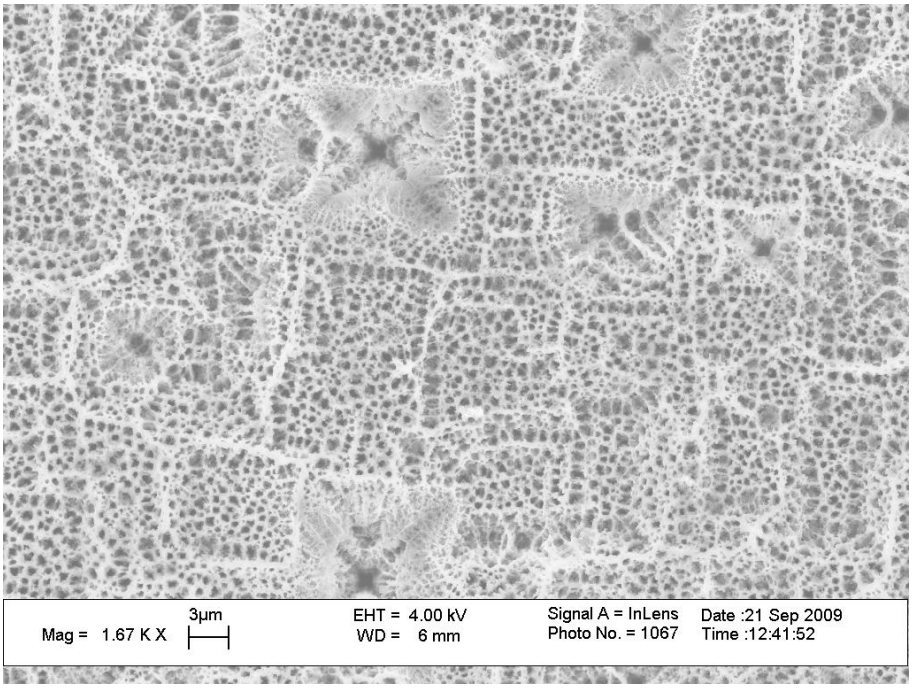

Figure 2.16 Rectangular-shaped pore domains are observed in the n-type silicon. Pore walls are directed along the {100}, and pores form in the directions normal to the walls.

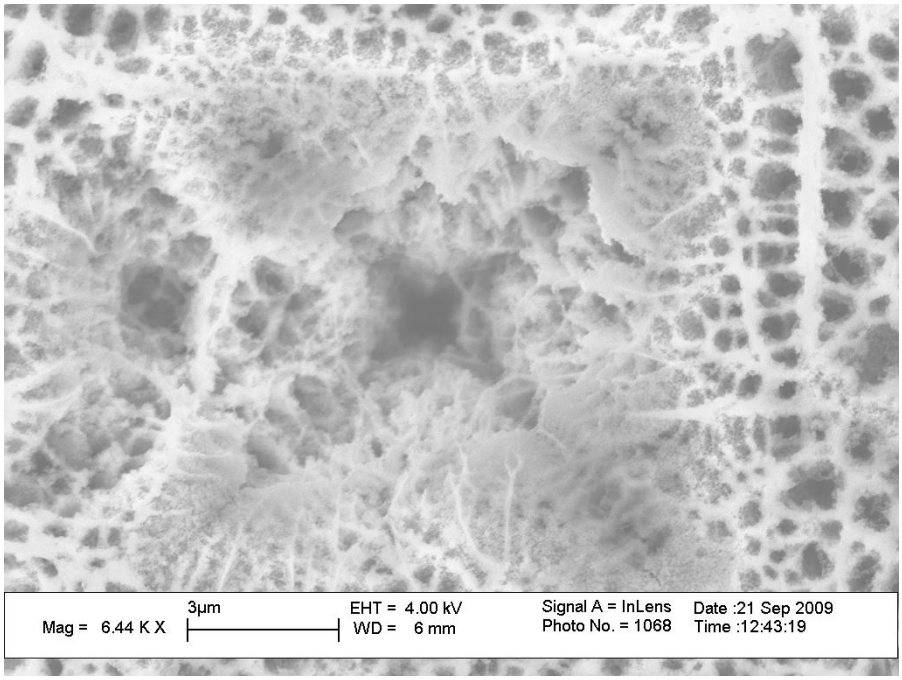

Figure 2.17 A rectangular-shaped pore domain with a side length of about 9 µm. Pores with diameters of about 1 µm inside the walls of the pore domain can be observed.

Branched pores originating at the walls of other pores and perpendicular to them can be seen in the structure shown in **Figure 2.18**. It can also be observed in the figure that the rectangular-shaped pore domains have increased in depth and formed macroscale pores. Indeed, after sufficient time, depending on the HF concentration and current density, the rectangular-shaped pore domains increase in depth and form the macropores known for n-type silicon as shown in **Figure 2.19**. While branched pores have less mechanical strength than non-branching pores, the pore density can account for up to 80% of the total surface area.

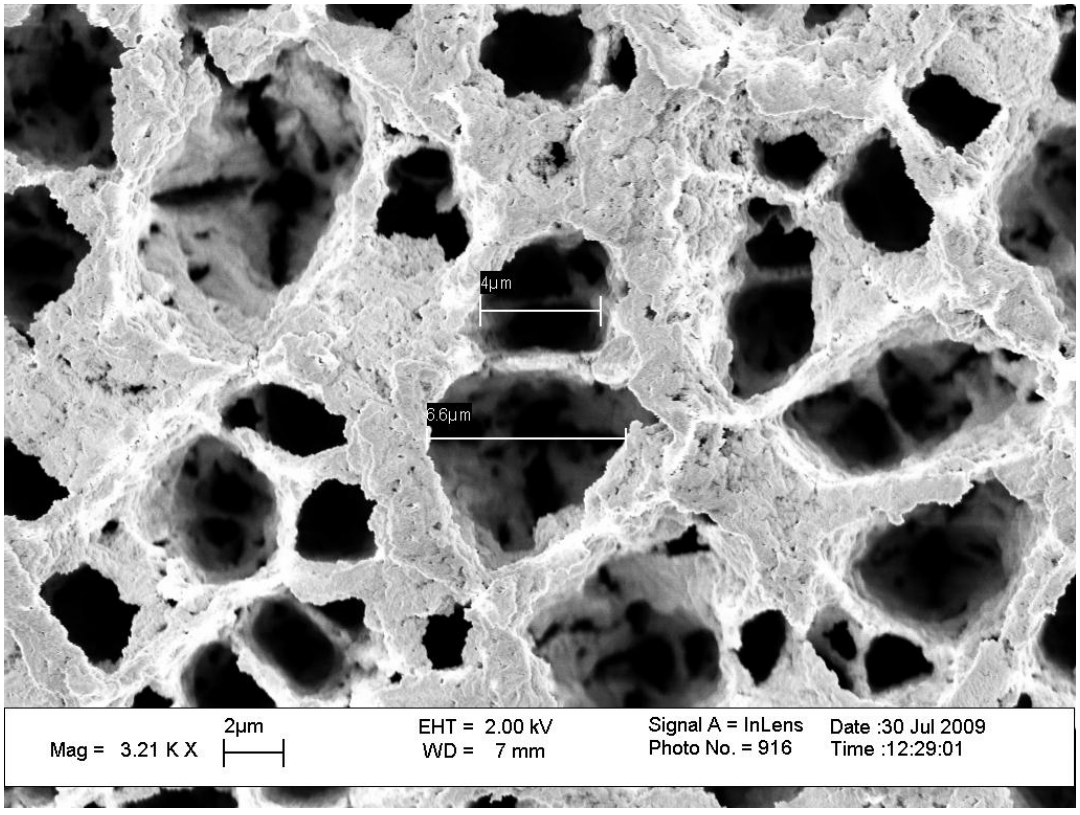

Figure 2.18 In n-type silicon, pores are rectangular-shaped. Pores can be seen originating in the walls of the pore domains.

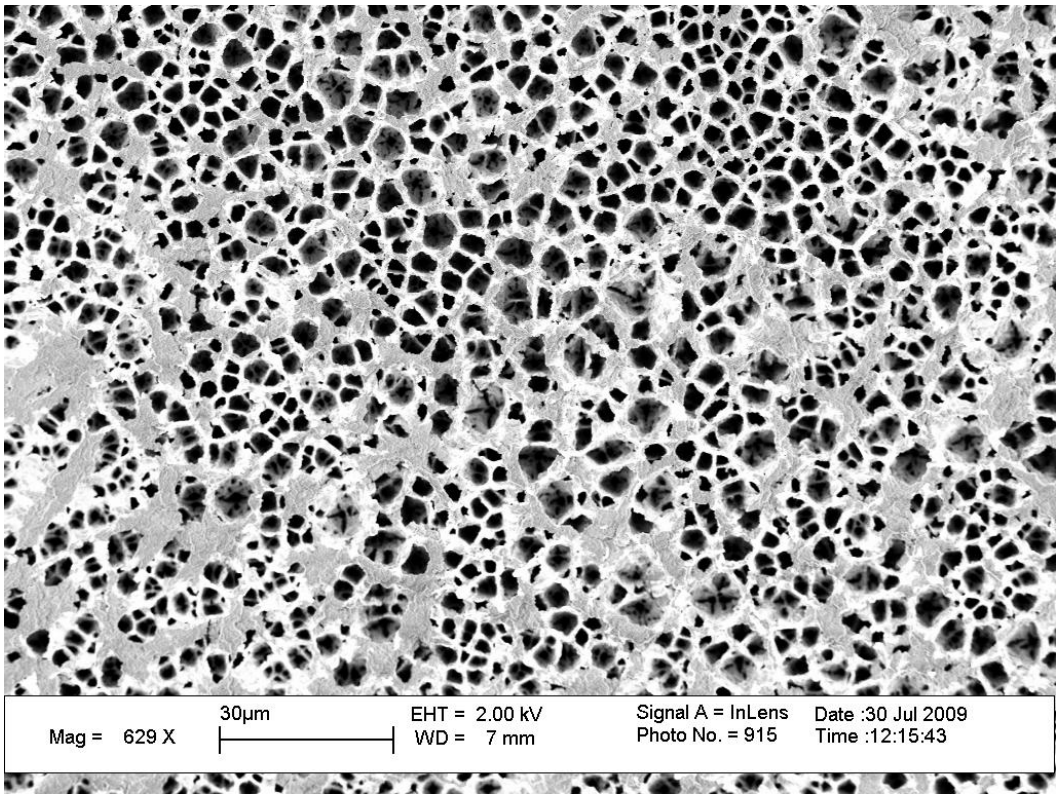

Figure 2.19 The large pore domains increase in depth forming the macropores in the n-type silicon.

2.4.3. Porous Silicon Membranes

The resulting porous silicon membranes were highly porous and had a thickness in the range 1- 3 µm. The average pore diameters at the top openings were in the range 0.5~ 2 µm. **Figure 2.20** shows a scanning electron microscope image of one of the structure that support a porous silicon membrane. The anisotropically-etched walls of the structure are inclined at 54.7^{o}, as was discussed earlier. **Figure 2.21** shows the surface of the porous silicon membrane.

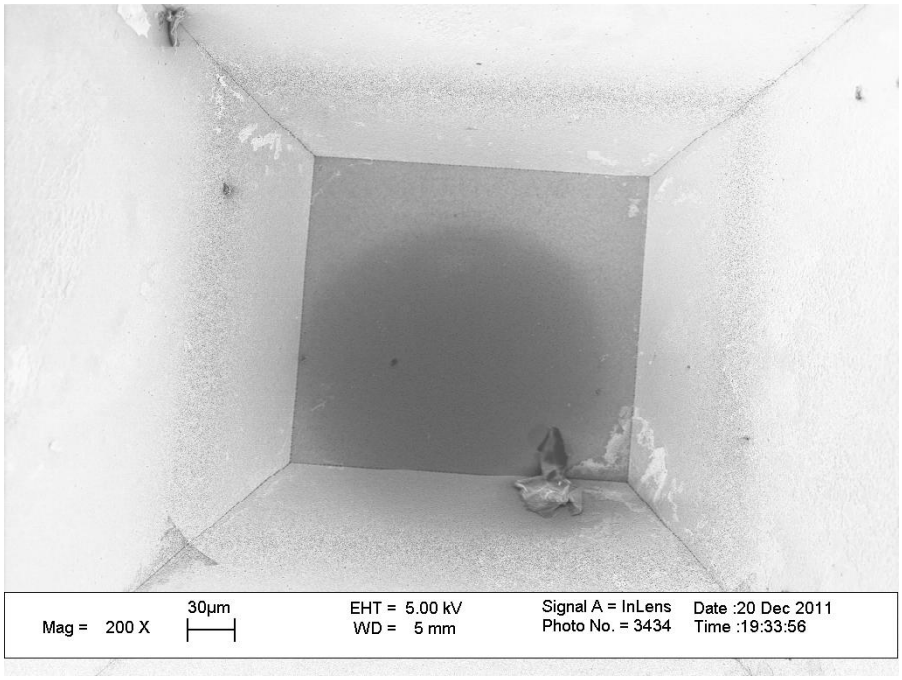

Figure 2.20 The silicon structure with the anisotropically-etched walls at an angle of 54.7^{o} with a fully developed porous silicon membrane seen by the scanning electron microscope (top).

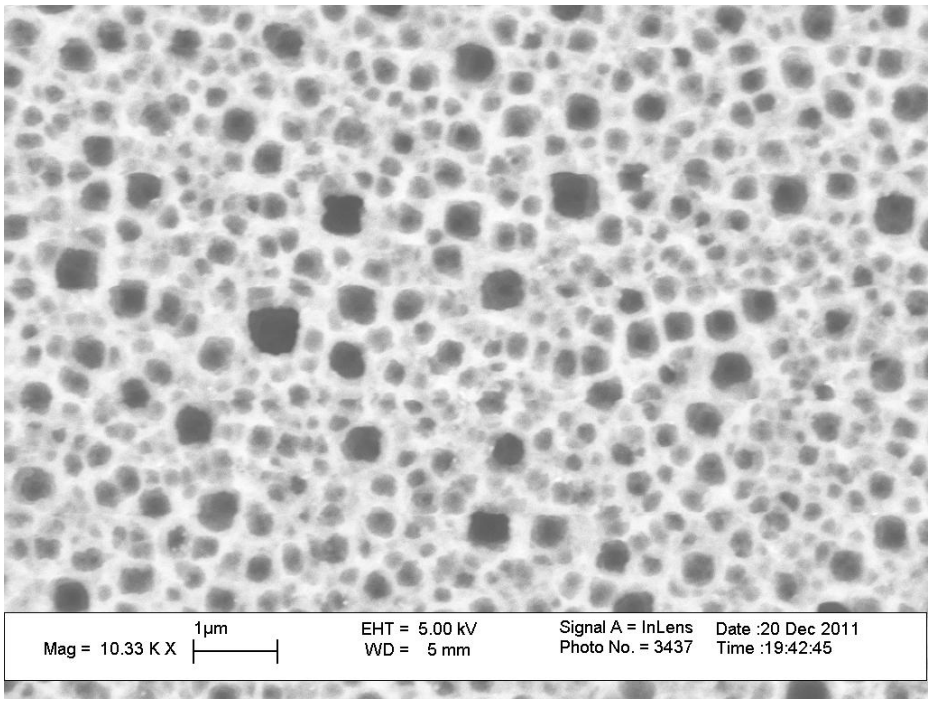

Figure 2.21 The porous silicon membrane of the structure shown in Figure 2.20.

Side view images of a membrane are shown in **Figure 2.22** and in **Figure 2.23**. The sidewall thickness is indicated by the arrows shown in the figure. Pore diameters decrease to a few hundred nanometers at the backside of the membrane. A variation in the thickness of the porous silicon membrane is observed in **Figure 2.23**, indicating that both electropolishing and pore formation take place at the same time. Silicon electropolishing may be readily overcome by fine-tuning the current density and time [32]. Thickness of the porous silicon membranes was in the range 1~3 μm.

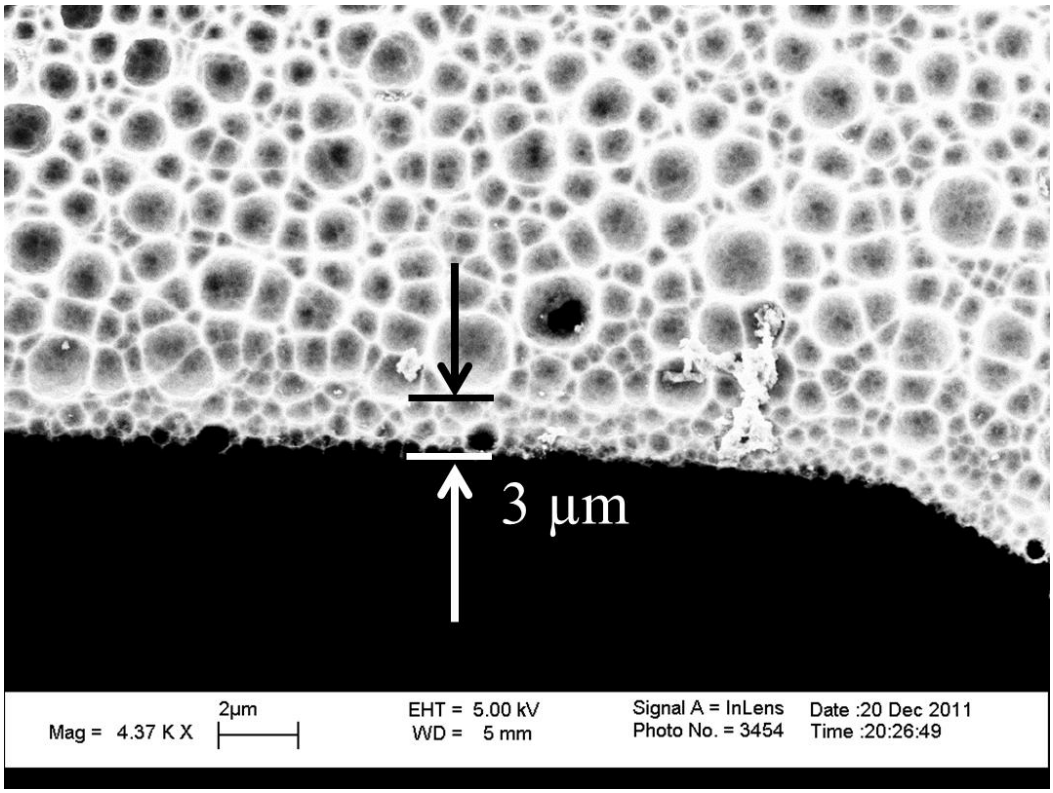

Figure 2.22 A side view of a porous silicon membrane.

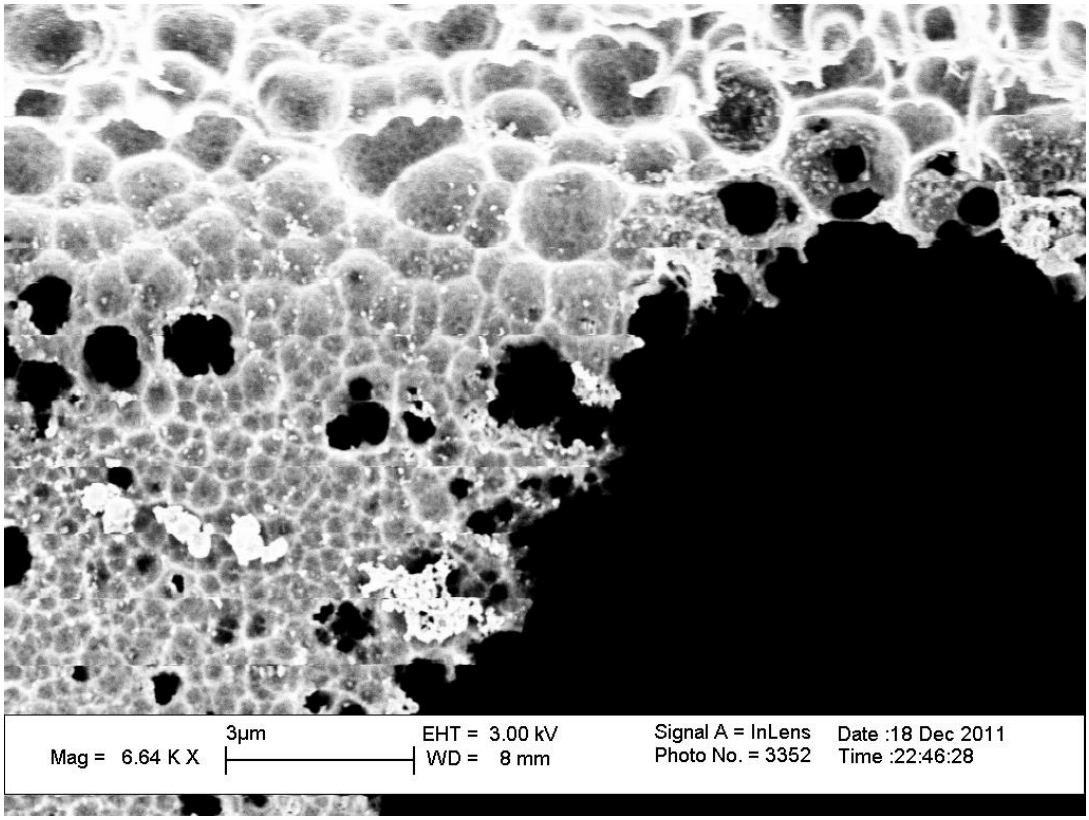

Figure 2.23 A partially collapsed porous silicon membrane.

Out of the 36 structures in the array with which the electrochemical etching started, 14 (39%) of them experienced a partial or full collapse in their porous silicon membranes. The main reasons for the membrane's collapse are the damage resulting from the water capillary force, and over etching. These sources of damage and the solutions to prevent them are presented in the next section.

The average pore diameters of 0.5~ 2 µm achieved in this technique are far less than the diameters over which functional lipid bilayer membranes with incorporated proteins have been demonstrated in literature. In the Montal-Mueller method [41], lipid bilayers are formed on an aperture as wide as 1.0 cm, bilayer membranes have been formed also under water on an aperture with an area as large as 10 mm^2 using the

painting method [42]. Lipid bilayer membranes with incorporated proteins have been demonstrated to form using the painting method on an aperture of a diameter 150 - 200 μm, with the epithelial sodium channel (ENaC) proteins incorporated into them [3] [2]. However, due to the large areas of the apertures, those LBMs lacked stability and could not last for more than a few minutes.

2.4.4. Challenges in Formation of Porous Silicon Membranes

Damages to porous silicon membranes can be attributed to four main reasons:

1. Over Etching
2. Stresses due to formation of pores on the {100} walls
3. The water capillary effect
4. Electropolishing.

Of all of these sources of damage, water capillary effect has the largest impact. It can be reduced significantly by immersive rinsing in ethanol, as will be discussed later in this section.

Figure 2.24 shows an example of a structure that experienced a partial collapse. Rectangular-shaped patterns can be observed in some of the collapsed parts of the membrane. The boundaries of these collapsed regions are likely to be the (100) crystallographic planes of the rectangular-shaped pore domains. The crystallographic dependency, known for the n-type porous silicon [32], was introduced in section 2.4.2.

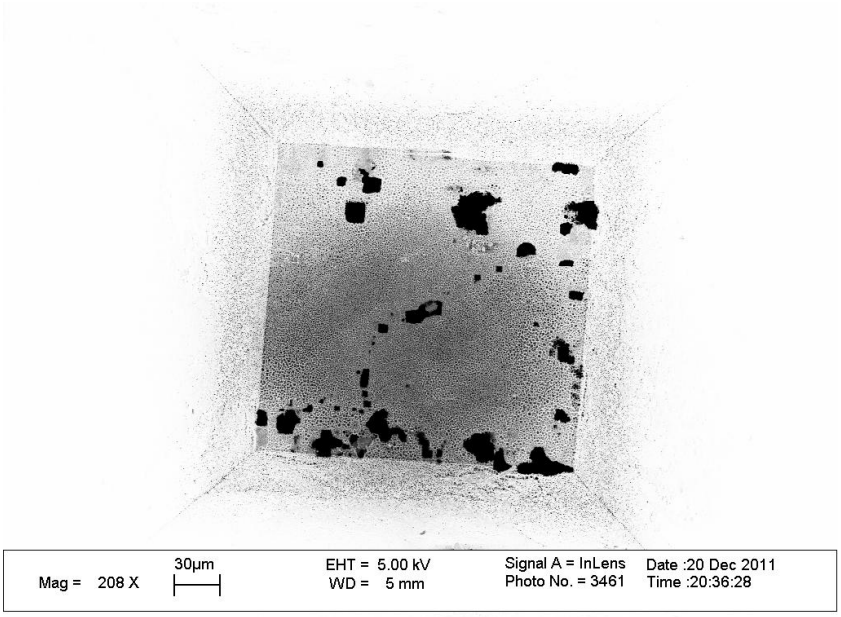

Figure 2.24 A membrane with rectangular-shaped collapsed sections.

The collapse observed in the structure above, is attributed to two main sources: water capillary force and the stresses on the {100} walls of the pores, resulting from pores originating inside the walls and normal to the {100} planes. Water capillary effect is known to induce damage on porous silicon; Zhen-Kun et. al. suggest that capillary forces can significantly increase tensile stresses to as high as 330% [43]. Immersive rinsing of the porous silicon structure in ethanol reduces the damage due to capillary effect. Ethanol has a surface tension of about 22 mN/m at room temperature compared to 72 mN/m for water.

Figure 2.25 shows the effect of the water capillary force on a macroscale level, while on the microscale level this effect is seen in the structure shown in **Figure 2.26**. To reduce the water capillary effect, every time the porous silicon structure is wetted in water, should be followed by immersive rinsing in ethanol.

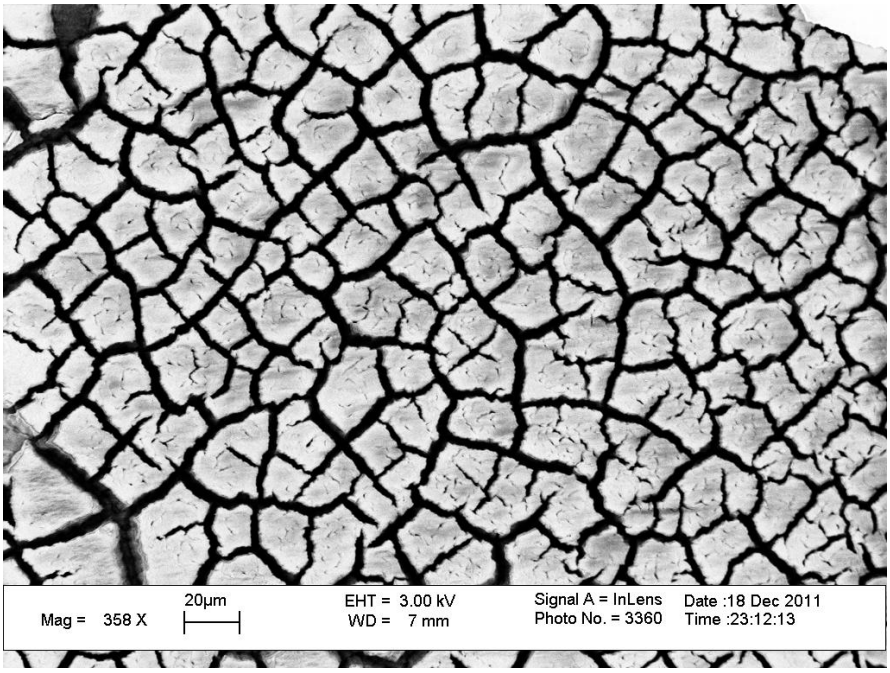

Figure 2.25 The effect of water capillary effect on porous silicon on the macroscale level. This effect may be reduced by dipping the porous silicon structure in ethanol after being wetted in water.

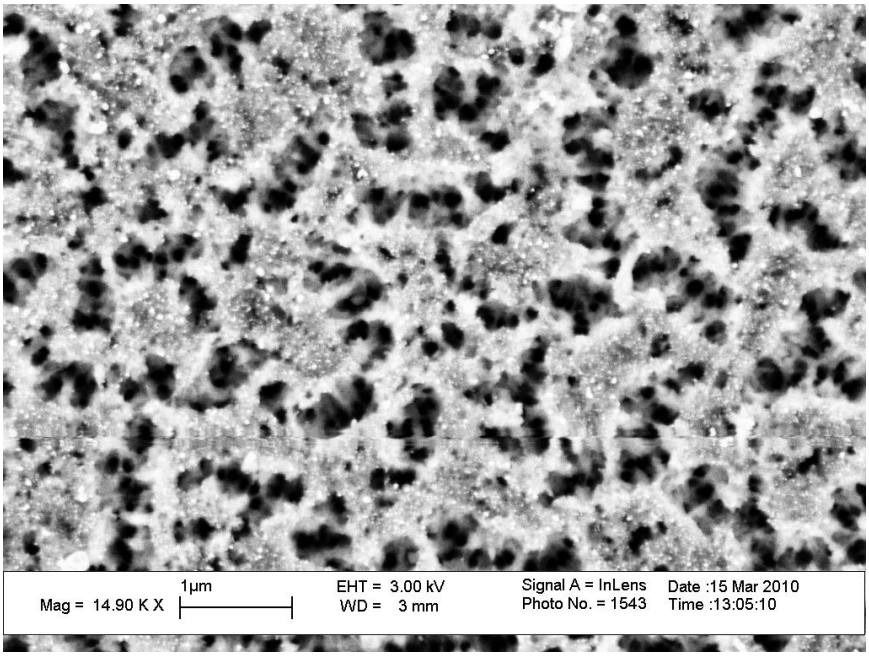

Figure 2.26 The water capillary effect seen on the microscale level in which damage is induced on the walls of the individual pores.

Figure 2.27 shows another structure with a large collapsed part. The collapsed membrane is shown in a SEM image. An optical micrograph is also shown in the figure to illuminate the structure and clarify to the reader that there is no surface underneath in the dark regions seen in the SEM images. The collapse in this structure is attributed to over-etching of that part. Improvement to over-etching may be achieved by electrochemical etching the part in a horizontal orientation rather than vertical one, and by providing a contact to the electrode that is at a uniform distance from each of the structures in the array.

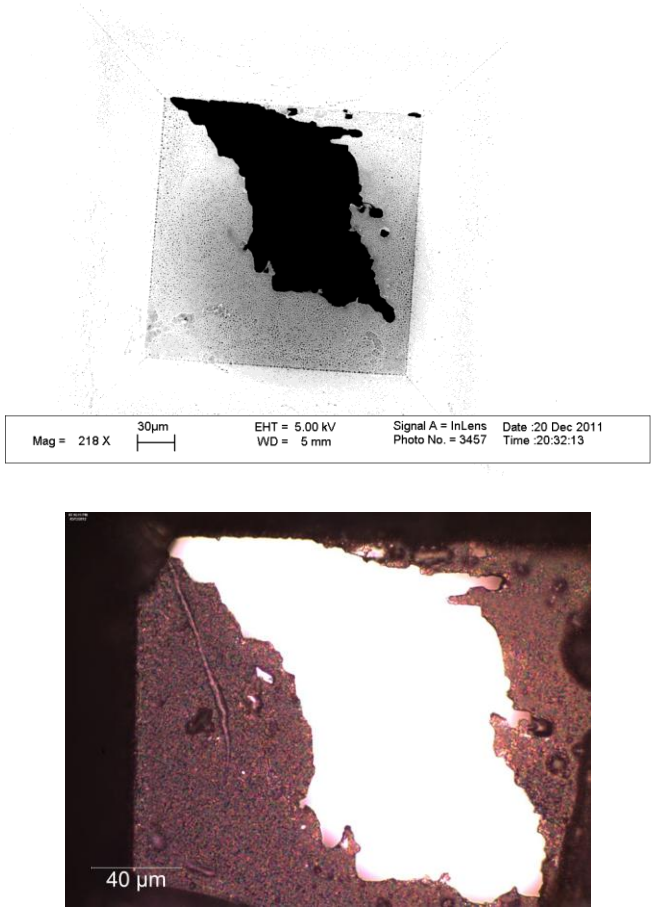

Figure 2.27 A partially collapsed porous silicon membrane due to over etching seen under the scanning electron microscope (top), and in an optical micrograph (bottom).

The effect of the stresses induced on the {100} walls is best seen in the structure shown in **Figure 2.28**, in which a collapsed rectangular-shaped section is clearly visible. The reader should clearly observe cracks along orthogonal axes. Also note the irregular pore formation that occurs as the membrane is etched through the regions that did not crack or break off. This is due to local changes in electrostatic fields present as pores etch through the membrane.

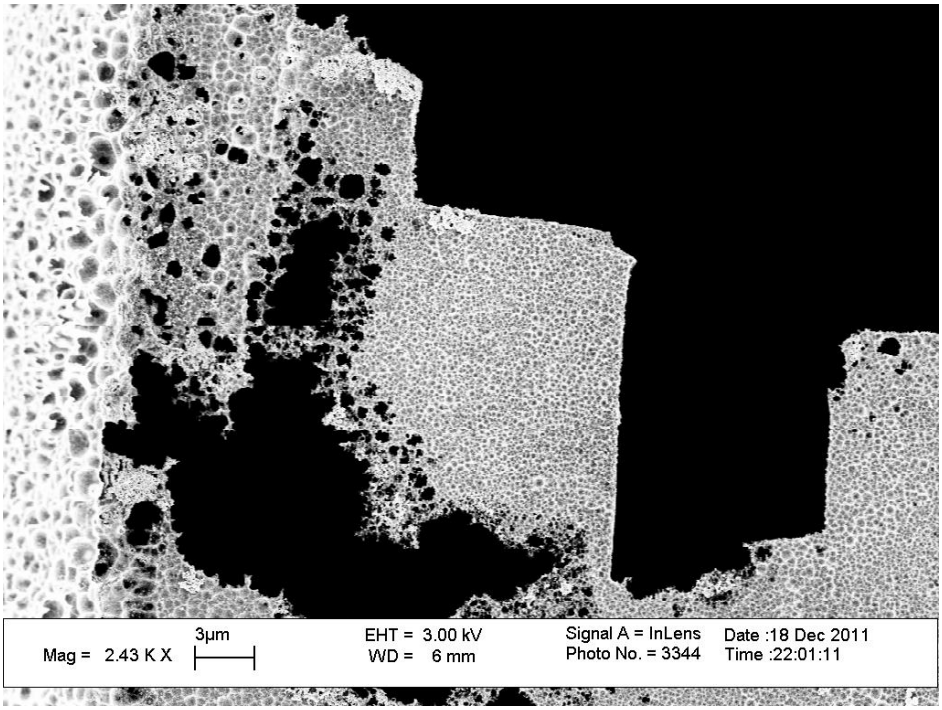

Figure 2.28 A membrane with a partial collapse.

If the operating point at which electrochemical etching is not chosen properly, then the process may enter the regime were both pore formation and electropolishing take place, or even it may entirely be in the electropolishing regime (refer to **Figure 2.1**), this causes a non-homogenous surface profile as seen in the structure in **Figure 2.29**.

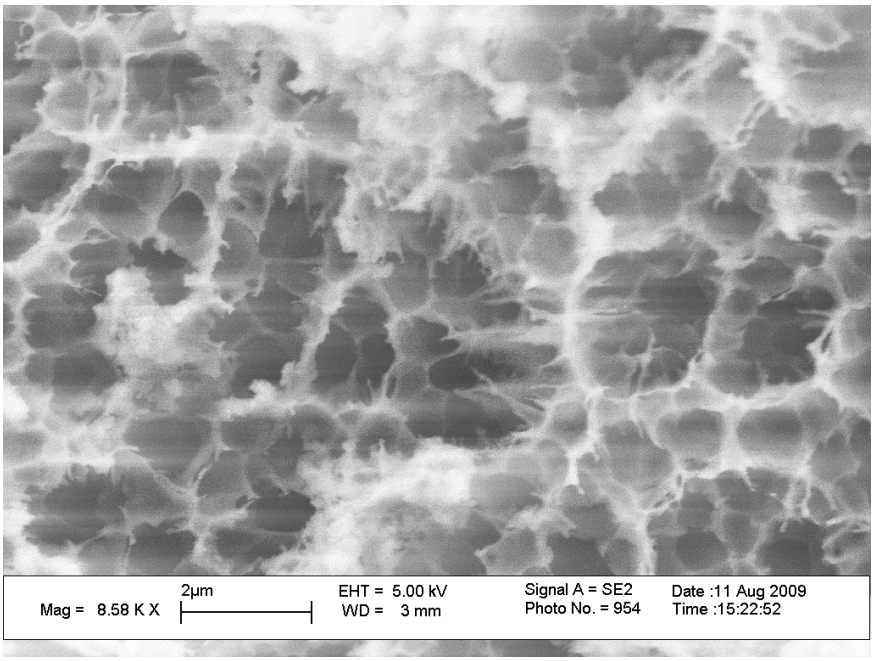

Figure 2.29 A common challenge in porous silicon results from the simultaneous formation of pores and electropolishing, resulting in a rough surface profile with a loss of pore uniformity.

2.5. Conclusion

A process has been developed to fabricate supported porous silicon membranes, in which a two-chamber device is fabricated. The structure is fabricated using conventional photolithography to transfer a pattern to an SOI wafer, followed by reactive ion etching and anisotropic wet etching to form the structure that supports the porous silicon membrane. Finally, electrochemical etching is used to form the porous silicon layer. The two chambers are separated by a porous silicon membrane with a thickness of less than 3 µm, and porous all the way through. The final dimensions of the porous silicon membrane are about $190 \times 190 \times 3\ \mu m^3$.

Several challenges arise when fabricating porous silicon membranes, such as membrane collapse due to over-etching, water capillary forces, increased stresses on the

{100} walls, and electropolishing. The main source of damage in porous silicon membranes is the water capillary effect, which may be reduced by immersive rinsing in ethanol. Other methods to reduce and eliminate these challenges also have been investigated. In subsequent chapters, these techniques are used to produce membrane for use in the investigation of transmembrane proteins fused into lipid bilayer membranes in a two-chamber structure (one chamber on each side of the LBM) with full visual and physical access to both chambers.

CHAPTER 3

DEPOSITION OF THE LIPID BILAYER MEMBRANE

3.1. Introduction

As the name suggests, lipid bilayer membranes are thin membranes with thicknesses of few nanometers of two layers of lipid molecules. The most prominent examples of lipid bilayer membranes are the plasma membrane, which isolates the biological cell from its surroundings, and the cell nucleus membrane, which marks the boundaries of the cell nucleus. There are many other cellular organelles that are equipped with membranes to separate their interior from exterior environments such as the mitochondria, Golgi apparatus and endoplasmic reticulum. Biological membranes are usually composed of phospholipids, which have hydrophilic head groups and hydrophobic fatty acid tails.

Several techniques for forming supported lipid bilayers have been presented in literature [44] [45] [46] [47] [48] [49], some of the commonly used techniques include the following:

- **Lipid vesicle spreading:** this technique is the conventional method in which lipids are spread over the substrate as shown by Brian and McConnell in [44].
- **Spin coating technique:** this method is probably the most recent, it was studied extensively by Krapf et. al. [45] and Simonson and Bagatolli [46].

- **Montal-Mueller method:** This technique was shown to form lipid bilayers on an aperture as wide as 1.0 cm [41].
- **Painting method:** [2] [42] This method was used to form bilayer membranes under water on an aperture with an area of 10 mm^2 [42], but those bilayers lacked stability, and failed to incorporate large proteins in them [41]. The painting method was used to form a lipid bilayer on an aperture as wide as 150 - 200 μm and incorporate the ENaC proteins into it [2] [3].
- **The Langmuir-Blodgett and Langmuir-Schafer techniques:** [47] [48] [49] These two techniques together offer one more degree of freedom over other methods by controlling the packing density of the lipid molecules and better homogeneity over the direct spreading method. They are also more convenient to transfer a lipid bilayer on a delicate substrate as porous silicon without inducing structural damage to it than the more recent spin-coating method. Moreover height differences in the coated lipid layers have been observed in spin-coating techniques [45], and there would always be uncertainty of the number of bilayers being spin- coated.

The deposition of the lipid bilayer membrane is done using the Langmuir-Blodgett and Langmuir-Schaffer techniques for the advantages listed above. The Langmuir–Blodgett trough at the lab of Dr. Ramon Cerro in University of Alabama in Huntsville is used for this purpose, and is shown in **Figure 3.1**.

Figure 3.1 The Langmuir-Blodgett Trough at the Department of Chemical Engineering in the University of Alabama in Huntsville.

3.2. Phospholipids

In mammalian cells, there are three main phospholipids that constitute the cellular membranes: phosphatidylethanolamine, phosphatidylserine, and phosphatidylcholine. A phospholipid molecule is composed of a glycerol with an attached phosphate group to which is attached a head group. The glycerol is linked to two fatty acid chains through ester bonds [5]. The phospholipids used in this work have the same head structures as phosphatidylserine and phosphatidylcholine, but with longer fatty acid chains to enhance formation of lipid bilayer membranes over forming micelles. Structural details of the natural lipids are shown in **Figure 3.2**.

More than 50% of the total mass of the lipids of a typical mammalian cell is composed of the three phosphoglyceride lipids phosphatidylethanolamine, phosphatidylserine, and phosphatidylcholine; and the phospholipid sphingomyelin, which has sphingosine as a backbone rather than glycerol as in the other three phospholipids [5].

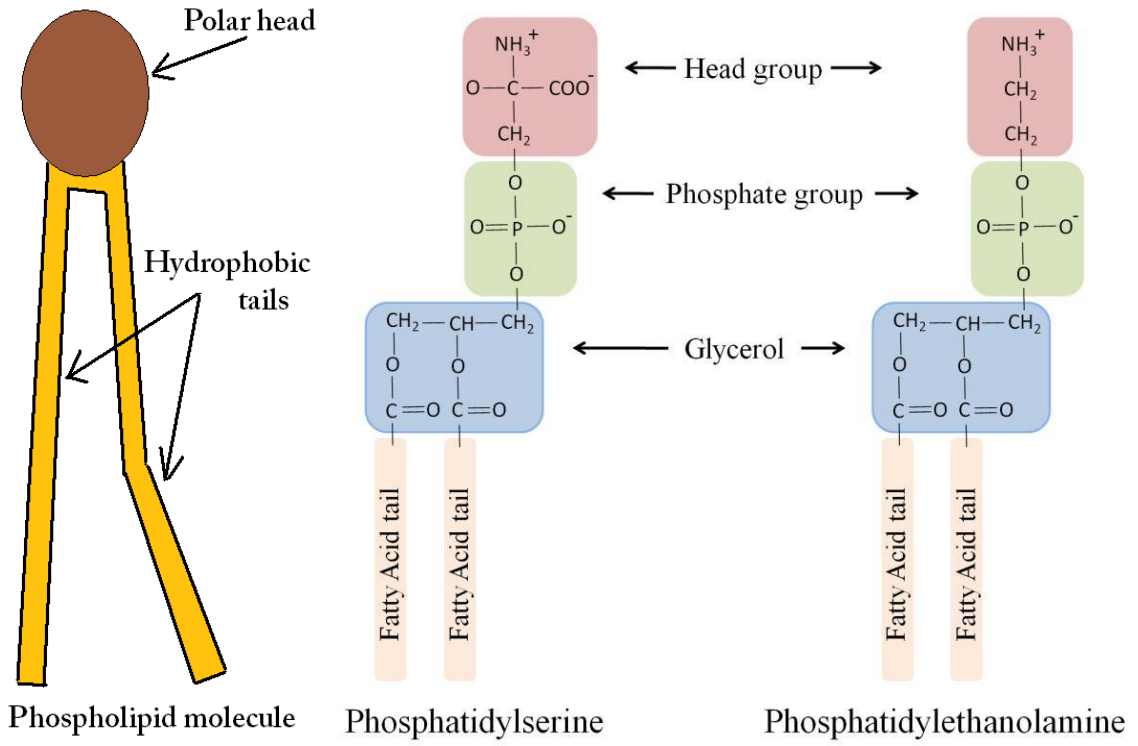

Figure 3.2 Structure of the phospholipid molecule (left). The two phospholipids used in this work are derived from the phosphatidylserine and phosphatidylethanolamine phospholipids.

For forming a lipid bilayer membrane, two synthetic phosphoglyceride lipids: 1,2-diphytanoyl-*sn*-glycero-3-phosphoserine ($C_{46}H_{89}NO_{10}PNa$) and 1,2-diphytanoyl-*sn*-glycero-3-phosphoethanolamine ($C_{45}H_{90}NO_8P$), were mixed in a one-to-two parts ratio. The lipids were supplied by the Alabama-based Avanti Polar Lipids, Inc., with a purity of more than 99%. This lipid composition is reported to have high chances of forming stable bilayer membranes, and enhance the possibility of fusion of the ENaC protein into the bilayer [2] [3]. Phospholipids with long fatty acid chains (typically longer than 12 carbon atoms) are known to form bilayer membranes more readily than micelles when spread over a surface [50]. Each of the lipids was supplied in a chloroform solution with a concentration of 10 mg/ml. The natural phospholipids phosphatidylserine and

phosphatidylethanolamine are two of the most common phospholipids in biological membranes, comprising 25% of the plasma membrane of red blood cells and more than 70% of that of the Escherichia coli (E. Coli) bacteria [5]. Furthermore, composition of the lipid bilayer membrane affects the activity of ion channels when incorporating active proteins into them.

3.3. Materials and Method

To form the lipid bilayer on the porous silicon structure, the Langmuir-Blodgett (LB) trough is first cleaned with chloroform, then filled with De-ionized (DI) water, the water surface is cleaned by aspiration until an acceptable Pressure-Area isotherm is achieved. The phospholipids dissolved in chloroform are then spread on the water surface. A total of 9 μL of the phospholipid mixture is added to the surface of the deionized water subphase in the trough, and then is left to sit for few minutes to allow for the chloroform solvent to evaporate as indicated by a slight rise in surface pressure that clears out as the chloroform evaporates. The lipids are then compressed symmetrically by two barriers at a speed of 30 cm^2/min; the trough had a total area of 922 cm^2 (20 cm x 46.1 cm). A solid tight packing of the lipid monolayer is reached at a surface pressure of 40~50 mN/m at which the recorded surface area is about 450 cm^2. The surface pressure is measured using a Wilhelmy plate. Tight packing of lipid bilayers is a feature biologically achieved by the presence of cholesterol in mammalian cell membranes. Indeed, the addition of oxidized cholesterol to the lipid mixture has been shown in studying ENaC protein structure [3]. Further compression results in the collapse of the monolayer [51]. The formed layer may be interpreted as a two-dimensional solid [52].

Further compression results in the collapse of the monolayer into three –dimensional micelles [51] [53].

A monolayer was transferred to the porous silicon surface by the Langmuir-Blodgett method in which the substrate is retracted upwards at a speed of 2 mm/min in an LB trough by Nima Technology LTD at room temperature and ambient pressure. These experiments have shown that the decrease in the area of monolayer on the water surface was greater than the area coated on the porous silicon substrate, indicating a deposition transfer ratio greater than or equal to unity, as defined by Langmuir and Schafer in [54]. This step constitutes the vertical left of the first monolayer as introduced by Langmuir and Blodgett [48], the second monolayer is deposited using the horizontal left method introduced by Langmuir and Schaefer [49], by bringing the hydrocarbon chains of the monolayer on the porous silicon and of the monolayer in the air-water interface to contact. The deposition of the lipid bilayer is illustrated in **Figure 3.3**. Optical images of a porous silicon surface before and immediately after deposition of a lipid bilayer membrane are shown in **Figure 3.4**.

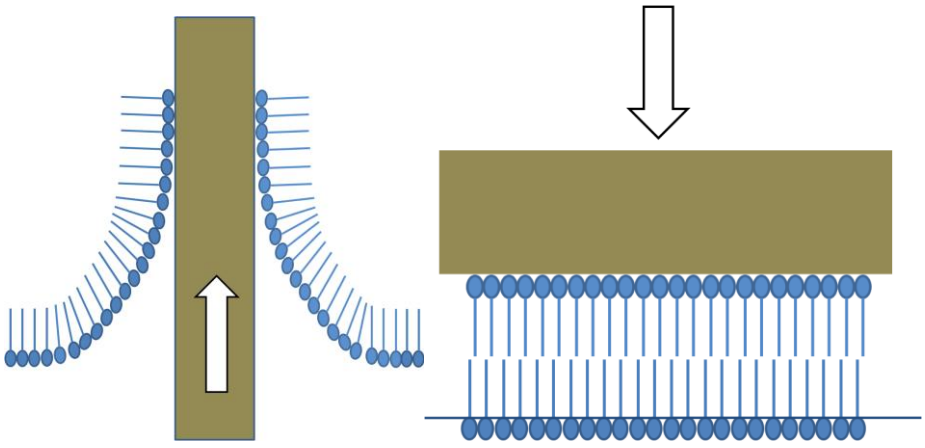

Figure 3.3 Deposition of the first layer using Langmuir- Blodgett technique (left). Deposition of the second layer by means of the Langmuir- Schaefer technique (right).

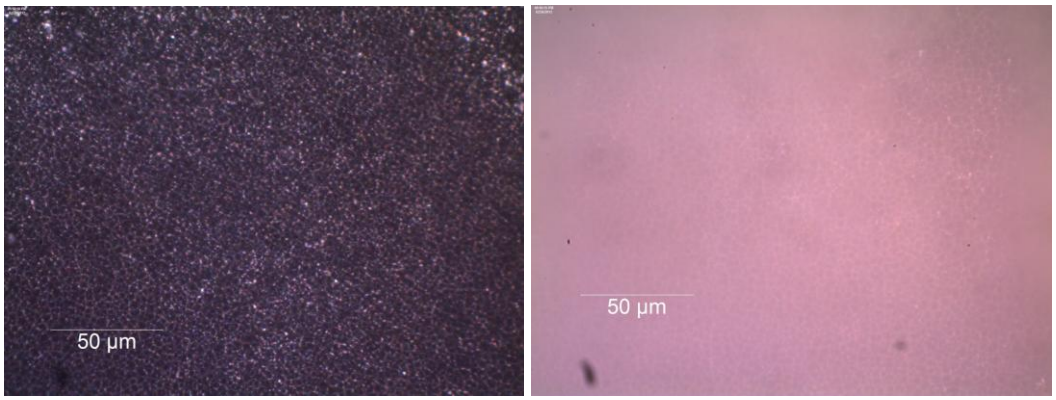

Figure 3.4 A porous silicon substrate before deposition (left) and immediately after deposition of a Lipid Bilayer Membrane (right).

3.4. The Drag-Out Problem

Deposition of thin films of liquids on solid flat surfaces by means of dip coating is common in industrial applications. Thickness of the coated layer has been investigated thoroughly in literature [55] [56] [57] [58] [59] [60] [61]. In their work, Landau and Levish [55] evaluated the thickness of the film as a function of the dragging speed, fluid viscosity, fluid surface tension, and fluid density, by considering two regions: the region of the liquid that is dragged by the flat surface and the region of the liquid at the meniscus. They show that the thickness of the liquid film may be found from the Prandtl boundary layer equations. However, their work is limited to flows with a very small capillary number [56]. In their work Jin and Acrivos [57] show a numerical solution of the problem based on solving the steady state Navier-Stokes system of equations. Darhuber et. al. [58] show in their work that when the surface is chemically heterogeneous, the film thickness depends on the geometry and pattern of the surface, as well as the speed, viscosity, density, and surface tension of the fluid.

3.4.1. Assumptions

Several assumptions are made in these studies:

- The substrate has an infinite flat solid surface: this assumption is necessary to negate the effect of the edges of the solid surface [55]. Also it leads to the assumption that the thickness of the liquid film approaches h_0 at a distance far away from the origin, along the y-axis [57] [58] (see **Figure 3.5**).
- The flow has a low value of Reynolds number: this assumption results in a laminar boundary layer problem, thus the difficulty of the analysis is reduced significantly as the flow properties are not time dependent in laminar flow [57].
- The flow is at a steady state: the velocity of removal is constant, resulting in a system of steady-state Navier- Stokes equations [57].
- The liquid has a constant density and viscosity [57].
- At any point in the liquid far away from the plate, the velocity is zero.

3.4.2. Analysis

To investigate the drag-out problem resulting from dipping and withdrawing a substrate at a low speed from a liquid, the y-axis is taken to be along the substrate movement, and the x-axis is taken to be in the plane of the liquid-air interface. The drag-out problem when a pure liquid is used is shown in **Figure 3.5** below. **Figure 3.5**-right shows the drag-out problem when a surfactant is present.

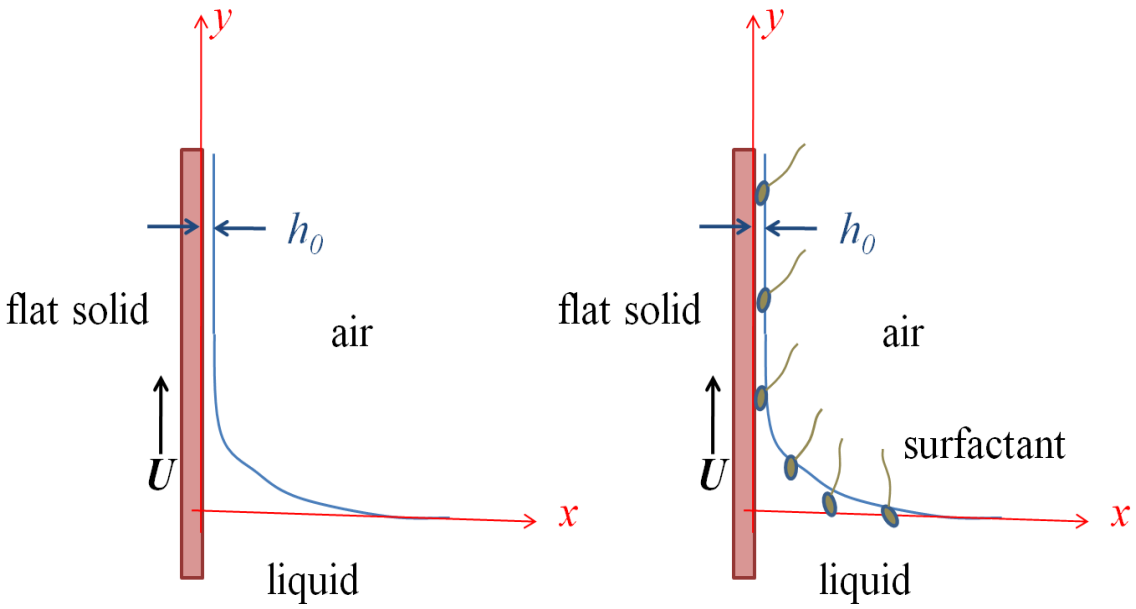

Figure 3.5 The drag-out problem in a pure liquid (left). The drag-out problem in the presence of a surfactant (right).

There are three main forces that affect the thickness. When a surfactant is added, a forth force also has to come into consideration. These forces are as follows:

1. Gravitational Force
2. Capillary Forces
3. Viscous Forces
4. Marangoni forces (only when surfactants are present) [59] [60].

Furthermore, there are three regions in the drag-out problem, as demonstrated in **Figure 3.6**, at the thin-film region, only the viscous forces govern the flow of the liquid. At the transition region, a balance has to take place between the capillary and viscous forces. While at the meniscus region, the capillary forces balance the gravitational forces [58].

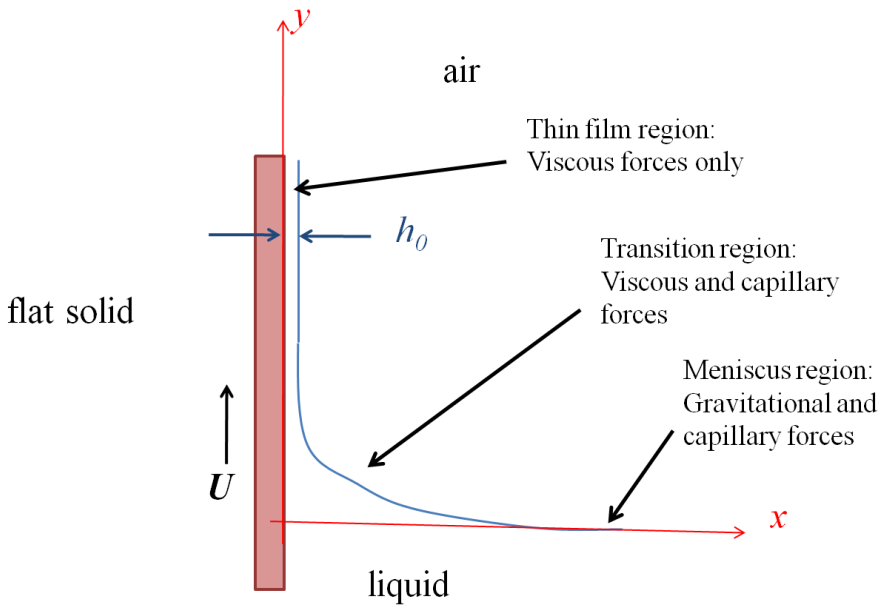

Figure 3.6 The three regions and the forces that govern each region.

The effect of each force is best understood by presenting the main models that were introduced.

1. **Gravitational Force:** In its simplest form, the force due to gravity is the hydrostatic pressure multiplied by the area of the liquid column:

$$F_{gravity} = \rho g h A. \qquad \textbf{Equation 3.1.}$$

Here, ρ is the density of the liquid, g is the gravitational acceleration, and A is the area of the cross section of the fluid column.

2. **Viscous Force:** In its fundamental form, the viscous force is given by

$$F_{viscosity} = \frac{\mu A u}{h}, \qquad \textbf{uation 3.2.}$$

where μ is the viscosity of the liquid and u is the speed (see **Figure 3.7**).

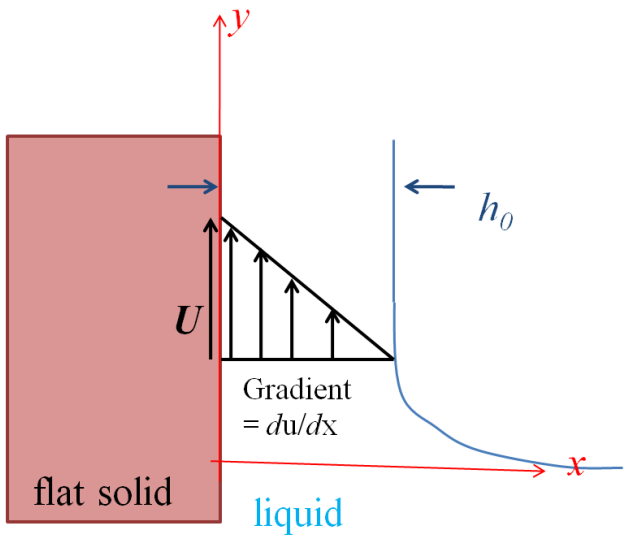

Figure 3.7 The viscous force

In this simple model, equilibrium is established between the viscous and gravitational forces:

$$F_{viscosity} = F_{gravity} \qquad \textbf{Equation 3.3.}$$

$$\frac{\mu A u}{h} = \rho g h A$$

$$h = \frac{\overline{\mu u}}{\rho g}$$

This model however, ignores the capillary force, which significantly reduces its accuracy, because the capillary rise is very influential [58]. In a more accurate model, introduced by Landau and Levish [55], the thin film is treated as a Prandtl boundary layer, which requires solving the Navier-Stokes equations. The effect due to the capillary forces was introduced, but the gravitational force was neglected. Another important factor neglected in this model is the normal pressure resulting from the viscous force

[58]. Therefore this model is only valid for laminar flows that have very small capillary numbers. Using the coordinate system defined in **Figure 3.5**, the region bounded by $y > 0$ and $0 < x < h$, the Prandtl boundary layer equations are:

$$v\frac{\partial^2 u}{\partial x^2} = \frac{1}{\rho}\frac{\partial p}{\partial y} + g, \qquad \textbf{Equation 3.4.}$$

$$\frac{\partial p}{\partial x} = 0. \qquad \textbf{Equation 3.5.}$$

The equations above assume the following boundary conditions:

- The no-slip condition given by:

$$u = u_{plate}\ at\ x = 0$$

- Continuity of pressure at the interface so that pressure inside the liquid is equal to the capillary pressure, and absence of tangent pressure:

$$p = p_{capillary} = -\gamma\frac{\partial^2 h}{\partial y^2}\ at\ x = h(y) \qquad \textbf{Equation 3.6.}$$

$$\frac{\partial u}{\partial x} = 0\ at\ x = h\ \ y\ .$$

In the equation above, γ is the surface tension. The pressure on the interface is the same as the pressure inside the liquid, this pressure equality falls from the second equation of the Prandtl boundary layer, thus in this model, the pressure inside the liquid is equal to the capillary pressure.

3. Capillary Force:

In their works Landau and Levish [55] and Wilson [56] assumed that a balance occurs between the capillary and viscous forces, and the gravitational force was neglected. This assumption is valid for the transition region in **Figure 3.6**. The capillary force is integrated into the governing equations by the presence of the capillary pressure shown in the boundary conditions above as well as the capillary length and the capillary number which is given as:

$$l_{capillary} = \overline{\frac{\gamma}{\rho g}}, \qquad \textbf{Equation 3.7}$$

$$Ca = \frac{U\mu}{\gamma}, \qquad \textbf{Equation 3.8}$$

where ρ is the liquid density, g is the gravity, and μ is the fluid viscosity.

4. Marangoni Forces:

When surfactants are present, experiments performed by Daripa and Pasa in [59] using Landau's approximation (i.e. only valid for low capillary numbers) show that surface tension gradients are the major players in determining the thickness. In particular, it was found in [60] that the film becomes thicker when surfactants are added due to the presence of Marangoni forces. A surface tension gradient is present due to a gradient in the concentration of surfactants in the thin-film region. This surface tension gradient introduces a new boundary condition at *x= h(y)* that is a function of the change of surface tension in the *y*-direction $\frac{\partial \gamma}{\partial y}$ [59] [61].

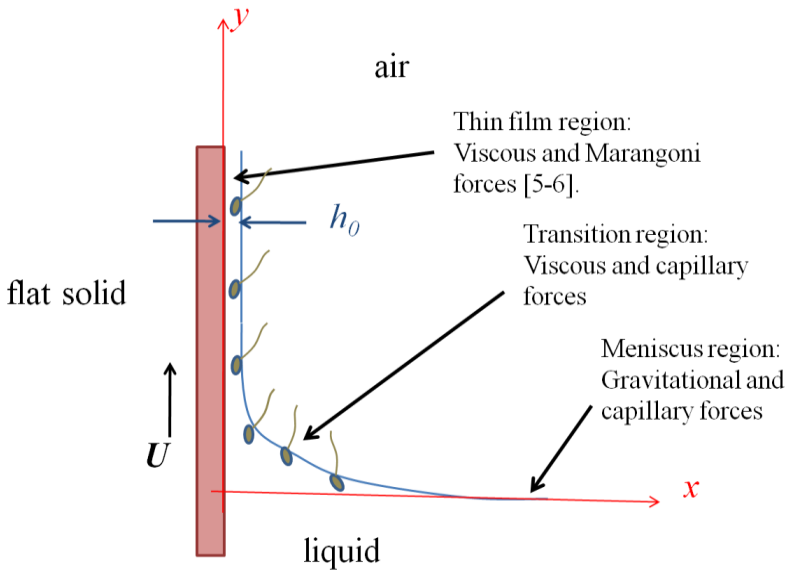

Figure 3.8 In the presence of surfactants, the forces governing the thin-film region are affected by the gradient of the concentration of the surfactants.

3.5. Results and Discussion

Membrane surfaces were characterized by contact angle measurement methods [62] as examined in the micrographs taken by Dr. Javier Montez and shown in **Figure 3.9**. Maintenance of the 10 µl pure deionized water drop on the surface of a deposited layer indicates the transfer of the lipid monolayer to the porous silicon surface. The large angle observed of about 112^{o} is due to the long hydrophobic tail of the phospholipids used. Immediately after the bilayer is deposited, the membrane is fully supported on the amphiphilic porous silicon mesh and water film that fills the pores during immersion. Upon evaporation of the water film underneath the lipid bilayer membrane, the formed bilayer bonds to the amphiphilic porous structure and is semi-supported on the porous silicon mesh, bridging over the 50~100 nm wide pores. It is reported that dry monolayers

may bridge over gaps as wide as 500 µm [52]. It was suggested from experiments performed on dipalmitoylphosphatidylcholine that the possibilities of van der Waals attractions between adjacent hydrocarbon chains increase with dehydration leading to a transition of the phase of the lipid bilayer to the gel phase [63]. The surface pressure at which the dense packing of the phospholipid molecules takes place is in the range 40 ~ 50 mN/m before collapse occurs. Using a value of 72 mN/m for the surface tension, γ, of pure water, the surface tension of the phospholipid monolayer is defined as [53]:

$$\gamma_{monolayer} = \gamma_{water} - \pi \qquad \textbf{Equation 3.9}$$

The equation above results in a value in the range 22-32 mN/m for the given range of surface pressure, π, which is within the range expected for phospholipid monolayers (about 25 mN/m) [53].

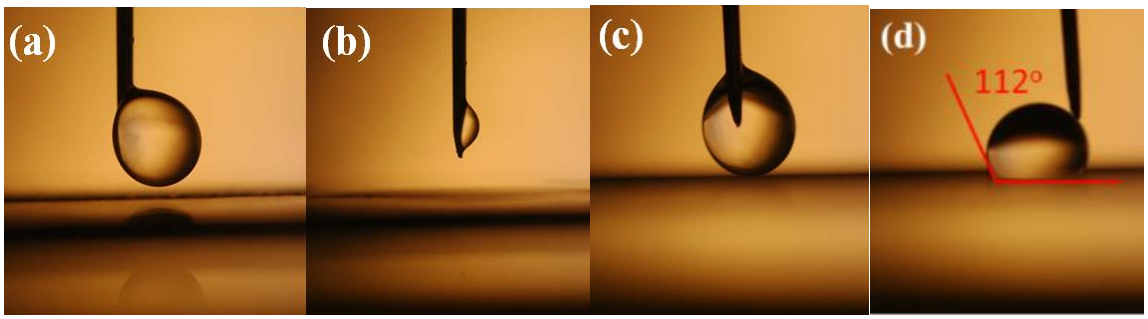

Figure 3.9 Contact angle measurement, water drop penetrates the highly porous silicon surface into the pores (images a and b). The water drop settles on the surface after formation of a lipid bilayer (images c and d). Images were taken by Dr. Javier Montez.

The surface pressure versus area-per-molecule isotherm of the phospholipid mixture (molecular weights 870.163 and 804.172 g/mol respectively) was constructed based on the experimentally achieved values of LB trough surface area and calculations using the lipid concentrations supplied by the manufacturer and mixing ratio of the lipid solutions. The area per molecule ($A_{molecule}$) in nm^2 is calculated from the total surface area (A_{total}) and number of lipid molecules ($N_{molecules}$), which in turn is calculated from the concentration of each of the two lipids in the mixed solution (C_1 and C_2), the molecular weight of each lipid (m_1 and m_2), Avogadro's number (N_A), and the volume of each of the lipid solutions used (V_1 and V_2).

$$A_{molecule} = \frac{A_{total}}{N_{molecules}} \qquad \textbf{Equation 3.10}$$

$$N_{molecules} = N_A \left(\frac{C_1 V_1}{m_1} + \frac{C_2 V_2}{m_2} \right) \qquad \textbf{Equation 3.11}$$

The isotherm plot presented in **Figure 3.10**, shows that the phospholipid molecules occupy an average molecular area of 0.68 - 0.73 nm^2 at the 2-dimensional solid phase region (i.e. at the peak surface pressure). The mean values of the molecular area achieved in the trough were in close agreement with that reported by Lis et. al. for egg phosphatidylserine in membranes at 25 ^oC of 0.50 – 0.70 nm^2. The surface pressures at which the lipid membranes have been coated (about 46 mN/m) were within the expected ranges for which supported lipid membranes of phosphatidylethanolamine form rather than micelles [50]. Thus, the experiment resulted in a phospholipid monolayer with a surface tension of 26 mN/m. The maximum surface pressure on water subphase

that can be achieved in a Langmuir- Blodgett trough at 20 ^{o}C is 73 mN/m because it is the difference between the surface tension with and without the monolayer [52].

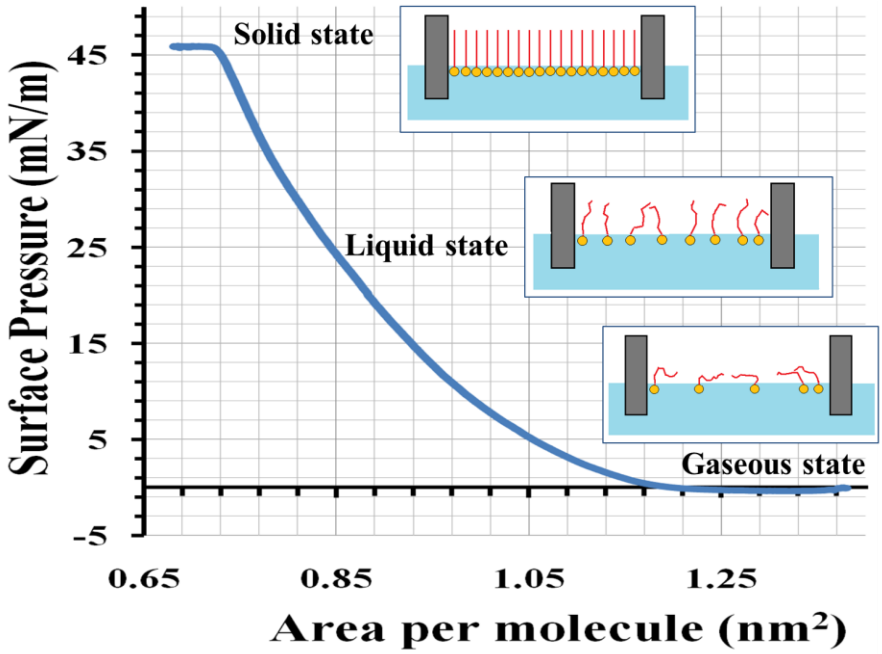

Figure 3.10 The surface pressure vs. area isotherm of phosphatidylserine and phosphatidylethanolamine lipids on deionized water subphase.

Black lipid membranes that have been formed on apertures with diameters of 1.0 cm [41] and 150 - 200 µm [2] lack rigidity and the mechanical stability to last more than a few minutes [64]. The lipid bilayer presented here is semi-supported due to presence of the highly-porous silicon underneath with pore diameters of about 1 – 2 µm and, as such, remains mechanically stable for longer durations. This stability allowed for supported lipid bilayer membranes to be investigated using atomic force microscopy (AFM) in the tapping mode [46].

3.6. Conclusion

This work shows for the first time the formation of a lipid bilayer membrane using the Langmuir-Blodgett and Langmuir-Schaefer techniques on porous silicon. These techniques result in the formation of tightly packed lipid bilayers when compared to other techniques such as direct vesicle spreading and Montal-Mueller methods. A mixture of the two phospholipids 1,2-diphytanoyl-*sn*-glycero-3-phosphoserine and 1,2-diphytanoyl-*sn*-glycero-3-phosphoethanolamine is used. The monolayers are formed at a surface pressure of 46 mN/m, each phospholipid monolayer demonstrated a surface tension of 26 mN/m. Tight packing is achieved at an average area per molecule of 0.68 - 0.73 nm^2. The application procedure presented in this chapter is important for fusion of the epithelial sodium channel (ENaC) proteins, which will be shown in the next chapter.

CHAPTER 4

INCORPORATION OF TRANSMEMBRANE PROTEINS

4.1. Introduction

In biological cells, membrane proteins handle most functions of the plasma membrane, allowing the cell to accommodate external environmental changes. The functionality of the biological membrane is generally determined by the types of membrane proteins it contains and their concentration. For example, in the nerve cell axon membrane, proteins constitute less than 25% of its mass. This membrane's main functionality is to provide electrical isolation from the surroundings, while membrane proteins constitute about 75% of the internal membrane of mitochondria, which is the ATP production organelle [5]. However, much of the functionality and structure of membrane proteins are yet to be understood, such as changes in protein conformation that result from changes in ion concentrations or during cargo transport [4]. Transmembrane proteins in particular, which penetrate through the lipid membrane, interact with both external and internal environments for the case of a biological cell. They also share the same physical property as lipid bilayers in that they are amphiphilic with their hydrophilic regions on the exterior sides and their hydrophobic region embedded in the interior of the lipid bilayer membrane.

Before continuing further, this chapter will introduce proteins to the reader: a protein is a molecule that is composed of amino acids that form a polypeptide chain.

Each amino acid is composed of a carbon atom bonded to hydrogen, an amino group, a carboxyl group, and a side chain. The amino group at one end of the polypeptide chain is called the Amino terminus (or N-terminus), and the carboxyl end is termed the carboxyl terminus.

Proteins may bind together forming larger proteins composed of more than one polypeptide chain, such as the epithelial sodium channel (ENaC) protein, which is usually composed of three protein subunits called α, β and γ subunits, as will be shown in the next section. The protein polypeptide chain folds into a three-dimensional conformation, which plays an important factor in the reactivity of the protein surfaces. One common three –dimensional fold in proteins is called the α helix, in which hydrogen bonds in the polypeptide backbone force the polypeptide chain to form a cylindrical shape. The α helix is commonly found in transmembrane proteins [5].

4.2. Structure of the Epithelial Sodium Channel Proteins

Transmembrane proteins have hydrophobic regions that pass through the bilayer membranes and hydrophilic regions outside the membrane. The epithelial sodium channel (ENaC) protein and bactriorhodopsin are two of the proton-pumping membrane proteins that received considerable attention [4] [2]. ENaC protein belongs to the ENaC/degenerin (DEG) family of proteins that was discovered in the 1990's and is only found in mammalian cells [65]. The protein subunits comprising ENaC are referred to as α, β and γ-Subunits. Also it was shown that the α-subunit is replaced by the δ-subunit to produce a conductance change [66]. Each subunit is composed of two α helices and an extracellular domain. The amino (NH_2-) terminus and the carboxyl (COOH-) terminus

are both located in the cytoplasm side of a cell membrane [67]. Each subunit of the ENaC/DEG family has a length of 500-700 amino acids [67]. Further reading about protein structure, interactions between proteins and lipid bilayers, and membrane protein biochemistry may be found in references [68] [69] [70] [71].

Structural analysis of proteins may be performed using atomic force microscopy (AFM), X-ray diffraction of purified and crystallized proteins [72], and electron microscopy [73]. However, only AFM imaging allows for an *in-vivo* environment of the protein. Protein functionality may be studied using fluorescence microscopy [4]. In atomic force microscopy, investigation of the protein may be done in the contact mode [4], or the tapping mode [46], or the mac mode [46]. The contact mode offers a high resolution visualization of the protein surface [74]. Also the forces applied by the AFM tip in the contact mode may be used to determine young's modulus of the membrane [4] but the force exerted by the tip may also damage the membrane and, therefore, limits the pore diameters underneath the biological membranes.

4.3. Preparation of Vesicles Containing Epithelial Sodium Channel Proteins

Vesicles containing the ENaC three proteins were prepared and supplied by Dr. Bakhrom Berdiev in the University of Alabama at Birmingham. The method to prepare the amiloride-sensitive Na^+ channel proteins of the ENaC/degenerin family was detailed by Berdiev and Benos in [2]. In brief, the method starts by linearization of plasmids containing the ENaC cDNA; the plasmid then undergoes an *in-vitro* transcription process into messenger RNA using T7 RNA Polymerase proteins. The translation process of the messenger RNA to ENaC proteins is done using the TNT transcription-translation kit.

Following a procedure to elute and concentrate the ENaC proteins, the proteins are reconstituted into proteoliposomes by incubating the proteins with the phospholipids phosphatidylethanolamine, phosphatidylserine, and phosphatidylcholine at a 50:30:20 ratio consecutively. Vesicles containing the ENaC proteins may also be prepared by injecting the cRNA molecules of each of the three subunits of the ENaC proteins into the oocytes of an adult female Xenopus [2].

4.4. Method

The Protein is purified beforehand as described in [2]. The protein used in this analysis is the epithelial sodium channel (ENaC) which is a transmembrane ion channel, as mentioned earlier. Protein incorporation was accomplished by spreading proteoliposomes containing ENaC protein at a close proximity over the lipid bilayer. Protein fusion may be enhanced by keeping the lipid bilayer at a -40 mV potential with respect to the surroundings [2] [3]. This negative potential improves reorientation of the transmembrane channels such that the amiloride-sensitive side, which is the side facing the exterior of a natural epithelial cell, faces one side [3]. The membrane is then left for few minutes to allow for protein fusion. After that the device is immediately taken for analysis in the atomic force microscope or for characterization of the total electrical impedance. Atomic force microscopy was performed in the lab of Dr. Darayas Patel at Oakwood University.

Unlike black lipid membranes, which lack rigidity and stability over time, the lipid bilayer here is semi-supported due to the presence of the porous silicon underneath. The lipid bilayer membranes in the gel phase with the proteins fused into them were then

investigated using atomic force microscopy (AFM). The tapping mode [75] is used for this analysis.

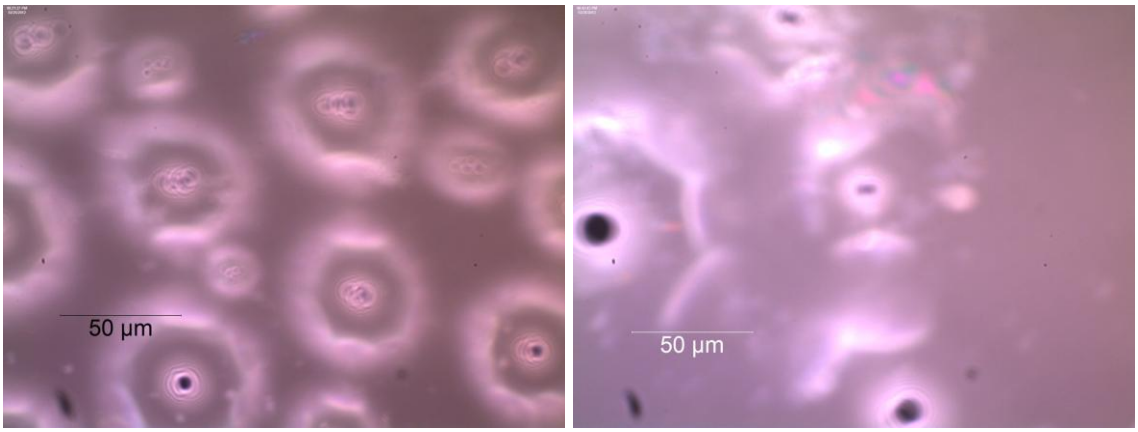

Figure 4.1 Optical images taken of the vesicles that contain the epithelial sodium channel (ENaC) proteins while spreading on a porous silicon substrate.

4.5. Results and Discussion

Characterization and analysis of supported lipid membranes with or without proteins incorporated into them may be performed using one of the following techniques:

1. **Atomic force microscopy:** This form of analysis is the ultimate technique due to the high resolution in the atomic scale. Both tapping mode [75] and contact mode [4] may be used.
2. **Capacitance measurement:** [2] This method is one of the oldest techniques of characterizing formation of lipid bilayer membrane. A good lipid bilayer is formed when a capacitance of about 0.67 – 0.95 pF/cm^2 is achieved [2] when the two phospholipids are used.

3. **Scanning electron microscopy:** [21] A disadvantage of this technique is that the environment at which the membrane is scanned is significantly different from the native environment of the lipids and proteins. In addition, the electron beam may damage the biological molecules.
4. **Ellipsometry:** [76] In this technique, the elliptic polarization of reflected light is measured and related to the thickness of the biological membrane under investigation.
5. **Raman spectroscopy:** [77] [78] [79] [80] [81] This technique has been shown to investigate interactions between lipids and proteins embedded in lipid bilayer membranes [81]. The Raman markers of lipids and proteins are shown in **Table 2** [81]. Although Raman spectroscopy equipment with an adequate resolution was not accessible at the time of this project, this method is presented here for completeness.

The ENaC channel is highly selective to sodium ions and is believed to be composed of three subunits (α, β, and γ) [82]. The stoichiometry of the ENaC channel is not exactly known; however, it is believed to have one of two stoichiometric models: the arrangement α:β:α:γ with the subunit α being the most abundant, the molecular weight reported for the α subunit is 95 KDa [22]. The second stoichiometric model is the 3α:3β:3γ [83] [84] with a molecular mass larger than 600 KDa [85].

Table 2. Raman modes of lipids and proteins

Raman Mode	**Wave number (cm^{-1})**	**location**	**Significance**
CH bending	1440, 1460	Lipid Acyl chain	Indicative of lateral packing
CH twisting	1296	Lipid Acyl chain	
CH deformation	970, 1229	Lipid Acyl chain	For unsaturated acyl chains
CH stretching	2800-3100 (2840, 2860, 2880, 2930, 2960, 3010)	Lipid Acyl chain, Amino acids	Indicative of chain packing and location of methylene in the acyl chain.
CC stretching	1064, 1080, 1089, 1133, 1660 (unsat C=C)	Lipid Acyl chain	
Phosphate group	860	Lipid Head group	
phosphodioxy group (PO_2^-)	1096	Lipid Head group	Indicative of H bonds
ethanolamine group	759	Lipid Head group	Marker for Phosphatidylethanolamine lipids
Choline group $N+(CH_3)_3$	717, 875	Lipid Head group	Marker for phosphatidylcholine lipids
OH stretching	3400, 3455	Water	
OH bending	1640	Water	Indicative of hydrogen bonding
Other modes	440, 550, 650, 730	Water	
Amide S	1395	Protein polypeptide chain	Indicative of protein contents that are not helical
Amide III	1200-1300	Protein polypeptide chain	
NH stretch	3300	Amino acids	
CH bending	1450	Amino acids	
Trp	1542, 1340, 1360	Amino acids	The intensity ratio I_{1360}/I_{1340} is an indication of hydrophobicity strength
Trp	883 or 877 or 871, and 1490	Amino acid	871 is an indicator of a strong H bond 883 is the marker of a weak H bond

Atomic force microscopy is superior to other imaging techniques, such as electron microscopy, in that images are taken in a biocompatible environment (room temperature and ambient pressure). **Figure 4.2** displays first-order topography AFM images of the structure at two different heights; the amplitude image is presented for better visualization of the edges and tips. The AFM images were taken using a PicoPlus atomic force microscope by Molecular Imaging, Inc., Arizona, at a scanning speed of 1 line/scan and a resolution of 516 x 516 pixels using the tapping mode. A silicon cantilever was used at the fundamental resonance frequency between 290 and 300 KHz and Hooke's spring constant of 40 N/m.

The AFM images present an attempt to visualize the incorporated ENaC protein complex on the fabricated structure with the lipid bilayer. The images in the top and middle rows show a 1 μm × 1 μm section. Large bodies that span the water-filled porous silicon surface are easily seen and believed to be aggregates of denatured ENaC protein. Protein denaturing and aggregation has been a known problem for proteins that experience an environmental change, such as in temperature, ion concentration, or pH level [86]. Another reason for protein agglomeration is the use of the spreading technique to incorporate protein. Protein incorporation may be better achieved if the proteins are deposited with the lipids simultaneously using the Langmuir-Blodgett and Langmuir-Schaefer techniques. The cross-sectional profiles along the lines labeled 1 and 2 on the image in the middle row are shown in the bottom row.

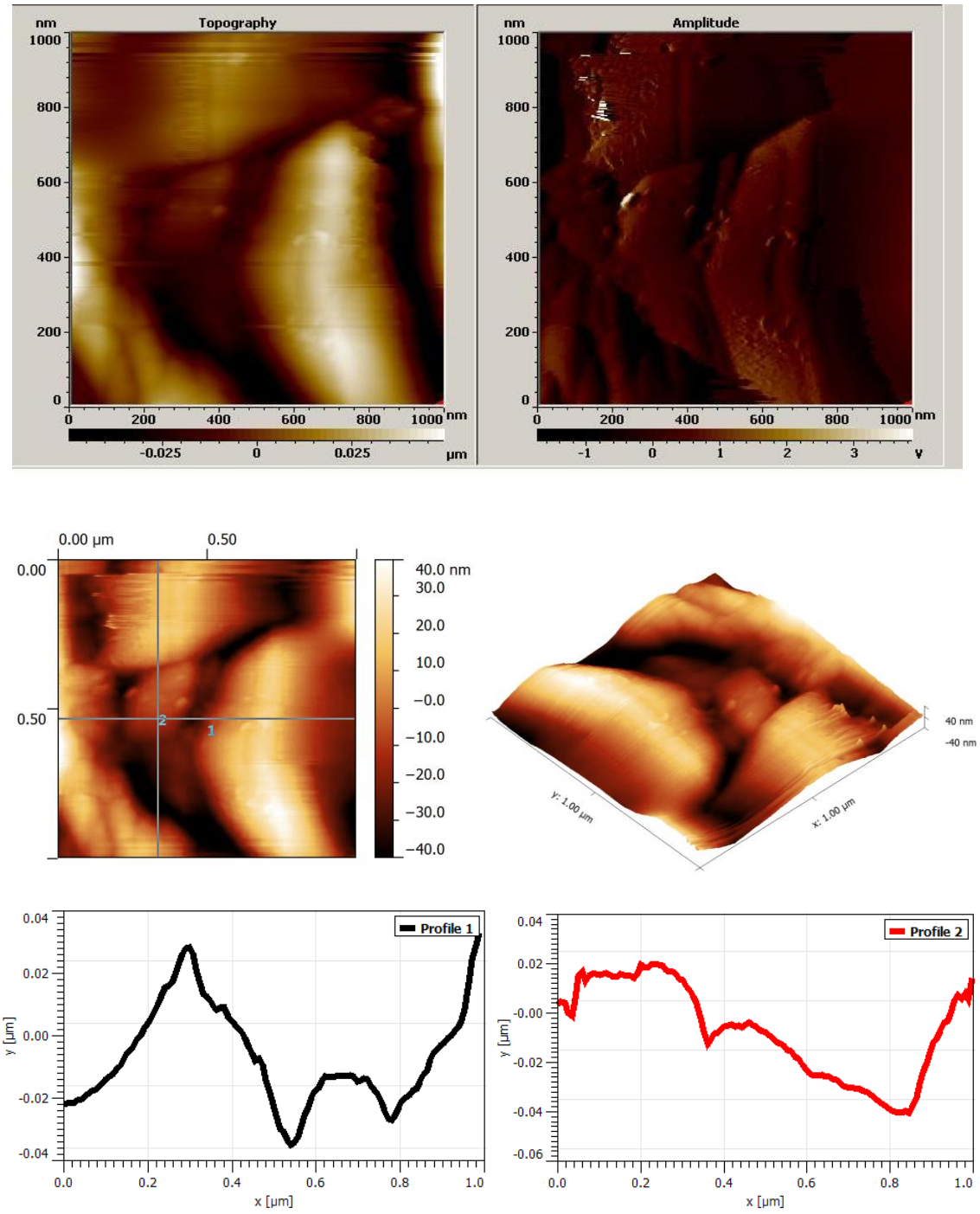

Figure 4.2 Atomic force microscope (AFM) images of ENaC protein complexes in an artificial lipid bilayer. Topography and amplitude images (top row), Topography image with lines marked for cross-sectional profiling, and in 3D view (middle row). Cross sectional profiles at the lines 1 and 2 (bottom row). AFM images are taken at the lab of Dr. Darayas Patel in Oakwood University.

A 2 μm × 2 μm section and its 3-dimensional view are displayed in **Figure 4.3**. The agglomerated proteins in the lipid bilayer membrane are shown to partially span the pores. The 10 μm × 10 μm topography images show that the transmembrane protein tends to form round-shaped objects with diameters of about 500 nm, these complexes are due to hydrophilic and hydrophobic interactions and the high insolubility for which transmembrane proteins are known to exhibit. Vertical and horizontal cross sectional profiles are also shown. From the profiles, it can be inferred that the bodies have heights as large as 400~500 nm.

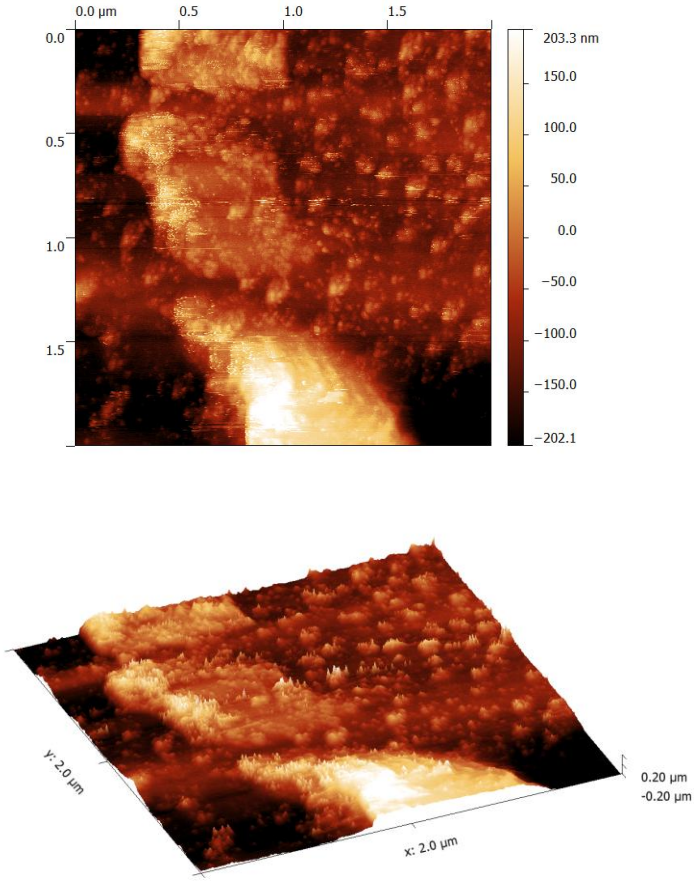

Figure 4.3 Protein complexes within a lipid bilayer membrane partially and fully spanning water-filled pores in a 2 μm × 2 μm area (top) and a computer-built three dimensional image (bottom).

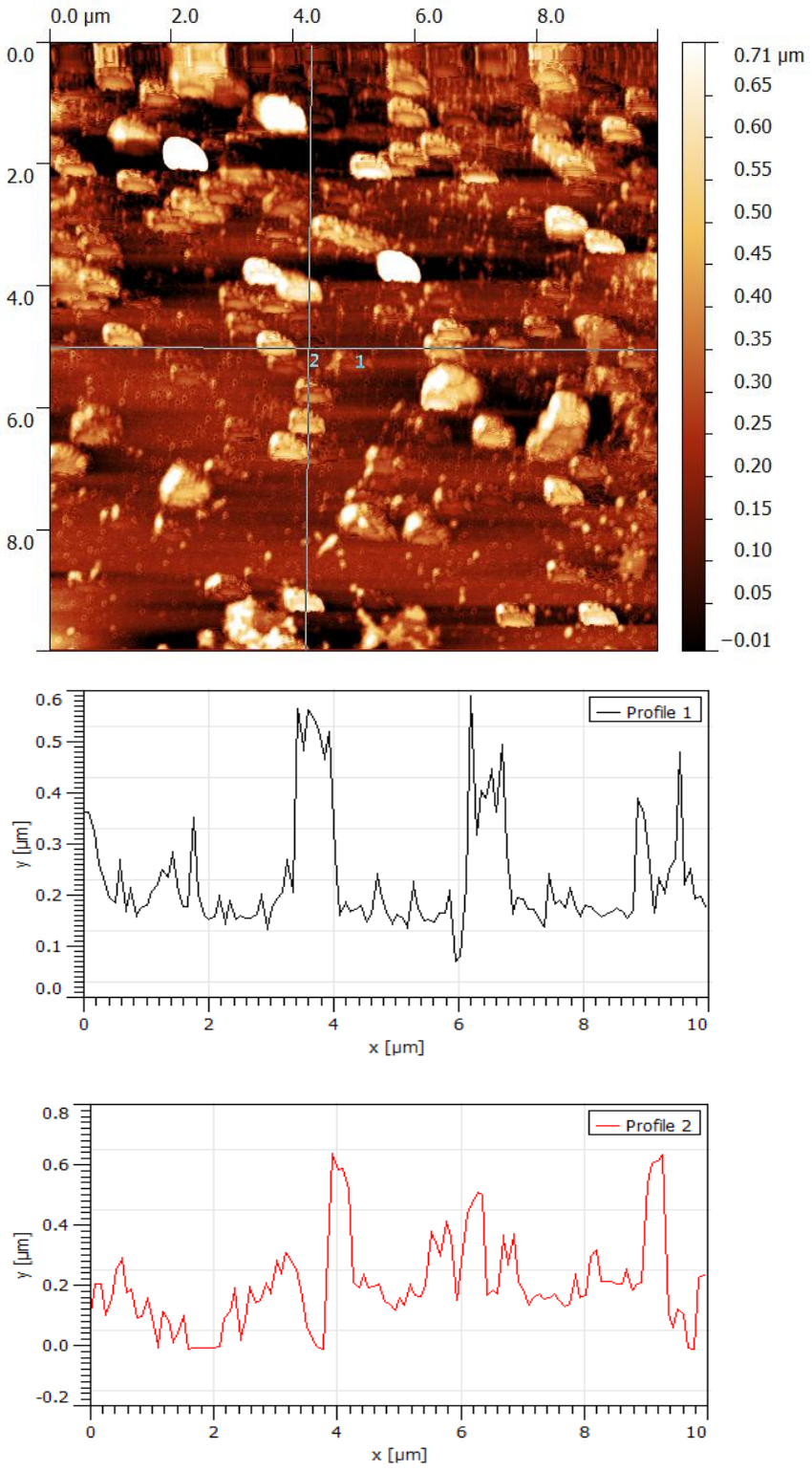

Figure 4.4 A 10 µm × 10 µm area of the protein complexes (top row). Surface profiles at the vertical (middle) and horizontal (bottom) cross sections at the lines indicated in the figure.

4.6. Conclusion

This is the first work in literature to demonstrate the formation of lipid bilayers with incorporated epithelial sodium channel (ENaC) proteins that are supported on a porous silicon substrate using atomic force microscopy (AFM). The epithelial sodium channel proteins form transmembrane ion channels that are fused into the lipid bilayer membranes by direct spreading of vesicles containing the three proteins that make up the ENaC channel. The main challenge associated with protein incorporation is protein denaturing due to due to the environmental sensitivity of the proteins. Protein denaturing results in forming clusters of agglomerated transmembrane proteins with diameters of about 500 nm, as shown by atomic force microscopy. The next chapter details the characterization of these ion pumps using electrochemical impedance spectroscopy.

CHAPTER 5

CHARACTARIZATION USING ELECTROCHEMICAL IMPEDANCE SPECTROSCOPY

5.1. Introduction

Several methods have been used to study environmental interactions with proteins fused into lipid bilayer membranes such as atomic force microscopy [4], surface plasmon resonance (SPR) [87] [88], and quartz crystal microbalance (QCM) techniques [89]. However, these methods are not suitable for characterizing protein channels in which an ion transfer takes place, in which case electrical impedance and capacitance measurement techniques are required [90] [91]. Voltage and current-clamp techniques [92], or the refined patch-clamp technique [6], and electrical impedance spectroscopy (EIS) techniques [93] [94] [90] [95] [1] historically have been used to study lipid bilayer membranes. The patch-clamp technique for investigating the protein channels has been used by Dr. Berdiev in his lab at the University of Alabama at Birmingham, as shown in **Figure 5.1** below. A planar lipid bilayer membrane is formed between two *cis* and *trans* compartments, and the Epithelial Sodium Channel proteins are fused into the lipid bilayer using a glass rod. Measurements were taken using Ag/AgCl electrodes in a 3% agar and 3M KCl solution, with the voltage applied to the *cis* compartment while the *trans* compartment is held at ground.

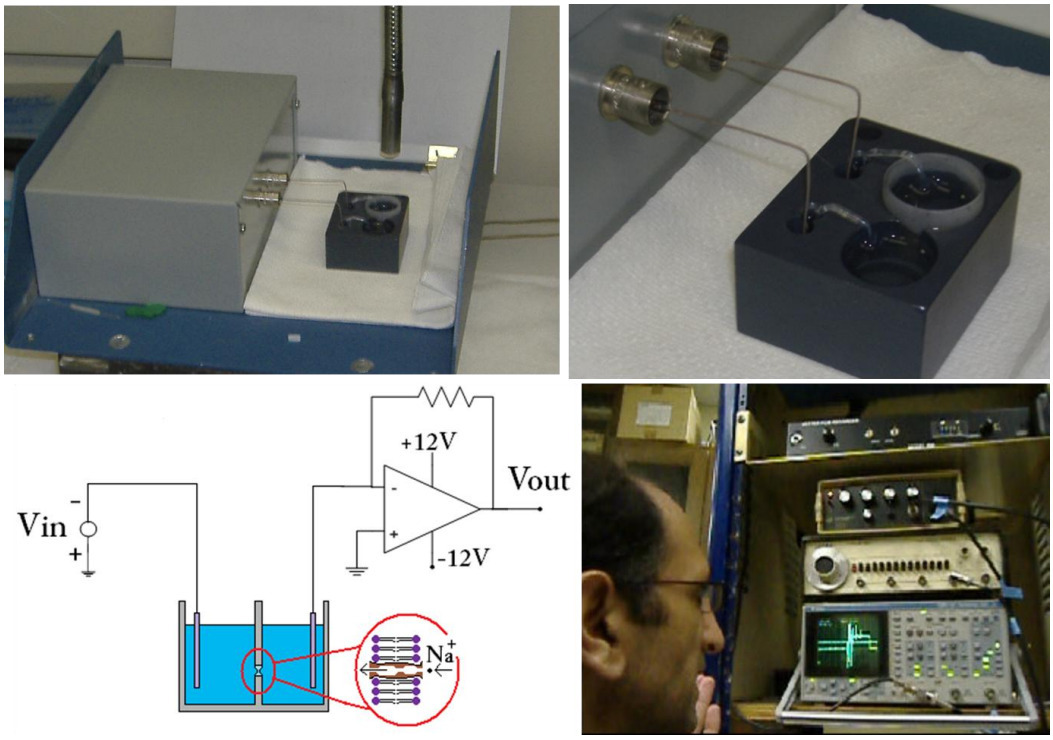

Figure 5.1 The setup used to perform electrical capacitance measurements of a lipid bilayer membrane by Dr. B. Berdiev at the University of Alabama at Birmingham.

When a lipid bilayer membrane is subjected to an external electric field that is high enough to overcome the energy barrier of the membrane, electric breakdown occurs in which electric conductance of the membrane increases dramatically. This breakdown starts by forming hydrophobic pores in the lipid bilayer. If the diameter of these pores is wide enough, they progress to the more stable hydrophilic pores by reorienting the lipid molecules such that minimum free energy is attained when the hydrophilic heads form the pore walls [96]. After the applied electric field is removed, the lipid bilayer membrane returns to its initial low conducting state, thence, is the name reversible electric breakdown [97].

Reversible electric breakdown of lipid bilayer membranes was investigated in literature [96] [92]. It was shown to be caused by accruement of hydrophilic pores [92]. Hydrophobic pores, on the other hand, were believed to have short transient lives and limited or no contribution to conductivity of lipid bilayer membranes [96]. The two phospholipids used in this work have long hydrophobic chains (longer than 15 carbon atoms), which increase the energy barrier for pore formation.

Electric breakdown of the membranes has been measured using the voltage-clamp technique by Chernomordik et. al. [92] and the charge-pulse relaxation method by Benz et. al. [98]. The Presence of cholesterol in the lipid bilayer membrane is known to enhance its packing, it was reported by Benz et. al. [98] that lipid bilayers experienced irreversible mechanical breakdowns that were not experienced in oxidized cholesterol membranes.

The reported electric collapse of the cell membrane in red blood cells was found to occur at an electric field of 1-10 V/cm [99]. Chernomordik et al [92] report that the resistance of human erythrocyte membranes is in the range 2-10 GΩ, and 0.5-1 GΩ in mice fibroblast L-cells. On the other hand, in experiments performed on phosphatidylcholine and phosphatidylserine bilayers, the LBM capacitance was shown to be in the range of approximately 0.35-0.6 $\mu F/cm^2$ depending on the content of cholesterol and pH value [100]. After the incorporation of protein channels into the lipid bilayer membranes, pore formation in the membranes is stabilized but may increase at the vicinity of the proteins [96] [101].

This chapter presents the electrical properties of the device composed of artificial lipid bilayer membranes from synthetic phospholipids deposited on electrochemically-fabricated porous silicon membranes with incorporated transmembrane proteins into the

lipid bilayers. This analysis uses the electrical impedance spectroscopy technique. The LBMs are formed using the Langmuir-Blodgett [48] and Langmuir- Schaeffer [49] [54] techniques. The lipids used for LBM formation in this work have been previously demonstrated to be used for incorporating the epithelial sodium channel (ENaC) proteins by Berdiev and Benos [2] and Ismailov et. al [3]. They used the negatively charged phosphatidylserine and the neutral lipid phosphatidylethanolamine to form the lipid bilayer membrane.

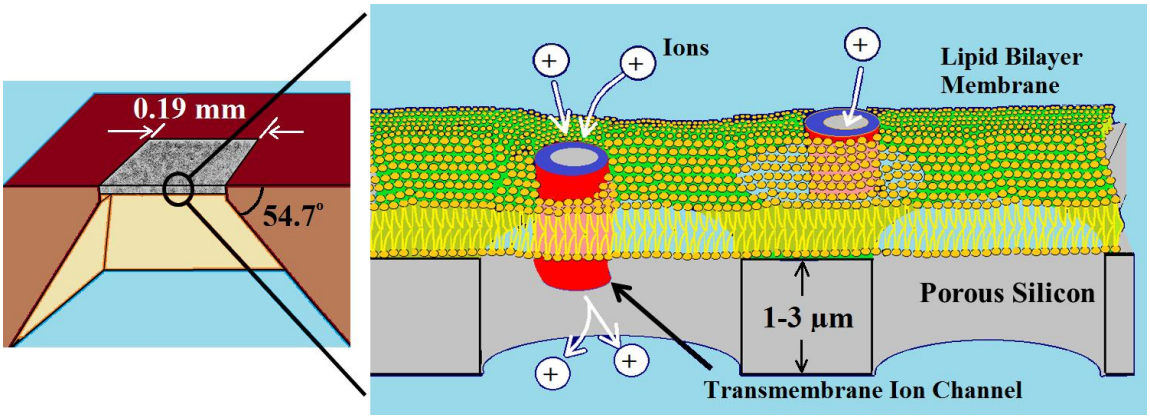

Figure 5.2 ENaC transmembrane channel proteins fused into a LBM deposited on the porous silicon membrane

5.2. Experimental Setup

Porous silicon was prepared electrochemically [32], as was outlined in Chapter 2, on a n-type silicon substrate with a low-resistivity and a crystallographic direction of <100> in an ethanoic Hydrofluoric acid (HF) solution. In brief the process was to fabricate a porous silicon structure that has a thickness of about 3 µm and pore of about 0.2~2 µm. In this process, a volumetric concentration of 49% HF: 95% Ethanol:

Deionized Water equal to 30:15:55 was used (Safety measures should be taken when handling the highly toxic HF acid). The electrochemical cell was light-illuminated and at room temperature. A driving current density of about 10-15 mA/cm^2 was applied for a duration of about 20-30 minutes. The sample was then immersed in a DI water bath for 10 minutes, then immediately immersed in Ethanol to reduce the water capillary effect when drying. The resulting porous silicon membrane had an area of about 3.6×10^{-4} cm^2. Samples resulting from this process that were used for the electrochemical impedance spectroscopy are shown in **Figure 5.3**.

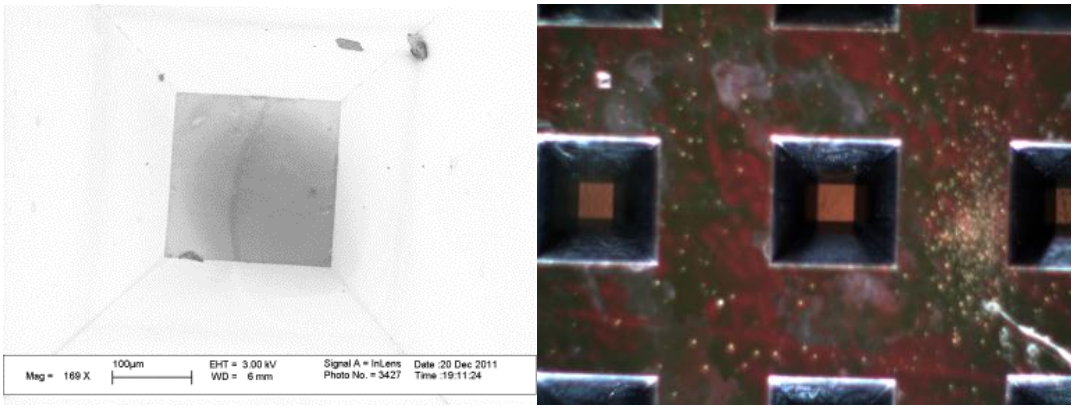

Figure 5.3 A scanning electron microscope image of the device carrying the porous silicon membrane (left). A micrograph of an array of the device structures (right).

The porous silicon membrane of the structure is shown in **Figure 5.4** (left). As was shown in Chapter 2, this membrane was less than 3-µm-thick with pore diameters of 0.2-2 µm. An image of the pores at a higher magnification is also shown to illustrate the high porosity of the membrane.

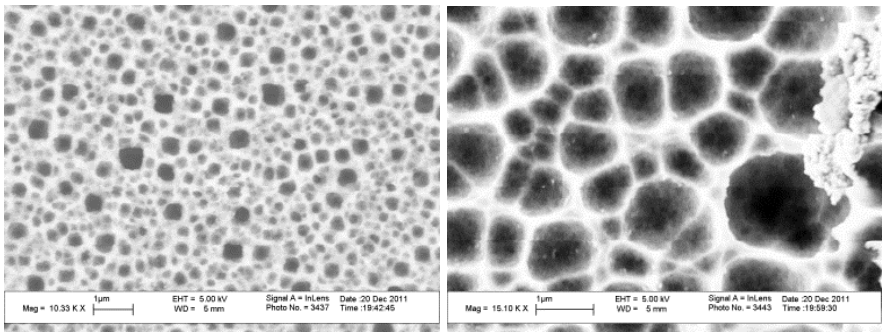

Figure 5.4 The Porous silicon membrane with about 0.2-2 µm wide pores shown at two different magnefications.

Prior to performing the experiments, all the 36 holes in the array at the backside of the sample were closed except for the hole on which EIS measurements are to be taken. An electrically-insulating tape is used for this purpose. This tape solely serves to provide an electrical insulation between the silicon substrate and the copper counter electrode in the electrochemical impedance spectroscopy as will be demonstrated in the next section. The porous silicon layer was wetted from both sides, and finally a copper foil was fixed tightly in place over the insulating tape to cover the back hole of the structure on which measurements are to be performed. The copper foil serves three functions: it forms the fourth edge of the lower compartment of the device, it also prevents the formation of a lipid bilayer membrane on the other side of the porous silicon membrane, and most importantly, it is the counter electrode used for the electrochemical impedance measurements. The experiment proceeds by taking electrochemical impedance spectra of the porous silicon layer alone. This system that is composed of the porous silicon alone is termed in this work as the Electrolyte-Porous Silicon system to account for the electrolyte resistance and porous silicon impedance.

For the set of experiments performed on the Electrolyte-Porous Silicon-LBM system, a lipid bilayer membrane was transferred to one side of the sample following the procedure outlined in Chapter 3. The two phosphoglyceride lipids, 1,2-diphytanoyl-*sn*-glycero-3-phosphoserine ($C_{46}H_{89}NO_{10}PNa$) and 1,2-diphytanoyl-*sn*-glycero-3-phosphoethanolamine ($C_{45}H_{90}NO_8P$), were used in a one-to-two parts ratio. The lipid bilayer deposition on the device is illustrated in **Figure 5.5**

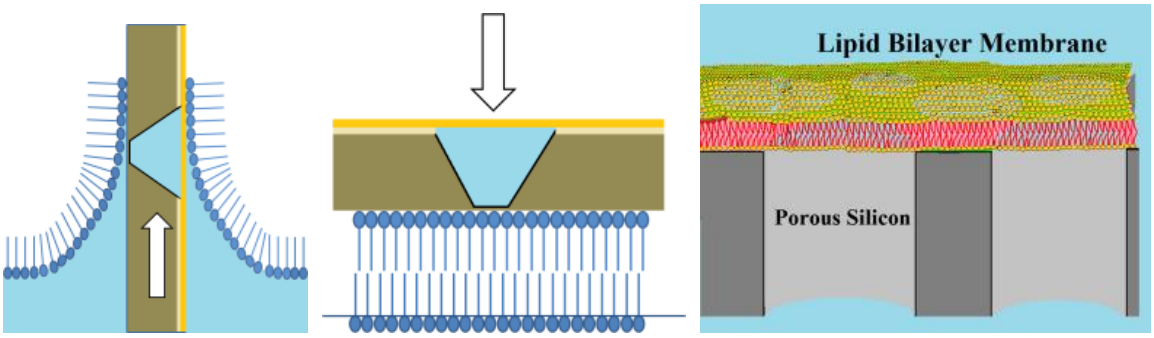

Figure 5.5 Schematic demonstration of the Langmuir- Blodgett (left), the Langmuir-Schaeffer (center) techniques, and the deposited LBM spanning the porous silicon structure (right).

After performing the experiment, the porous silicon sample was rinsed in water and was kept in a condition such that the need for wetting and dewetting is reduced as possible to avoid inducing damage to the porous silicon layer due to the water capillary effect. The same procedure then was repeated in the same day. Immediately after LBM deposition, ENaC channel protein vesicles were spread on the lipid bilayer membrane to take electrochemical impedance measurements of the Electrolyte-Porous Silicon-LBM-ENaC system.

Characterization of the electrochemical impedance was performed at room temperature using a Princeton Applied Research VersaSTAT3 potentiostat. The experiments were performed in two-electrode and three-electrode setups.

5.2.1. The Two-Electrode Setup

In the first set of experiments, a two-electrode system was made, in which the working electrode is a platinum coiled wire in one compartment, and the counter electrode is the copper foil that forms the cover of the lower compartment. The top compartment is simply a drop of the electrolyte solution. This experimental setup is shown in **Figure 5.6**.

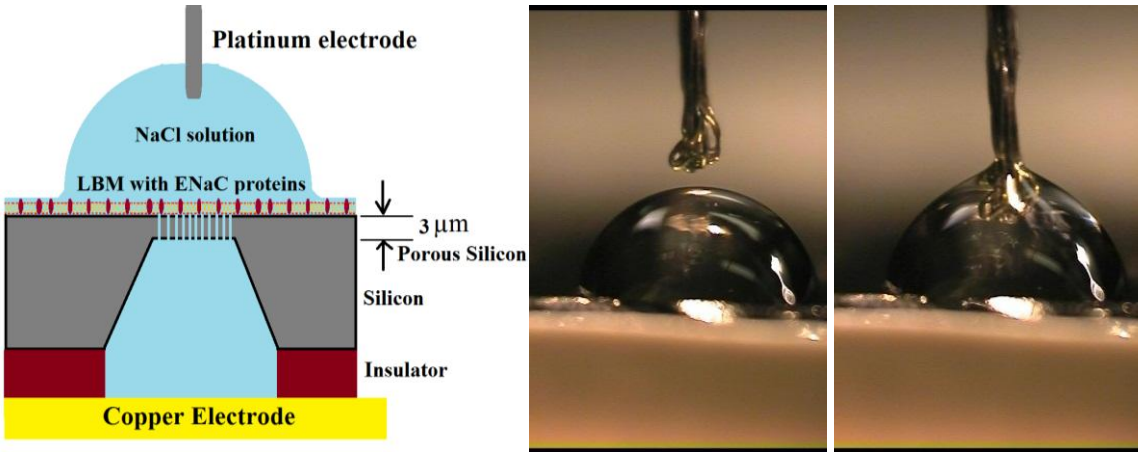

Figure 5.6 Illustration of the experimental setup of the two-electrode system for electrochemical impedance spectroscopy (left). The platinum electrode approaching the electrolyte drop (center), and engaging into the system (right).

5.2.2. The Three-Electrode Setup

In a three-electrode system, measurements are taken through a working electrode, an auxiliary (or counter), and a reference electrode. A coiled platinum wire was used as

the working electrode, the counter electrode was a copper foil that tightly covers the 0.9 mm × 0.9 mm back hole of the structure supporting the porous silicon layer. The reference electrode was a standard 4M potassium chloride (KCL) saturated with silver chloride electrode by Accumet, with a thin extension. This extension was built in the lab to fit in the micro electrochemical system. The height and location of the reference and working electrodes from the porous silicon surface were adjustable by a precision translation stage.

In their work, Naumowicz et. al. [94] performed EIS measurements on lipid bilayer membranes formed from 3-sn-phosphatidylcholine and 1,2-dimyristoyl-sn-glycero-phosphoethanolamine covering an area of about 0.04-0.08 cm^2 using sinusoidal signals of a peak amplitude of 4 mV. On the other hand, it was reported by Ohki [100] that the breakdown potential measured for phosphatidylcholine is over 200 mV in the pH range 4-8. In this work, a 100 mV sinusoidal signal was applied in the range of frequencies 0.1-100,000 Hz. The peak amplitude of the applied signal is comfortably below the breakdown potential reported by Ohki [100] for phosphatidylcholine. It is also high enough to take into account the porous silicon layer impedance with accurate measurements.

Lipid bilayer membranes were deposited on one side of the porous silicon layer. For the case of a full system comprising porous silicon with lipid bilayer membranes and transmembrane proteins, the proteoliposomes containing the ENaC transmembrane channel proteins were spread immediately after LBM deposition. The 0.1 M electrolyte solution was prepared using a 99% purity sodium chloride (NaCl) dissolved in Deionized water. A schematic illustration of the three-electrode experimental setup is shown in **Figure 5.7**. As in the two-electrode setup, the cell is composed of two upper and lower

compartments. The working electrode is a platinum wire, the reference electrode is positioned in close proximity and in the same compartment with the working electrode as seen in the figure. The counter electrode is tightly sealed to the insulating tape and closes the lower compartment of the cell as was described previously. Ions flow between the two compartments with the applied potential to close the electrochemical circuit.

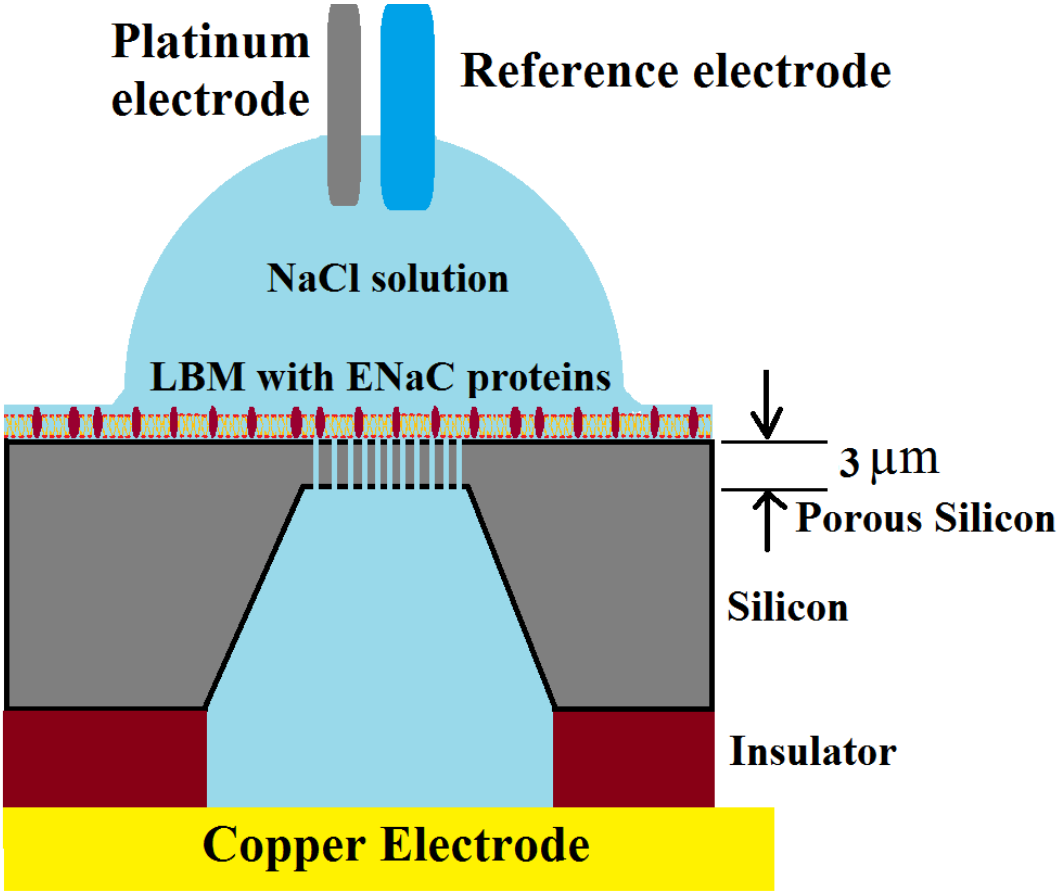

Figure 5.7 Experimental setup, the working electrode is a platinum coiled wire, and the counter electrode is a copper foil. A standard 4M KCL with AgCl reference electrode is used.

The experimental setup around the device consists of electrodes, light sources, microscopes, precision stages, and data acquisition and analysis equipment. This setup is shown in **Figure 5.8**. Microscopes are used for live visualization and monitoring of the system.

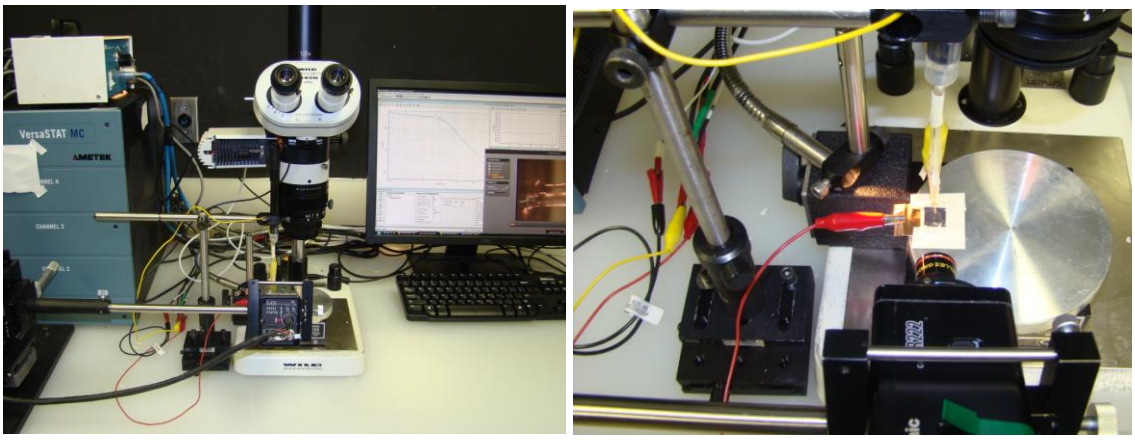

Figure 5.8 The actual experimental setup showing the device connected to the electrodes which in turn are connected to the potentiostat. Microscopy equipment are used for live visualization and clearance adjustment purposes.

Microscope images of the platinum working electrode and the reference electrode before and after engaging into the electrolyte are shown in **Figure 5.9**. Clearance between the two electrodes, as well as the distance between the electrodes and the porous silicon surface, are adjusted by a side camera equipped with a 6.7x magnification lens, and the high precision stages as shown above in **Figure 5.8**. The distance between the working and the reference electrodes was less than 1 mm. Electrolyte vaporization should also be continuously monitored to avoid altering the experiment; it further can result in damaging the porous silicon surface.

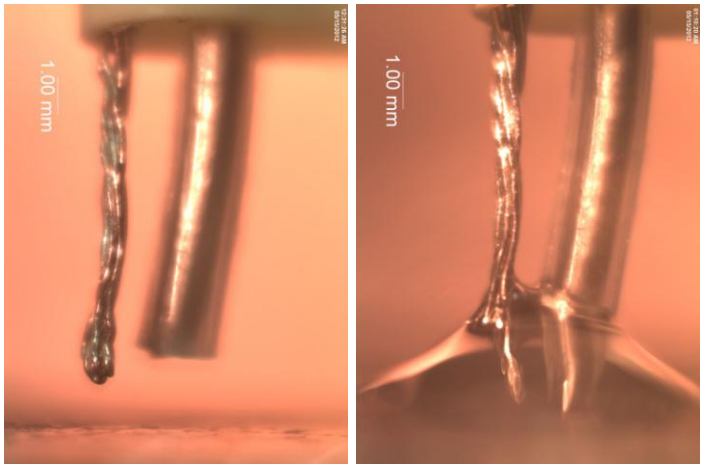

Figure 5.9 The working and reference electrodes before and after engaging into the electrolyte solution.

5.3. Results and Discussion

Lipid bilayer membranes that are deposited by the Langmuir-Blodgett and Langmuir–Schaeffer techniques are known to exhibit high rigidity, as was discussed previously, when compared to lipid membranes deposited by self-assembly. Another major drawback of self-assembly techniques is that the capacitance of the self-assembled lipid membrane is known to vary with time before it reaches a stable value due to the thinning of the lipid bilayer membrane [7] [102]. The lipid bilayer here is supported on the porous silicon layer underneath. The formation of the lipid bilayer may be easily verified by the contact angle method, as shown in **Figure 5.10** below, where a contact angle of approximately 95^{o} of a DI water drop on the porous silicon surface after LBM deposition indicates a successful deposition of the lipid bilayer membrane, when compared to the contact angle of water on the porous silicon surface. LBMs may also be visually monitored under light illumination [94]. A micrograph of a LBM that formed over a 850 µm x 850 µm hole is shown in **Figure 5.10** (right).

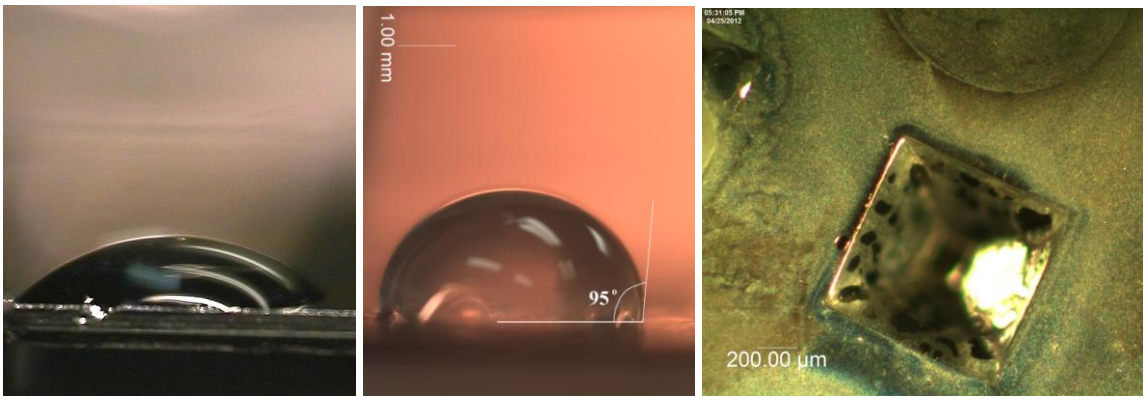

Figure 5.10 A contact angle of about 45^{o} is observed on the back surface of the porous silicon membrane (left). After deposition of the lipid bilayer membrane, an angle of about 95^{o} is observed (middle). A micrograph of a light-illuminated lipid bilayer membrane that formed across a 850 µm x 850 µm hole (right).

A lipid bilayer membrane is electrically modeled as an impedance composed of a resistance in parallel with a capacitor [91]. Addition of the ENaC channels is modeled by adding another impedance in parallel with the LBM impedance. In series with them is the impedance of the porous silicon membrane and the electrolyte resistivity. The simplest equivalent circuit of an electrochemical system takes into account the impedance of the electrolyte solution. This impedance is modeled as a pure resistance $R_{electrolyte}$ connected in series with the equivalent circuit of the full device, since the entire current must pass through the electrolyte [103]. The impedance of the system includes the series combination of the impedance of the system and the electrolyte resistance.

In the case when the electrochemical impedance spectra are taken for the porous silicon membrane alone, the equivalent circuit includes the impedance of the porous silicon membrane in series with the electrolyte resistance as shown in **Figure 5.11** below.

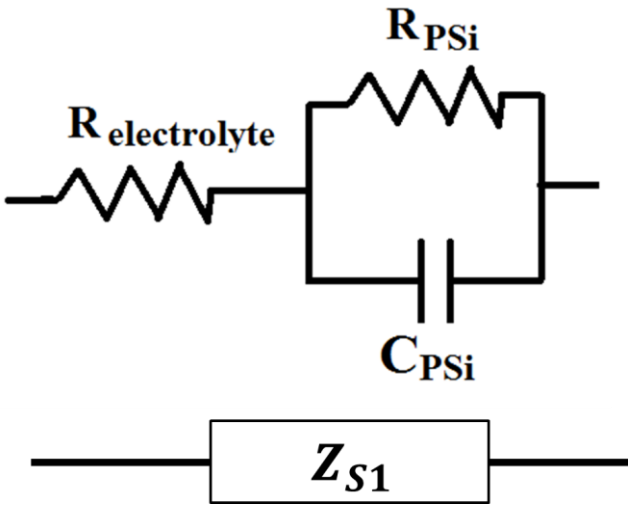

Figure 5.11 The equivalent impedance of the system composed of the porous silicon membrane in the electrolyte solution.

The impedance resulting from this case will be referred to as Z_{S1}, and it can be shown to be equal to:

$$Z_{S1} = R_{electrolyte} + \frac{R_{PSi}}{1+R_{PSi}^2 C_{PSi}^2 \omega^2} - j\frac{R_{PSi}^2 C_{PSi}\omega}{1+R_{PSi}^2 C_{PSi}^2 \omega^2} \quad . \qquad \textbf{Equation 5.1}$$

Which has the real and imaginary components as follows:

$$Z_{S1_{Re}} = R_{electrolyte} + \frac{R_{PSi}}{1+R_{PSi}^2 C_{PSi}^2 \omega^2}, \qquad \textbf{Equation 5.2}$$

$$Z_{S1_{Im}} = Z_{PSi_{Im}} = \frac{R_{PSi}^2 C_{PSi}\omega}{1 + R_{PSi}^2 C_{PSi}^2 \omega^2}. \qquad \textbf{Equation 5.3}$$

It can be noted from the real part of the impedance that:

$$\omega^2 = \frac{R_{PSi}}{R_{PSi}^2 C_{PSi}^2 \ Z_{S1_{Re}} - R_{electrolyte}} - \frac{1}{R_{PSi}^2 C_{PSi}^2} \qquad \textbf{Equation 5.4}$$

After that, dividing the imaginary by the real part, and substituting for ω^2 by the expression above then rearranging, we get:

$$Z_{S1_{Re}} - R_{electrolyte} - \frac{R_{PSi}}{2}^2 + Z_{S1_{Im}} = \frac{R_{PSi}}{2}^2 \qquad \textbf{Equation 5.5}$$

This is the equation of a circle of radius $R_{PSi}/2$ with its center at $(Z_{S1_{Re}}, Z_{S1_{Im}}) = (R_{electrolyte} + \frac{R_{PSi}}{2}, 0)$ [104]. When the imaginary impedance is plotted against the real impedance of the system, the resulting plot is referred to as the Nyquist plot. The resulting Nyquist plot of this system is shown in **Figure 5.12**.

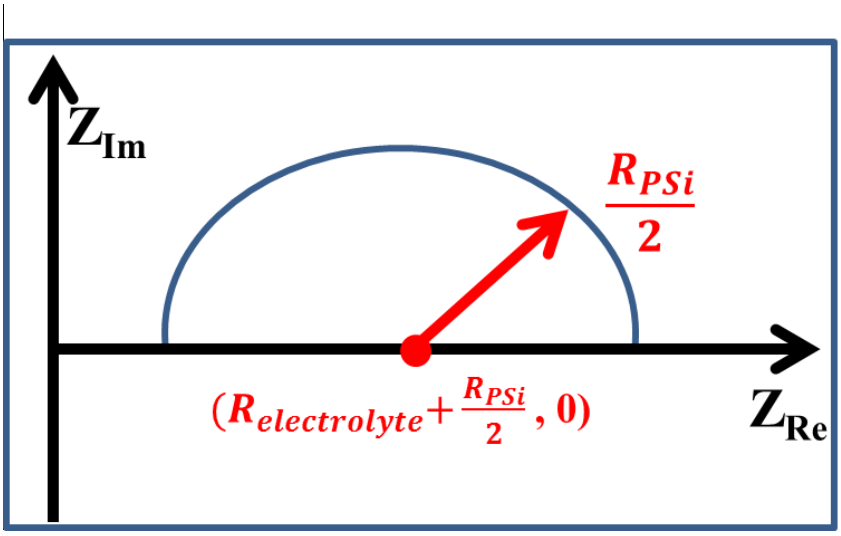

Figure 5.12 The Nyquist plot that results for a system described by Equation 5.5.

The second system Z_{s2} is composed of the electrolyte, porous silicon membrane, and a lipid bilayer membrane deposited on the porous silicon. This system is referred to as the Electrolyte-PSi-LBM system, the equivalent impedance of this system is composed of the equivalent impedance of the lipid bilayer membrane in series with the impedance of the porous silicon membrane and the electrolyte resistance [90] [94]; thus, the lipid bilayer membrane is in series with the impedance Z_{s1}, as is demonstrated in **Figure 5.13**.

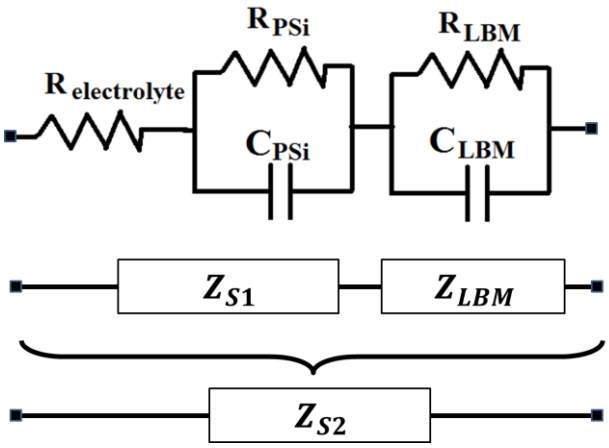

Figure 5.13 The equivalent impedance of the system composed of the porous silicon membrane with a deposited lipid bilayer membrane on it in the electrolyte solution.

The real and imaginary components of the impedance Z_{s2} are given by the following:

$$Z_{S2_{Re}} = R_{electrolyte} + \frac{R_{PSi}}{1 + R_{PSi}^2 C_{PSi}^2 \omega^2} + \frac{R_{LBM}}{1 + R_{LBM}^2 C_{LBM}^2 \omega^2} \qquad \textbf{Equation 5.6}$$

$$Z_{S2_{Im}} = Z_{PSi_{Im}} + Z_{LBM_{Im}} \qquad \textbf{Equation 5.7}$$

$$Z_{S2_{Im}} = \frac{R_{PSi}^2 C_{PSi}\omega}{1 + R_{PSi}^2 C_{PSi}^2 \omega^2} + \frac{R_{LBM}^2 C_{LBM}\omega}{1 + R_{LBM}^2 C_{LBM}^2 \omega^2} \qquad \textbf{Equation 5.8}$$

Thus:

$$Z_{LBM_{Im}} = Z_{S2_{Im}} - Z_{PSi_{Im}} = \frac{R_{LBM}^2 C_{LBM}\omega}{1 + R_{LBM}^2 C_{LBM}^2 \omega^2} \qquad \textbf{Equation 5.9}$$

$$Z_{LBM_{Re}} = Z_{S2_{Re}} - Z_{PSi_{Re}} - R_{electrolyte} = \frac{R_{LBM}}{1+R_{LBM}^2 C_{LBM}^2 \omega^2} \ . \qquad \textbf{Equation 5.10}$$

Finally, the third system Z_{S3} is formed when the ENaC vesicles are spread on the lipid bilayer membrane to incorporate the transmembrane ion channels. **Figure 5.14** shows the equivalent impedance of this porous silicon membrane with a deposited lipid bilayer membrane on it and the transmembrane epithelial sodium ion channel proteins incorporated into the lipid membrane. In this circuit model, the equivalent impedance of the transmembrane ion channels is in parallel with the equivalent impedance of the lipid bilayer membrane.

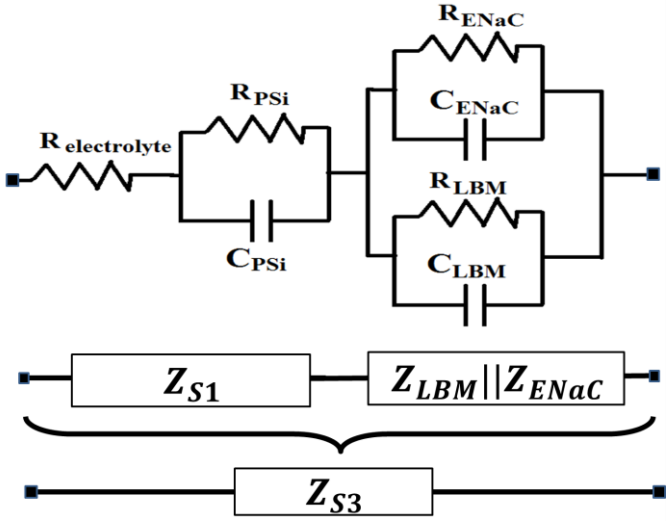

Figure 5.14 The equivalent impedance of the Electrolyte-PSi-LBM-ENaC system.

The real and imaginary impedances are given by:

$$Z_{S3_{Re}} = R_{electrolyte} + \frac{R_{PSi}}{1 + R_{PSi}^2 C_{PSi}^2 \omega^2} + \frac{R_t}{1 + R_t^2 C_t^2 \omega^2} \quad \textbf{Equation 5.11}$$

$$Z_{S3_{Im}} = \frac{R_{PSi}^2 C_{PSi} \omega}{1 + R_{PSi}^2 C_{PSi}^2 \omega^2} + \frac{R_t^2 C_t \omega}{1 + R_t^2 C_t^2 \omega^2} \ , \quad \textbf{Equation 5.12}$$

where

$$R_t = \frac{R_{LBM} R_{ENaC}}{R_{LBM} + R_{ENaC}} \quad \textbf{Equation 5.13}$$

$$C_t = C_{LBM} + C_{ENaC} \ . \quad \textbf{Equation 5.14}$$

To determine the impedance of the lipid bilayer and the transmembrane proteins, the impedance spectra over the range 0.1 Hz to 100 KHz were measured for the porous silicon membrane alone as a control experiment. Then measurements were taken with the addition of the lipid bilayer membrane, and finally, with the spreading of the ENaC vesivcles in a two-electrode system and in a three-electrode system.

5.3.1. The Two-Electrode System Measurements

The impedance spectra achieved when a two-electrode system was used, are shown in **Figure 5.15**. From the figure, it can be seen that the impedance of the system increases significantly when a lipid bilayer membrane is deposited on the porous silicon membrane. The impedance of the system composed of porous silicon-lipid bilayer membrane- ENaC proteins has a level in between the previous two systems. This is attributed to the formation of transmembrane ion channels once the ENaC

proteoliposomes are spread on the lipid bilayer. It also validates the circuit model of the system shown in **Figure 5.14**, in which the ENaC impedance is in parallel with the lipid bilayer membrane impedance.

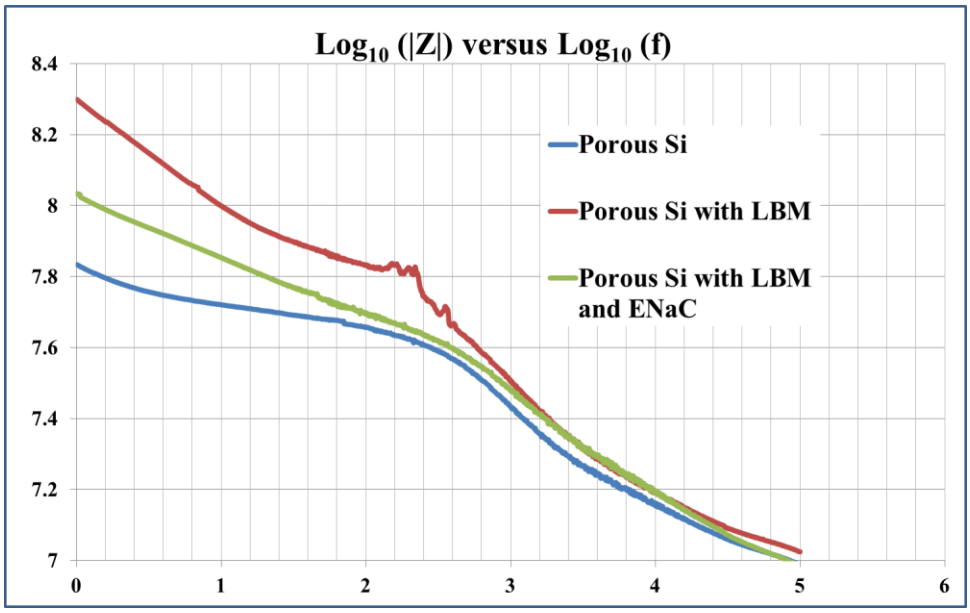

Figure 5.15 Variation of the electrical impedance with frequency in a logarithmic scale for the three systems using two-electrode measurements.

The Nyquist plots of the three systems show the variation of the imaginary impedance of each of the three systems with the real impedance, as shown in **Figure 5.16**. A linear behavior can be seen in the three systems at very low frequencies. This is attributed to the presence of a capacitance in series with the resistance of each of the three regimes such as the pseudocapacity [103]. It can be shown that at low frequencies, a linear relationship exists between the imaginary and real impedances due to the presence of the impedance termed the Warburg impedance. This impedance is a function of mass-transfer rather than charge transfer [103].

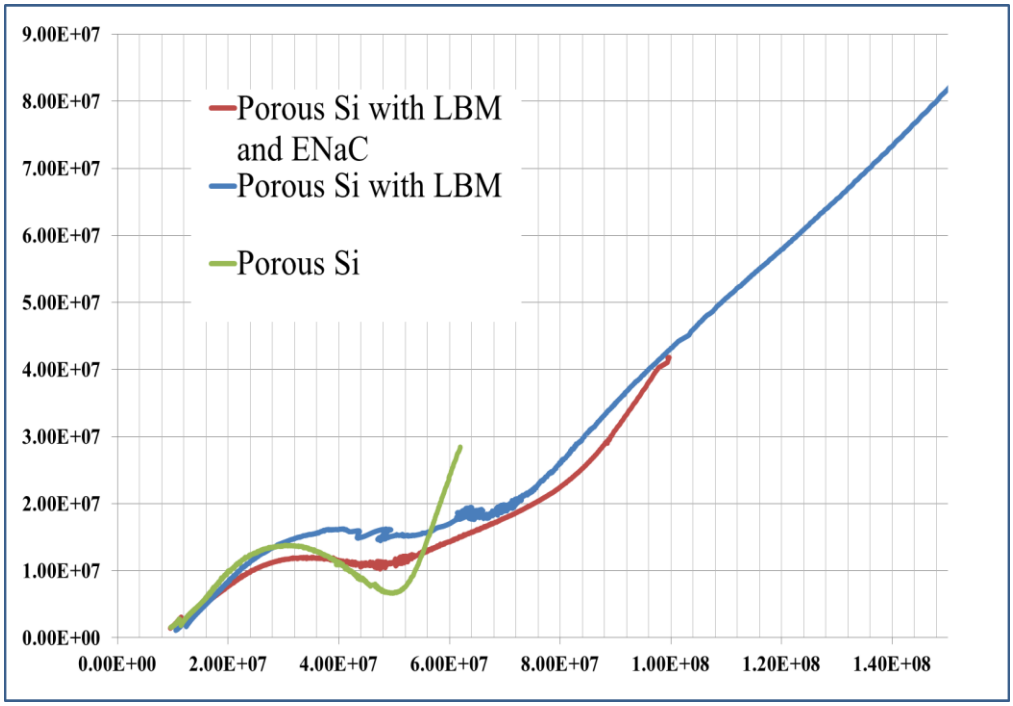

Figure 5.16 Nyquist plot for the three systems using two-electrode measurements.

5.3.2. The Three-Electrode System Measurements

A three-electrode system offers a higher level of accuracy than the two-electrode system. The impedance spectra of each of the three regimes are shown in **Figure 5.17** in a logarithmic scale. From the figure, it can be seen that the impedance decreases with increasing frequency for all regimes, no significant difference is observed at high frequencies. This difference is attributed to the decrease of the reactance known to be inversely proportional to the frequency. The system composed of a porous silicon with a lipid bilayer membrane has a higher impedance than the system with incorporated protein channels. The high impedance in the porous silicon-LBM system is expected and is attributed to the low permeability of the LBM to ions. This low permeability results in an increase in the impedance. Following the incorporation of the ion channel proteins, the

impedance decreases due to the presence of the sodium channels in the lipid bilayer. This difference in the impedance is more prominent at low frequencies, which is due to the decrease in the difference between the impedances with increasing frequencies as pointed earlier.

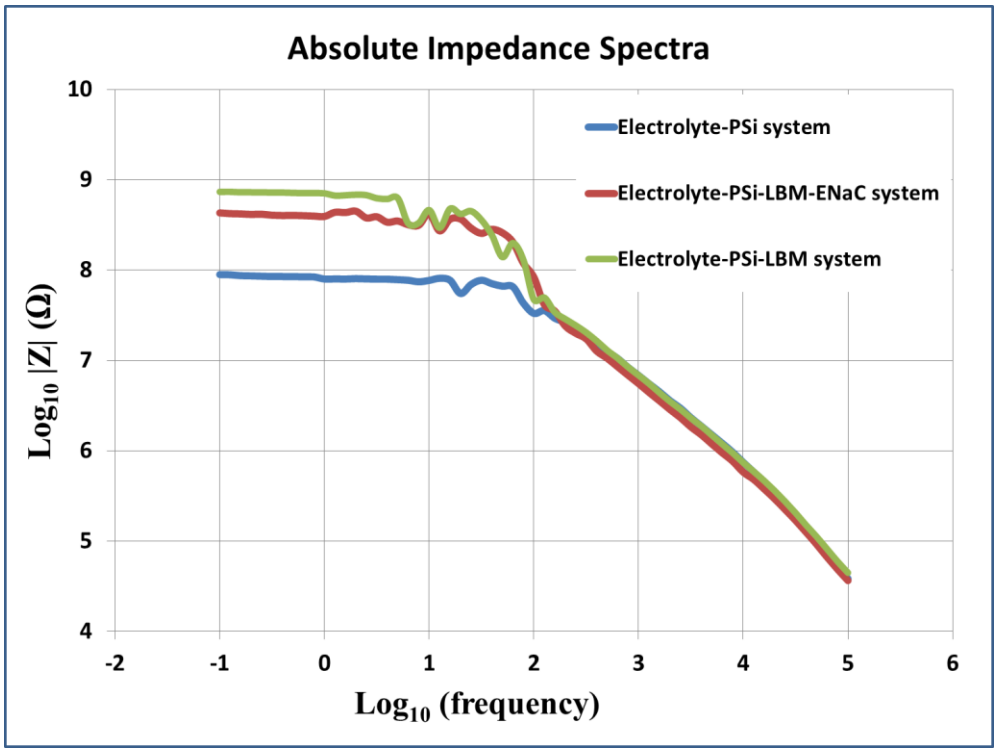

Figure 5.17 Electrochemical Impedance Spectra of the system before and after deposition of a lipid bilayer membrane and transmembrane protein fusion.

The Nyquist plot of the electrolyte-porous silicon system is shown in **Figure 5.18**. The plot shows a second-order polynomial regression of the imaginary versus real impedance of the system over the range of frequencies 0.1 Hz – 100 KHz. From the

figure, a resistance of the 0.19 mm × 0.19 mm porous silicon membrane in the 0.1M NaCl electrolyte can be seen to be equal to about 0.8×10^{8} - 1×10^{8} Ω, which is equal to the diameter of the semicircle, as was shown previousely.

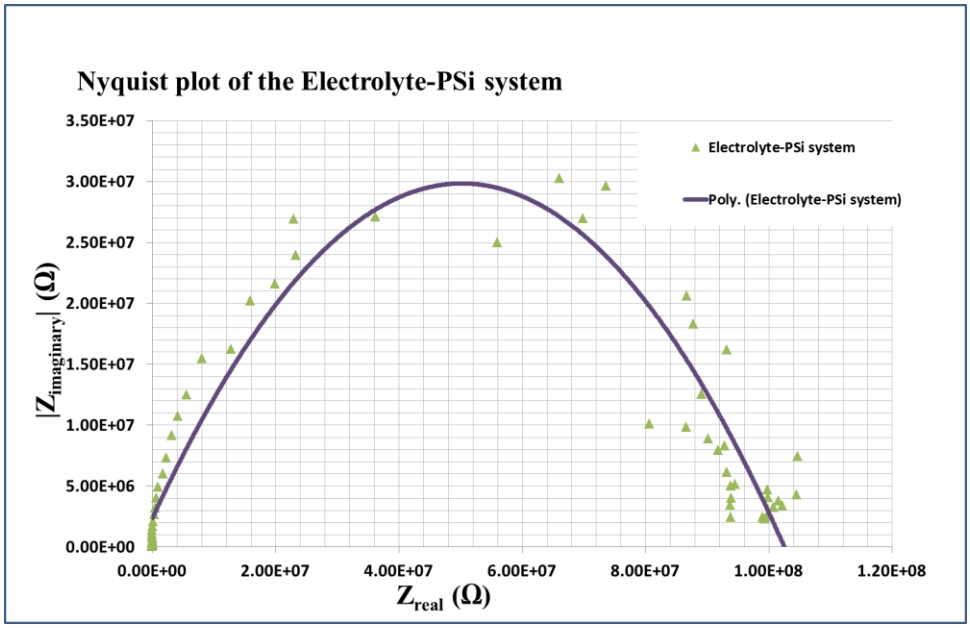

Figure 5.18 Nyquist plot of the system composed of the electrolyte and the porous silicon membrane in the 0.1 M NaCl electrolyte.

When normalized with respect to the area, the resistance of the 0.00036 cm^2 porous silicon membrane is about 32.5 KΩ.cm^2, and the capacitance measures about 1.39 μF/cm^2. In their work, Gold et. al. [105] show that a porous silicon membrane of a 40-70 μm thickness fabricated in a 100 mm silicon wafer had a resistance of about 36.4 Ω and a capacitance of about 1.7×10^{-4} F when a 8M H_2SO_4 electrolyte is used. Normalizing these values obtained by Gold et. al. result in a resistance and a capacitance of about 2.86 KΩ.cm^2 and 2.16 μF/cm^2 consecutively. The difference in the resistance of approximately one order of magnitude is attributed to the different electrolytes used (0.1M NaCl in this work and 8M H_2SO_4 in the work of Gold et. al. [105]), resulting in a

different electrolyte-semiconductor interface. The Helmholtz capacitance of silicon was shown to be about 3μF/cm^2 in an aqueous solution of 0.5M KCL and 0.1M $K_4Fe(CN)_6$ [106]. Furthermore, the absolute impedance of the porous silicon membrane is comparative to the impedance of the SiO_2-coated dual electrode sensor shown Lundgren et. al. [90] to be equal to 10^7 Ω at a frequency of about 100 Hz when a 0.01 M Tris buffer solution with 0.1 M NaCl is used.

EIS measurements obtained after depositing the lipid bilayer on the porous silicon membrane show a significant increase in real and imaginary impedances. The Nyquist plot of the electrolyte-porous silicon-lipid bilayer membrane system is shown in **Figure 5.19** below. Data fitting for all the figures presented here is performed using a second-order polynomial in Microsoft Excel. It can be observed in the figure that the impedance increased by an order of magnitude. The data spreading in the figure is due to the impedance oscillations of silicon in the range of about 10-100 Hz.

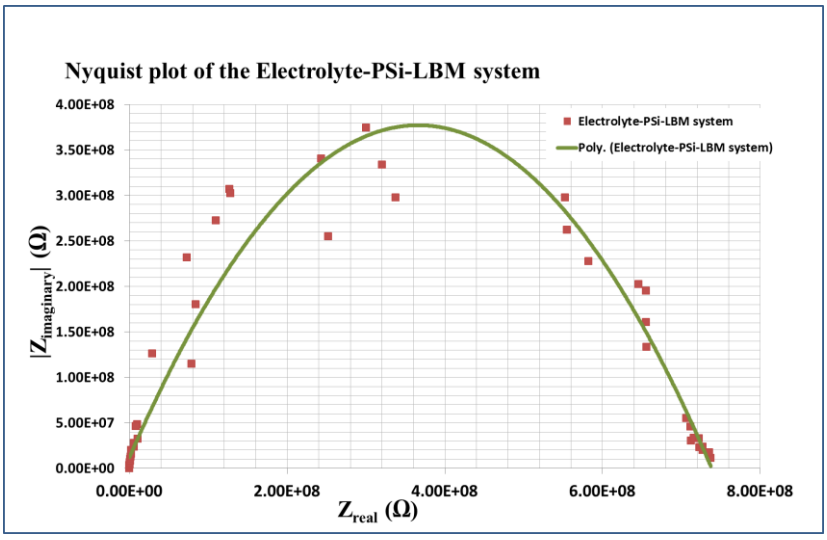

Figure 5.19 Nyquist plot of the system composed of the electrolyte, the porous silicon membrane, and the deposited lipid bilayer membrane in a 0.1 M NaCl electrolyte.

The epithelial sodium channel proteins were then fused into the lipid bilayer membrane by spreading vesicles containg the the three proteins at close proximity to the lipid membrane. The sample was continuousely maintained under wet conditions to avoid inducing damage in the porous silicon membrane under the capillary force of the evaporating water and to prevent denaturing of the proteins. The Nyquist plot of the EIS measurements performed on the system that is composed of the porous silicon membrane with the lipid bilayer membrane and the fused proteins, is shown in **Figure 5.20**. Reduction in the real and imaginary impedances by 50% is observed when compared to the Nyquist plot presented in **Figure 5.19**, indicating s shunted equivalent ciruit. Data spreading in the figure is due to impedance oscillations in the silicon as was shown previousely.

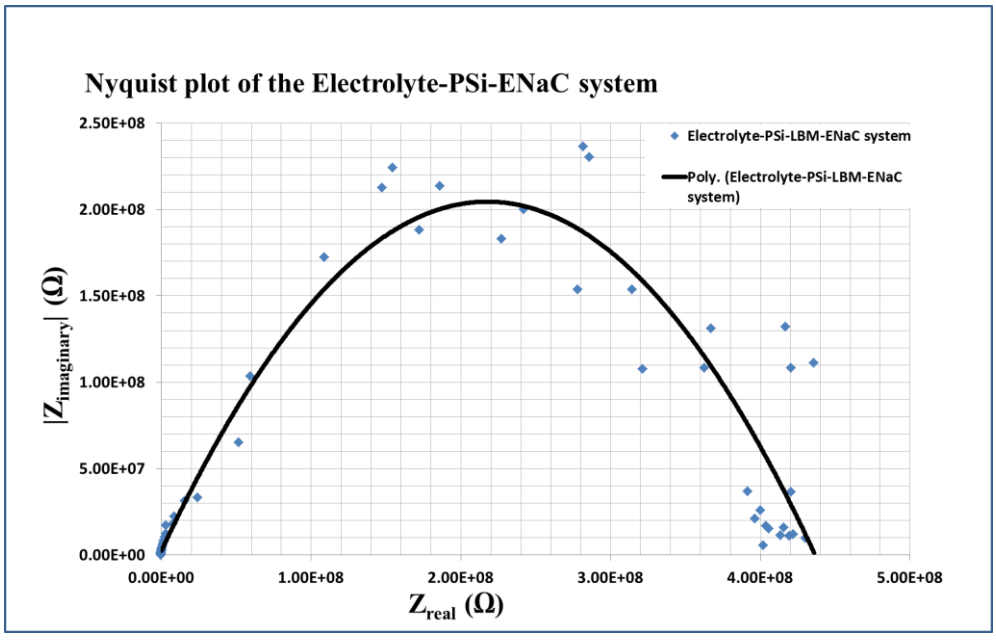

Figure 5.20 Nyquist plot of the system composed of the electrolyte, the porous silicon membrane, with the lipid bilayer membrane and the fused ENaC proteins in a 0.1 M NaCl electrolyte.

When plotting all the three systems together, nested plots are achieved as shown in **Figure 5.21**. Note in the figure that the system composed of porous silicon and the lipid bilayer membrane has the largest impedance. The impedance then decreases after the incroporation of the ENaC channels, while the porous silicon membrane has the lowest impedance. These results clearly show that a conduction occurs across the lipid bilayer membrane through the ion channels. The data scattering that occurs at about 10-100 Hz (as can be seen in **Figure 5.17**) is inherent in the system and is associated with silicon. Although noise is present in each of the three systems, it is in the same range of values obtained for the system it originated from as can be seen in the figure.

The electrolyte resistance constantly measured a value of 5~10 KΩ. As pointed previousely, the resistance of the porous silicon membrane in the electrolyte measured about 3.25×10^4 $\Omega.cm^2$ and showed, on average, a capacitance of approximately 1.39 $\mu F/cm^2$. The lipid bilayer membrane showed a capacitance of approximately 0.194 $\mu F/cm^2$, and a resistance of about 2.35×10^5 $\Omega.cm^2$. The ENaC channels resulted in a capacitance of about 0.222 $\mu F/cm^2$ and a resistance of about 1.81×10^5 $\Omega.cm^2$.

To verify these results, the solutions to **Equation 5.1** to **Equation 5.14** were plotted for the frequency range 0.1 Hz to 100 KHz for each of the experimental restistance and capacitance values measured and presented above. These simulations (plotted in **Figure 5.22**.) validate the equivalent circuit model by producing comparative results. The nyquist plots of the simulated equations above verify the equivalent circuit model of the system, and the values that were obtained for the individual components. The impedance spectra may be normalized by multiplying the impedance of each of the three systems by the area of the porous silicon membrane and replotting, as shown in **Figure 5.23**.

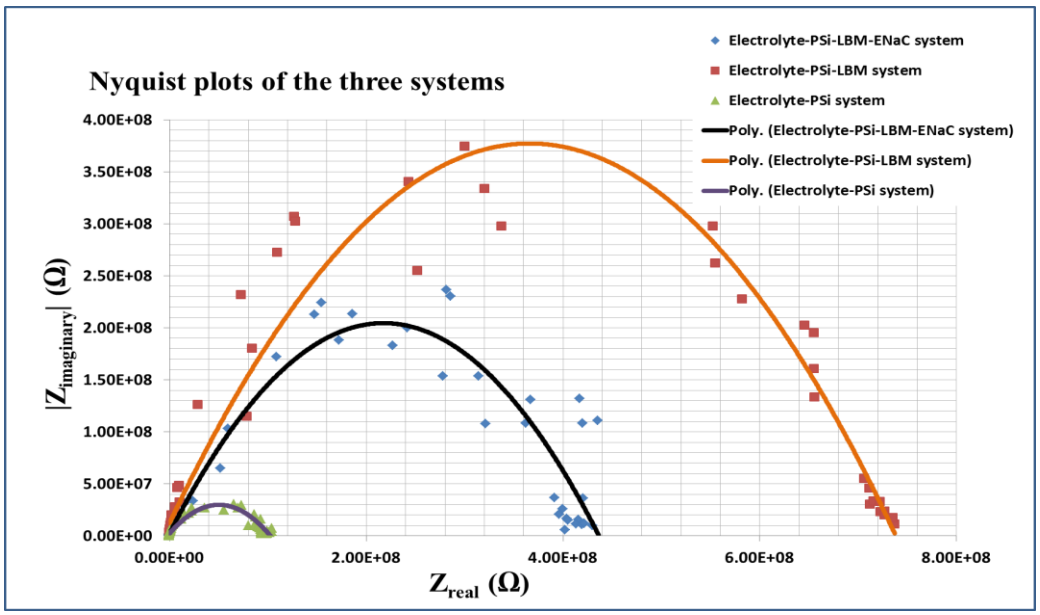

Figure 5.21 Variation of the imaginary impedance with the real part of the impedance over the frequency range 0.1 Hz – 100KHz.

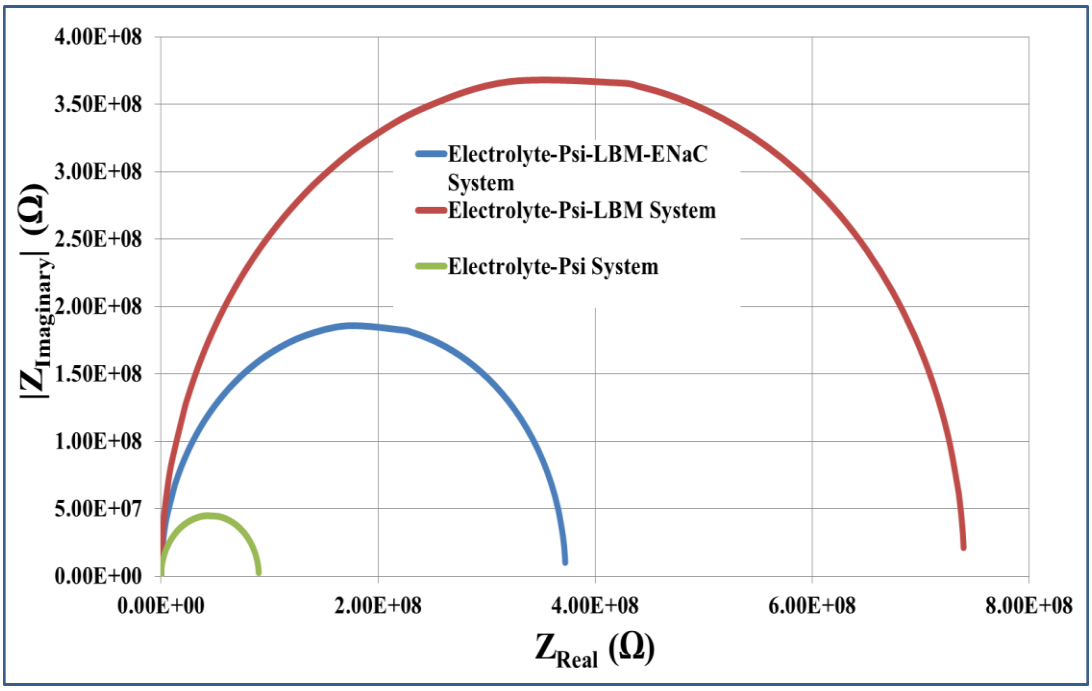

Figure 5.22 The nyquist plots produced by the numerical model.

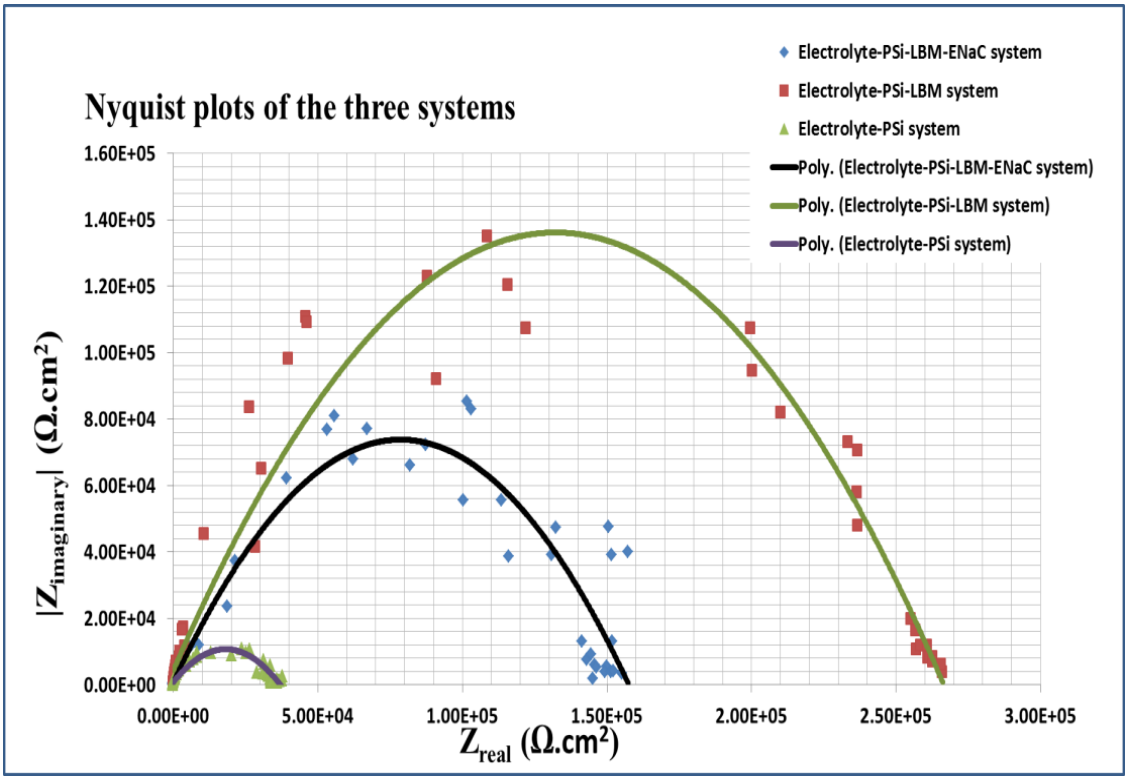

Figure 5.23 The nyquist plots of the three systems in $\Omega.cm^2$.

The impedance values obtained in these nyquist plots are in close agreement with those obtained for the closely related phospholipid phosphatidylcholine by Naumowicz et. al. [107] and [94], in which the real impedance of a phosphatidylcholine membrane in a 1mM KCl electrollyte was found to be about 5×10^5 $\Omega.cm^2$ with a capacitance of about 0.62 $\mu F/cm^2$. The spectra also closely agree with the impedance spectra shown Naumowicz et. al. [108] for phosphatidylcholine-decanoic acid, and phosphatidylcholine-decylamine, which were found to have resistances in the range 1.5-2.5×10^5 $\Omega.cm^2$, with a pure phosphatidylcholine resistance of 2.30×10^5 $\Omega.cm^2$, the capacitances of decanoic acid and decylamine were shown to be 2.552 and 0.047 $\mu F/cm^2$. The capacitance of the lipid bilayer membrane obtained in this work is also in close

agreement with that obtained for black lipid membranes of the same phosopholipid structure and composition found by Berdiev and Benos to be 0.67-0.95 μF/cm^2 [2]. Also it is within a close range to the capacitance obtained by Lundgren et. al. [90] for the lipid 1-palmitoyl-2-oleoyl-sn-glycero-3-ethylphosphocholine shown to be 1.16 μF/cm^2.

5.3.3. Conclusion

Electrochemical impedance spectroscopy was used to characterize the porous silicon platform with a lipid bilayer membrane deposited on it, and with transmembrane proteins incorporated into the lipid membrane. The epithelial sodium channel (ENaC) proteins were used for this purpose. Results of the three-electrode measurements show that the electrochemical impedance of the porous silicon layer increases significantly after the deposition of the lipid bilayer membrane, and then reduce following the incorporation of the transmembrane channel proteins. The resistance and capacitance of the porous silicon membrane in the electrolyte measured about 3.25×10^4 Ω.cm^2 and 1.39 μF/cm^2 consecutively. The lipid bilayer membrane showed a resistance of about 2.35×10^5 Ω.cm^2 and a capacitance of about 0.194 μF/cm^2. The ENaC channels resulted in a capacitance of about 0.222 μF/cm^2 and a resistance of about 1.81×10^5 Ω.cm^2. The capacitance and resistance values of the porous silicon membrane, the lipid bilayer membrane, and the tranamembrane proteins obtained in this work are in close agreement with those shown in literature.

CHAPTER 6

CONCLUSIONS AND FUTURE RESEARCH

6.1. Conclusions and Discussion

In this work a device is fabricated to allow for investigation and characterization of transmembrane ion channels. This device is composed of a two-chamber structure; the two chambers are separated from each other by a porous silicon membrane. A lipid bilayer membrane then is deposited on one side of the membrane and followed by incorporation of transmembrane ion channel proteins into the lipid membrane.

The two-chamber device is fabricated from a silicon-on-insulator (SOI) wafer in a top-down approach. It is composed of an electrochemically-fabricated porous silicon membrane that is less than 3 μm thick and porous all the way through, supported from the sides and separating the two chambers. The final dimensions of the porous silicon membrane are about 190 × 190 × 3 μm. Such membrane allows for investigating transmembrane proteins fused into lipid bilayer membranes in a two-chamber structure (one chamber on each side of the LBM) with full visual and physical access to both chambers. The electrochemically-fabricated porous silicon was chosen over other forms of porous materials because the photoluminescence and biodegradability of porous silicon, which prove more beneficial for in-vivo monitoring of membrane proteins.

Membrane proteins are known to be the targets of most drug delivery systems. The porous silicon membrane was characterized using scanning electron microscopy (SEM).

The Lipid bilayer membrane is formed from two synthetic phospholipids: 1,2-diphytanoyl-*sn*-glycero-3-phosphoserine ($C_{46}H_{89}NO_{10}PNa$) and 1,2-diphytanoyl-*sn*-glycero-3-phosphoethanolamine ($C_{45}H_{90}NO_8P$). The Langmuir- Blodgett and Langmuir-Schaefer techniques are used to form the lipid bilayer membrane on the porous silicon surface. The lipid membrane formation is accomplished at a surface pressure of 46 mN/m, at which each phospholipid monolayer demonstrated a surface tension of 26 mN/m. Tight packing of the phospholipid molecules is achieved at an average area per molecule of 0.68 - 0.73 nm^2. Measurements of the contact angle of DI water on the surface of a deposited lipid bilayer membrane constantly show angles of 90^o or higher.

The Epithelial Sodium Channel (ENaC) transmembrane proteins then are fused into the lipid bilayer membrane by direct spreading. Atomic force microscope images taken in the tapping mode of the transmembrane proteins after spreading the protein vesicles into the lipid bilayer showed that the transmembrane proteins agglomerated into clusters with diameters of about 500 nm. This indicated the environmental sensitivity for forming functional ENaC protein complexes on porous silicon.

Characterization of the functionality of the device that is composed of the transmembrane proteins fused into a lipid layer that is deposited on the porous silicon structure, was performed using electrochemical impedance spectroscopy (EIS). Measurements were performed in a two-electrode and a three-electrode experimental setup. Both measurement techniques showed a significant increase in impedance following the deposition of a lipid bilayer membrane on the porous silicon layer. This

impedance decreases slightly following the incorporation of epithelial sodium channel proteins into the lipid membrane.

The electrolyte-PSi system had a capacitance of about 1.39 $\mu F/cm^2$ and a resistance of about 3.25×10^4 $\Omega.cm^2$. The lipid bilayer membrane had a capacitance of about 0.194 $\mu F/cm^2$ and a resistance of about 2.35×10^5 $\Omega.cm^2$. The epithelial sodium channel (ENaC) proteins resulted in a capacitance of about 0.222 $\mu F/cm^2$ and a resistance of about 1.81×10^5 $\Omega.cm^2$.

6.2. Future Research

In this work, lipid bilayer membranes were formed on one side of the porous silicon membrane to incorporate the transmembrane proteins. Future work involves incorporating transmembrane proteins on both sides of the 3 μm thick porous silicon structure to allow for protein-protein interactions on both sides of the porous silicon membrane.

The final device upon completion resembles the cellular membrane of the E. Coli bacteria, which includes a highly-porous cell wall in between the lipid bilayers. This wall provides the mechanical stability that the cholesterol-free cell membrane lacks [85]. The structure and the bacterial cell wall are illustrated in **Figure 6.1**. This structure may be utilized to examine structures and functionalities of numerous transmembrane proteins, such as proton permeability of bacteriorhodopsin [80].

In the porous silicon formation process, the percentage of collapsed parts due to over-etching may be reduced by providing a uniform current density to each of the silicon layers in the patterned array, and completely eliminating hydrogen bubble formation.

This reduction in pore collapse may be achieved by performing the porous silicon formation experiments using the design shown in **Figure 6.2** below, which is based on the setup presented by Lehmann [109].

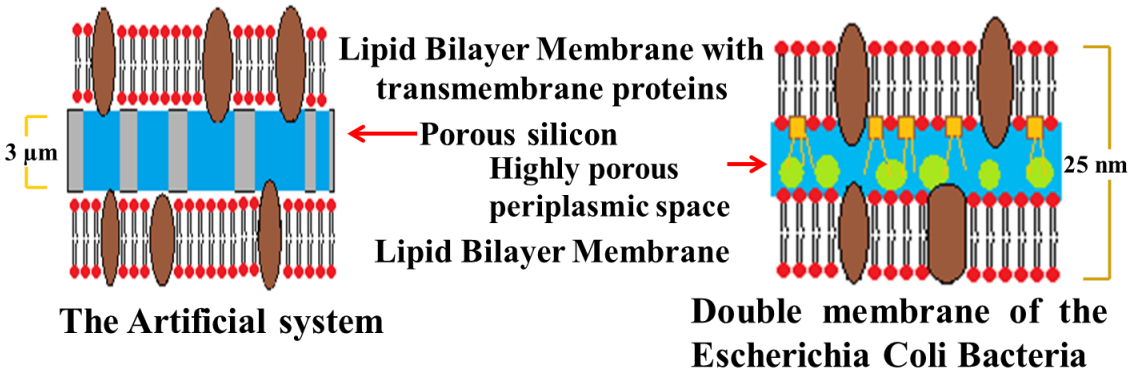

Figure 6.1 The similarity between the structure with two lipid bilayer membranes and the cellular wall of the E. Coli bacteria.

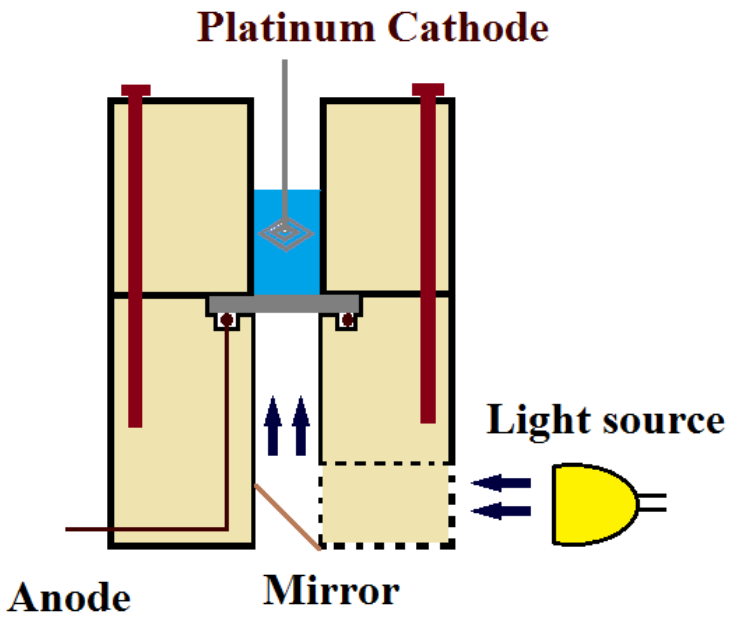

Figure 6.2 The design of the suggested experimental setup to improve pore formation and reduce probability of collapse of porous silicon membranes.

The reduction of collapse of the porous silicon membranes is achieved by taking into account the following treatments:

1. Alleviation of surface discrepancy: Hydrogen bubbles that form during the electrochemical etching of silicon are known to cause surface discrepancy. Although this problem may be solved by the addition of a wetting agent, such as ethanol or isopropanol, positioning the silicon substrate in a horizontal direction also contributes in eliminating this problem. While in the vertical direction, the hydrogen bubbles slide along the silicon surface, causing them to stay in contact with the surface for longer durations, horizontal positioning of the wafer permits the hydrogen bubbles to escape from the surface of the silicon as soon as they form.
2. Improvement of current distribution in the silicon substrate: By allowing the electrode to encircle the silicon substrate, the uniformity of distance of the porous silicon regions from the electrode is improved. This uniformity in distance from the electrode, yields more homogenous porous regions.
3. Improved insulation of the electrodes from the HF acid. The location of the electrode underneath the silicon substrates provides more insulation to it from the HF acid. Furthermore, the silicon substrate can be accessed easily from underneath for light illumination without subjecting the light source to the hazard of HF vapor.

REFERENCES

[1] S. Smeazzetto, M. D. Zotti and M. R. Moncelli, "A new approach to detect and study ion channel formation in microBLMs," *Electrochemistry Communications,* vol. 13, pp. 834-836, 2011.

[2] B. Berdiev and D. Benos, "Epithelial Sodium Channel in Planar Lipid BiLayers," *Methods in Molecular Biology,* vol. 337, pp. 89-99, 2008.

[3] I. Ismailov, M. Awayda, B. Berdiev, J. Bubien, J. Lucas, C. Fuller and D. Benos, "Triple-barrel Organization of ENaC, a Cloned Epithelial Na+ Channel," *The Journal of Biological Chemistry,* vol. 271, pp. 807-816, 1996.

[4] R. P. Goncalves, G. Agnus, P. Sens, C. Houssin, B. Bartenlian and S. Scheuring, "Two-chamber AFM: probing membrane proteins separating two aqueous compartments," *Nature Methods,* vol. 3, pp. 1007-1012, 2006.

[5] B. Alberts, A. Johnson, J. Lewis, M. Raff, K. Roberts and P. Walter, Molecular Biology of the Cell, 5th ed., New York: Garland Science, 2008.

[6] A. Staruschenko, R. Booth, O. Pochynyuck, J. Stockand and Q. Tong, "Functional Reconstitution of the Human Epithelial Na+ Channel in a Mammalian Expression System," in *Ion Channels: Methods and Protocols*, vol. 337, Totowa, NJ, Humana Press Inc., 2006, pp. 3-13.

[7] W. Römer and C. Steinem, "Impedance Analysis and Single-Channel Recordings on Nano-Black LipidMembranes Based on Porous Alumina," *Biophysical Journal,* vol. 86, pp. 955-965, 2004.

[8] O. Mori and T. Imae, "AFM investigation of the adsorption process of bovine serum albumin on mica," *Colloids and Surfaces B: Biointerfaces*, vol. 9, pp. 31-36, 1997.

[9] O. Worsfold, N. H. Voelcker and T. Nishiya, "Biosensing Using Lipid Bilayers Suspended on Porous Silicon," *Langmuir,* vol. 22, pp. 7078-7083, 2006.

[10] R. Martin-Palma, M. Manso-Silvan and V. Torres-Costa, "Biomedical applications of nanostructured porous silicon: a review," *Journal of Nanophotonics,* vol. 4, pp. 042502, 2010.

[11] J. Park, L. Gu, G. Maltzahn, E. Ruoslahti, S. Bhatia and M. Sailor, "Biodegradable luminescent porous silicon nanoparticles for in vivo applications," *Nature Materials,* pp. 331-336, 2009.

[12] C. Thibault, F. Carcenac, E. Dague, J. Chalmeau and C. Vieu, "Porous silicon membrane, with an integrated aqueous supply, for two chamber AFM," *Microelectronic Engineering,* vol. 86, pp. 1393–1395, 2009.

[13] J. Schmidt, "Stochastic Sensors," *Journal of Materials Chemistry,* vol. 15, pp. 831-840, 2005.

[14] S. Kellenberger and L. Schild, "Epithelial Sodium Channel/Degenerin Family of Ion Channels: A variety of Functions for a Shared Structure," *Physiological Reviews,* vol. 82, pp. 735-767, 2002.

[15] J. West and N. Halas, "Applications of Nanotechnology to Biotechnology: Commentary," *Current Opinion in Biotechnology,* vol. 11, pp. 215-217, Current Opinion in Biotechnology 2000.

[16] D. LaVan, T. McGuire and R. Langer, "Small-scale systems for in vivo drug delivery," *Nature Biotechnology,* vol. 21, pp. 1184-1191, 2003.

[17] A. Vaseashta and D. Dimova-Malinovska, "Nanostructured and nanoscale devices, sensors and detectors," *Science and Technology of Advanced Materials,* vol. 6, pp. 312-318, 2005.

[18] M. P. Stewart and J. M. Buriak, "Chemical and biological applications of porous silicon technology," *Advanced Materials,* vol. 12, pp. 859-869, 2000.

[19] V. Lin, K. Motesharei, K. P. Dancil, M. Sailor and M. R. Ghadiri, "A Porous Silicon-Based Optical Interferometric Biosensor," *Science,* vol. 278, pp. 840-843, 1997.

[20] K. Buchholz, A. Tinazli, A. Kleefen, D. Dorfner, D. Pedone, U. Rant, R. Tampe, G. Abstreiter and M. Tornow, "Silicon-on-insulator based nanopore cavity arrays for lipid membrane investigation," *Nanotechnology,* vol. 19, pp. 445305-445311, 2008.

[21] M. Simion, L. Ruta, Mihailiscu, I. Kleps, A. Bragaru, M. Miu, T. Ignat and I. Baciu, "Porous silicon used as support for protein microarray," *Superlatticesand Microstructures,* vol. 11, pp. 1-8, 2008.

[22] D. Firsov, I. Gautschi, A. Merillat, B. Rossier and L. Schild, "The heterotetrameric architecture of the epithelial sodium channel (ENaC)," *The EMBO Journal,* vol. 17, pp. 344-352, 1998.

[23] L. Canham, "Silicon quantum wire array fabrication by electrochemical and chemical dissolution of wafers," *Applied Physics Letters 57,* pp. 1046-48, 1990.

[24] E. Lorenzo, C. J. Oton, N. E. Capuj, M. Ghulinyan, D. Navarro-Urrios, Z. Gaburro and L. Paves, "Porous silicon-based rugate filters," *Applied Optics,* vol. 44, pp. 5415-5421, 2005.

[25] A. E. Pap, K. Kordas, J. Vahakangas, A. Uusimaki, S. Leppavuori, L. Pilon and S. Szatmari, "Optical properties of porous silicon. Part III: Comparison of experimental and theoretical results," *Optical Materials,* vol. 28, pp. 506-513, 2006.

[26] J. Perez, J. Villalobos, P. McNeill, J. Prasad, R. Cheek, J. Kelber, J. Estrera, P. Stevens and R. Glosser, "Direct evidence for the amorphous silicon phase in visible photoluminescent porous silicon," *Applied Physics Letters,* vol. 61, pp. 563-565, 1992.

[27] J. Martínez-Duart, V. Parkhutik, R. Guerrero-Lemus and J. Moreno, "Electroluminescent porous silicon," *Advanced Materials* , vol. 7, pp. 226-228, 1995.

[28] P. Ferrand, R. Romestain and J. C. Vial, "Photonic band-gap properties of a porous silicon periodic planar waveguide," *Physical Review B,* vol. 63, pp. 115106-115109, 2001.

[29] M. Ghulinyan, J. Oton, G. Bonetti, Z. Gaburro and L. Pave, "Free-standing porous silicon single and multiple optical cavities," *Journal of Applied Physics,* vol. 93, pp. 9724-9729, 2003.

[30] C. C. Striemer and P. M. Fauchet, "Dynamic etching of silicon for broadband antireflection applications," *Applied Physics Letters,* vol. 81, pp. 2980-2982, 2002.

[31] T. James, A. Keating, G. Parish, L. Faraone and C. Musca, "A Technique for Fabricating Uniform Double-Sided Porous Silicon Wafers," *Electrochemical and Solid-State Letters,* vol. 10, pp. D130-D133, 2007.

[32] R. L. Smith and S. D.Collins, "Porous silicon formation mechanisms," *Journal of Applied Physics* , vol. 71, pp. R1-R22, 1992.

[33] C. T. Black, K. W. Guarini, G. Breyta, M. C. Colburn, R. Ruiz, R. L. Sandstrom, E. M. Sikorski and Y. Zhang, "Highly porous silicon membrane fabrication using polymer self-assembly," *Journal of Vacuum Science Technology B,* vol. 24, pp. 3188-3191, 2006.

[34] V. Lehmann and S. Rönnebeck, "The Physics of Macropore Formation in Low-Doped p-Type Silicon," *Journal of The Electrochemical Society,* vol. 146, pp. 2968-2975, 1999.

[35] X. Zhang, "Morphology and formation mechanisms of porous silicon," *J. Electrochem. Soc. ,* vol. 151, pp. C69-C80, 2004.

[36] K.-L. Chu, Porous Silicon Membrane Based Formic Acid Fuel Cells For Micro Power Generation, Saarbrucken, Germany: VDM Verlag Dr. Muller Aktiengesellschaft & Co., 2008.

[37] R. Puers, "Mechanical Silicon Sensors at K.U. Leuven," in *Themadag Sensors Proceeding*, Rotterdam, Netherlands, 1991.

[38] H. Seidel, L. Csepregi, A. Heuberger and H. Baumgartel, "Anisotropic Etching of Crystalline Silicon in Alkaline Solutions- Orientation Dependence and Behavior of Passivation Layers," *J. Electrochem. Soc.,* vol. 137, pp. 3612-3626, 1990.

[39] S. Chuang, "Preferential propagation of pores during the formation of porous sincon: A transmission electron microscopy study," *Applied Physics Letters,* vol. 55, pp. 675-677, 1989.

[40] M. J. Madou, Fundamentals of Microfabrication: The Science of Miniaturization, Second ed., Boca Raton, Florida: CRC Press, 2002, pp. 187-189.

[41] M. Montal and P. Mueller, "Formation of Bimolecular Membranes from Lipid Monolayers and a Study of Their Electrical Properties," *Proc. Nat. Acad. Sci.,* vol. 69, pp. 3561-3566, 1972.

[42] P. Mueller, D. Rudin, H. Ti Tien and W. Wescott, "Reconstitution of Excitable Cell Membrane Structure in vitro and its Transformation into an Excitable System," *Nature,* vol. 194, pp. 979-980, 1962.

[43] L. Zhen-Kun, K. Yi-Lan, Q. Yu, H. Ming and C. Hao, "Experimental Study of Capillary Effect in Porous Silicon Using Micro-Raman Spectroscopy and X-Ray Diffraction," *Chin. Phys. Lett.,* vol. 21, pp. 1377-1380, 2004.

[44] A. Brian and H. M. McConnell, "Allogeneic stimulation of cytotoxic T cells by supported planar membranes," *Proceeding of the National Academy of Science USA,* vol. 81, pp. 6159-6163, 1984.

[45] L. Krapf, M. Dezi, W. Reichstein, J. Kohler and S. Oellerich, "AFM characterization of spin-coated multilayered dry lipid films prepared from aqueous vesicle suspensions," *Colloids and Surfaces B: Biointerfaces,* vol. 82, pp. 25-32, 2011.

[46] A. C. Simonsen and L. A. Bagatolli, "Structure of Spin-Coated Lipid Films and Domain Formation in Supported Membranes Formed by Hydration," *Langmuir,* vol. 20, pp. 9720-9728, 2004.

[47] K. Blodgett, "Films Built by Depositing Successive Monomolecular Layers on a Solid Surface," *J. Am. Chem. Soc.,* vol. 57, pp. 1007-1022, 1935.

[48] K. Blodgett and I. Langmuir, "Built-up films of barium stearate and their optical properties," *Phys. Rev.,* vol. 51, pp. 964-982, 1937.

[49] I. Langmuir and V. Schaefer, "Activities of Urease and Pepsin Monolayers," *J. Am. Chem. Soc.,* vol. 60, pp. 1351-1360, 1938.

[50] P. Weschayanwiwat, J. Scamehorn and P. Reilly, "Surfactant Properties of Low Molecular Weight Phospholipids," *Journal of Surfactants and Detergents,* vol. 8, pp. 65-72, 2005.

[51] S. Baoukina, L. Monticelli, H. J. Risselada and D. P. Tieleman, "The molecular mechanism of lipid monolayer collapse," *Proc. Of the National Academy of Science,* vol. 105, pp. 10803-10808, 2008.

[52] G. Roberts, Langmuir- Blodgett Films, New York: Plenum Press page 19, 1990.

[53] T. Osborn and P. Yager, "Modeling Success and Failure of Langmuir-Blodgett Transfer of Phospholipid Bilayers to Silicon Dioxide," *Biophysical Journal,* vol. 68, pp. 1364-1373, 1995.

[54] I. Langmuir, V. Schaefer and H. Sobotka, "Multilayers of sterols and adsorption of digitonin by deposited monolayers," *J. Am. Chem. Soc.,* vol. 59, pp. 1751-1759, 1937.

[55] L. Landau and B. Levish, "Dragging of a Liquid by a Moving Plate," *Acta Physiochemica U.R.S.S,* vol. 17, pp. 42-54, 1942.

[56] S. Wilson, "The Drag-Out Problem in Film Coating Theory," *Journal of Engineering Mathematics,* vol. 16, pp. 209-221, 1982.

[57] B. Jin and A. Acrivos, "The Drag-Out Problem in Film Coating," *Physics of Fluids,* vol. 17, pp. 1-12, 2005.

[58] A. Darhuber, S. Troian, J. Davis and S. Miller, "Selective dip-coating of chemically micropatterned surfaces," *Journal of Applied Physics,* vol. 88, pp. 5119-5126, 2000.

[59] P. Daripa and G. Pasa, "The thickening effect of interfacial surfactant in the drag-out coating problem," *Journal of Statistical Mechanics: Theory and Experiment,* vol. 7, pp. 1-10, 2009.

[60] C. Park, "Effects of insoluble surfactant in dip coating," *J. Colloid Interface Sci.,* vol. 146, p. 382, 1991.

[61] K. Ruschak, "Caoting Flows," *Annual Review of Fluid Mechanics,* vol. 17, pp. 65-89, 1985.

[62] M. J. Rosa and M. de Pinho, "Membrane surface characterisation by contact angle measurements using the immersed method," *Journal of Membrane Science,* vol. 131, pp. 167-180, 1997.

[63] J. H. Crowe, L. M. Crowe, J. F. Carpenter and C. Aurell Wistrom, "Stabilization of dry phospholipid bilayers and proteins by sugars," *Biochem. J.,* vol. 242, pp. 1-10, 1987.

[64] T. Jeon, N. Malmstad, J. Poulo and J. Schmidt, "Black lipid membranes stabilized through substrate conjugation to a hydrogel," *Biointerphases,* vol. 3, pp. 96-100, 2008.

[65] S. Kellenberger and L. Schild, "Epithelial Sodium Channel/Degenerin Family of Ion Channels: A Variety of Functions for a Shared Structure," *Physiol. Rev.,* vol. 82, pp. 735-767, 2002.

[66] R. H. Meltzer, N. Kapoor, Y. J. Qadri, S. J. Anderson, C. M. Fuller and D. J. Benos, "Heteromeric Assembly of Acid-sensitive Ion Channel and Epithelial Sodium Channel Subunits," *The Journal of Biological Chemistry* , vol. 282, pp. 25548-25559, 2007.

[67] S. Coscoy and P. Barbry, "The ENaC/Deg family of cation channels," *Advances in Molecular and Cell Biology,* vol. 32, pp. 303-329, 2004.

[68] M. B. Jackson, Molecular and Cellular Biophysics, New York: Cambridge University Press, 2006.

[69] H. Fu, Protein- Protein Interactions- Methods and Applications, vol. Methods in Molecular Biology 261, New Jersey: Humana Press Inc., 2004.

[70] D. Vance and J. Vance, Eds., Biochemistry of Lipids, Lipoproteins and Membranes, First ed., Hungary: Elsevier, 2008.

[71] M. Luckey, Membrane Structural Biology with Biomedical and Biophysical Foundations, New York: Cambridge University Press, 2008.

[72] M. Caffrey, "Membrane protein crystallization," *Journal of Structural Biology,* vol. 142, pp. 108-132, 2003.

[73] J. Frank, "Single-particle imaging of macromolecules by cryo-electron microscopy," *Annu. Rev. Biophys Biomol Struct.,* vol. 31, pp. 303-319, 2002.

[74] S. Scheuring, H. Stahlberg, M. Chami, C. Houssin, J. Rigaud and A. Engel, "[46] S. Scheuring,Charting and unzipping the surface layer of Corynebacterium glutamicum with the atomic force microscope," *Molecular Microbiology,* vol. 44, pp. 675-684, 2002.

[75] L. J. Lis, M. McAlister, N. Fuller and R. P. Rand, "Interactions between neutral phospholipid bilayer membranes," *Biophysical Journal,* vol. 37, pp. 657-666, 1982.

[76] S. Kodera, T. Okajima, H. Iwabuki, D. Kitaguchi, S. Kuroda, T. Yoshinobu, K. Tanizawa, M. Futai and H. Iwasaki, "Detection of protein–protein interactions on SiO2/Si surfaces by spectroscopic ellipsometry," *Analytical Biochemistry,* vol. 321, pp. 65-70, 2003.

[77] G. Thomas, "Raman Spectroscopy of Protein and Nucleic Acid Assemblies," *Annu. Rev. Biophys. Biomol. Struct.,* vol. 28, pp. 1-27, 1999.

[78] T.-M. Fu, "Understanding immune protection mechanisms of an influenza A virus M2 peptide vaccine," *The Journal of Immunology ,* vol. 184, p. 52, 2010.

[79] S. D. Cady, T. V. Mishanina and M. Hong, "Structure of Amantadine-bound M2 transmembrane peptide of influenza A in lipid bilayers from magic-angle-spinning solid state NMR: the role of Ser31in Amantadine binding," *J. mol. Biol.,* vol. 385, pp. 1127-1141, 2009.

[80] Z. Wang, J. Bai and Y. Xu, "The effect of charged lipids on bacteriorhodopsin membrane reconstitution and its photochemical activities," *Biochemical and Biophysical Research Communications,* vol. 371, pp. 814-817, 2008.

[81] F. N. Petersen and C. Helix Nielsen, "Raman Spectroscopy as a Tool for Investigating Lipid- Protein Interactions," *Spectroscopy,* vol. 24, pp. 1-8, 2009.

[82] C. M. Canessa, L. Schild, G. Buell, B. Thorens, I. Gautschi, J. D. Horisberger and B. C. Rossier, "Amiloride-sensitive epithelial Na+ channel is made of three homologous subunits," *Nature,* vol. 367, pp. 463-467, 1994.

[83] P. M. Snyder, C. Cheng, L. S. Prince, J. C. Rogers and M. J. Welsh, "Electrophysiological and Biochemical Evidence That DEG/ENAC Cation Channels are Composed of Nine Subunits," *The Journal of Biological Chemistry,* vol. 273, pp. 681-684, 1997.

[84] A. Staruschenko, J. L. Medina, P. Patel, M. S. Shapiro, R. E. Booth and J. D. Stockand, "Fluorescence Resonance Energy Transfer Analysis of Subunit stoichiometry of the epithelial Na+ channel," *The Journal of Biological Chemistry,* vol. 279, pp. 27729-27734, 2004.

[85] C. A. Schnaitman, "Protein composition of the cell wall and cytoplasmic membrane of Escherichia coli," *Journal of Bacteriology,* vol. 104, pp. 890-901, 1970.

[86] C. Tanfor, "Protein Denaturation," *Advances in Protein Chemistry,* vol. 23, pp. 121-282, 1968.

[87] A. Plant, M. Brighamburke, E. Petrella and D. Oshannessy, "Phospholipid/Alkanethiol Bilayers for Cell-Surface Receptor Studies by Surface Plasmon Resonance," *Analytical Biochemistry,* vol. 226, pp. 342-348, 1995.

[88] K. Glasmästar, C. Larsson, F. Höök and B. Kasemo, "Protein Adsorption on Supported Phospholipid Bilayers," *Journal of Colloid and Interface Science,* vol. 246, pp. 40-47, 2002.

[89] F. Höök, M. Rodahl, B. Kasemo and P. Brzezinski, "Structural changes in hemoglobin during adsorption to solid surfaces: Effects of pH, ionic strength, and ligand binding," *Proceedings of the National Academy of Sciences of the United States of America,* vol. 95, pp. 12271-12276, 1998.

[90] A. Lundgren, J. Hedlund, O. Andersson, M. Branden, A. Kunze, H. Elwing and F. Hook, "Resonance-Mode Electrochemical Impedance Measurements of Silicon Dioxide Supported Lipid Bilayer Formation and Ion Channel Mediated Charge Transport," *Analytical Chemistry,* vol. 83, pp. 7800-7806, 2011.

[91] A. Studer, X. Han, F. K. Winklera and L. X. Tiefenauera, "Formation of individual protein channels in lipid bilayers suspended in nanopores," *Colloids and Surfaces B: Biointerfaces,* vol. 73, pp. 325-331, 2009.

[92] L. Chernomordik, S. Sukharev, I. Abidor and Y. Chizmadzhev, "Breakdown of lipid bilayer membranes in an electric field," *Biochimica et Biophysica Acta (BBA) - Biomembranes,* vol. 736, pp. 203-213, 1983.

[93] V. Atanasov, N. Knorr, R. Duran, S. Ingebrandt, A. Offenhausser, W. Knoll and I. Koper, "Membrane on a Chip: A Functional Tethered Lipid Bilayer Membrane on Silicon Oxide Surfaces," *Biophysical Journal,* vol. 89, pp. 1780-1788, 2005.

[94] M. Naumowicz, A. D. Petelska and Z. A. Figaszewski, "Impedance analysis of a phosphatidylcholine-phosphatidylethanolamine system in bilayer lipid membranes," *Electrochemica Acta,* vol. 51, pp. 5024-5028, 2006.

[95] R. Roskamp, I. Vockenroth, N. Eisenmenger, J. Braunagel and I. Koper, "Functional Tethered Bilayer Lipid Membranes on Aluminum Oxide," *ChemPhysChem,* vol. 9, pp. 1920-1924, 2008.

[96] R. W. Glaser, S. L. Leikin, L. V. Chernomordik, V. F. Pastushenko and A. I. Sokirko, "Reversible electrical breakdown of lipid bilayers: formation and evolution of pores," *Biochimica et Biophysica Acta,* vol. 940, pp. 275-287, 1988.

[97] L. Chernomordik, S. Sukharev, S. Popov, V. Pastushenko, A. Sokirko, I. Abidor and Y. Chizmadzhev, "The electrical breakdown of cell and lipid membranes: the similarity of phenomenologies," vol. 902, pp. 360-373, 1987.

[98] R. Benz, F. Beckers and U. Zimmermann, "Reversible electrical breakdown of lipid bilayer membranes: A charge-pulse relaxation study," *JOURNAL OF MEMBRANE BIOLOGY,* vol. 48, pp. 181-204, 1979.

[99] U. Zimmermann, G. Pilwat, F. Beckers and F. Riemann, "Effects of external electrical fields on cell membranes," *Bioelectrochemistry and Bioenergetics,* vol. 3, pp. 58-83, 1976.

[100] S. Ohki, "The Electrical Capacitamce of Phospholipid Membranes," *Biophysical Journal,* vol. 9, pp. 1195-1205, 1969.

[101] V. Dressler, K. Schwister, C. Haest and B. Deuticke, "Dielectricbreakdown of the erythrocytemembraneenhancestransbilayermobility of phospholipids," *Biochimica et Biophysica Acta (BBA) - Biomembranes,* vol. 732, pp. 304-307, 1983.

[102] R. Benz, O. Fröhlich, P. Lauger and M. Montal, "Electrical capacity of black lipid films and of lipid bilayers made from monolayers," *Biochim. Biophys. Acta,* vol. 394, pp. 323-334, 1975.

[103] A. J. Bard and L. R. Faulkner, Electrochemical Methods Fundamentals and Applications, Hoboken, NJ: John Wiley and Sons, Inc, 2001.

[104] A. J. Bard and L. R. Faulkner, Electrochemical Methods Fundamentals and Applications, Hoboken, NJ: John Wiley and Sons, Inc, 2001.

[105] S. Gold, K.-L. Chu, C. Lu, M. A. Shannon and R. I. Masel, "Acid loaded porous silicon as a proton exchange membrane for micro-fuel cells," *Journal of Power Sources,* vol. 135, pp. 198-203, 2004.

[106] X. G. Zhang, Electrochemistry of Silicon and Its Oxide, New York: Kluwer Academic/Plenum Publishers, 2001, p. 14.

[107] M. Naumowicz and J. Kotynska, "Impedance analysis of phosphatidylcholine membranes modified with valinomycin," *European Biophysics Journal,* vol. 35, pp. 239-246, 2006.

[108] M. Naumowicz, A. D. Petelska and Z. A. Figaszewski, "Impedance Analysis of Complex Formation Equilibria in Phosphatidylcholine Bilayers Containing Decanoic Acid or Decylamine," *Cell Biochem Biophys,* vol. 61, pp. 145-155, 2011.

[109] V. Lehmann, "The Physics of Macropore Formation in Low Doped n-Type Silicon," *Journal of The Electrochemical Society,* vol. 140, pp. 2836-2843, 1993.

VITA

Khalid Hasan Tantawi received his Bachelor of Science degree in Mechatronics Engineering in 2005 from the University of Jordan in Amman, Jordan. He received a double Master of Science degree in Aerospace Engineering from École nationale supérieure de l'aéronautique et de l'espace (SupAero) in Toulouse, France and University of Pisa in Pisa, Italy in 2007. Khalid obtained a masters degree in Electrical Engineering from the University of Alabama in Huntsville in 2011.

His research interests include porous silicon fabrication, lipid bilayer membranes, electrochemical impedance spectroscopy, photosensitive glass processing, glass science, composition and structural analysis of materials, and rigid and flexible body dynamics.